Parton Cascades and Hadronisation in High Energy Processes

Sandipan Mohanty

Department of Theoretical Physics
Lund University, Sweden

Thesis for the degree of Doctor of Philosophy

Thesis Advisors: Bo Andersson and Gösta Gustafson

Faculty Opponent: Andrzej Białas

To be presented, with the permission of the Faculty of Natural Sciences of Lund University, for public criticism in Lecture Hall F of the Department of Theoretical Physics on Friday, May 16th, 2003, at 10.30 a.m.

To my friends

This thesis is based on the following publications:

I B. Andersson, S. Mohanty and F. Söderberg,
The Lund Fragmentation Process for a Multi-gluon String According to the Area Law
European Physical Journal **C21**, 631–647 (2001).

II S. Mohanty
ALFS: A New String Fragmentation MC Based on the Lund Model
LU TP 03-09

III B. Andersson, S. Mohanty and F. Söderberg,
The λ-Measure and the Generalised Dipoles in the Lund Model
Nuclear Physics **B646**, 102–126 (2002).

IV S. Mohanty and F. Söderberg,
Coherence Chains and Bose-Einstein Correlations in the Lund Model
LU TP 03-08.

Contents

Introduction

What is essential is invisible to the eye.

Antoine De Saint-Exupery
in *The Little Prince*

To the best of our knowledge, all matter consists of a very small set of basic building blocks called quarks and leptons. There are six kinds of quarks and equally many kinds of leptons. Our very familiar electron is a lepton. We understand the electrons quite well, and we can persuade millions of millions of millions of those particles to move around and, for instance, play music for us. The electron has two heavier cousins: the muon and the tau lepton. They are almost identical to the electron in most of their properties, but they are a lot heavier and decay too quickly for "muonics" or "tauonics" to be possible. The three other leptons are the electron-neutrino, the muon-neutrino and the tau-neutrino. These particles are electrically neutral and very light. They interact so rarely with the other particles that it is extremely common for the neutrinos to pass through the whole earth completely oblivious to the presence of all other particles!

The six kinds of quarks are called "up" (u), "down" (d), "charm" (c), "strange" (s), "top" (t) and "bottom" (b). Most forms of matter known to us are made out of the u and d quarks and the electrons. The other quarks, as well as the leptons are produced in high energy processes in nature, or in man made experiments. They have very short life-times and decay into the u or d quarks, the electrons and the neutrinos.

The charged leptons interact with each other and with the quarks through three kinds of forces or interactions, the electromagnetic, the weak and the gravitational interactions. The neutrinos, which are electrically neutral, can not feel the electromagnetic interaction. The quarks interact through all these interactions, but they also participate in another kind of interaction, called the strong interaction.

One of the most puzzling aspects of this strong force is that any elementary particle which feels the strong force is necessarily in a "composite" made out of several elementary constituents. Such composites are called hadrons, and the most common examples are the proton (uud) and the neutron (udd). No quark has ever been observed free.

Just like the particles which experience the electric force have electric charge, the particles which participate in strong interactions are said to have a "strong charge". Equal amounts of positive and negative electric charge could be added to make an electrically neutral object. The "strong" charge however, comes in three kinds and all three kinds of the charge need to be added in a particular way to make something neutral. As this is reminds of the way colours mix, i.e., the three primary colours need to be mixed to make a neutral or white object, the strong charge is referred to as the "colour" charge, even though it has no connection whatsoever, with the colours we see. Likewise, the theory of strong interactions is referred to as "Quantum Chromo Dynamics" or QCD. One way of saying the above fact about particles interacting with the strong force never occurring free in nature, is to say that the QCD colour is confined, or that only those particles which are "white" can occur free in nature.

Apart from the particles, there are anti-particles in nature, which have the same masses as ordinary particles, but exactly the opposite charges. For instance, the electron which is negatively charged, has an anti-particle called the "positron", which has the same mass as the electron but is positively charged. A particle and its anti-particle can annihilate each other when they collide, and produce an equivalent amount of energy. This is why one does not normally come across a lot of anti-particles in daily life. Any anti-particles present in our world would very quickly meet with a corresponding particle and the two would annihilate each other. But anti-particles can be created in experiments.

An accelerated electric charge radiates electromagnetic radiation, and in the modern description, even this radiation comes in the form of particles called "photons". Colour charges can similarly emit a form of radiation represented by particles analogous to the photons. These particles are called "gluons". The photons and the gluons appear as particles, but they do not constitute matter. They are associated with forces or interactions. One very interesting property of the gluons is that they have colour charge, in contrast to the photons which do not have any electric charge. This means that as soon as a gluon is radiated, there are more charges present to radiate even more gluons, and so on. Some gluons may also decay into quark anti-quark pairs. Quarks and gluons are often referred to as "partons", and this process of creation of more and more coloured particles is referred to as a "parton cascade".

If quarks have never been seen, why do we think that they exist ? Different quarks have different electric charges. This means that the quarks in a proton for instance, will not always present a united front to every external object. An electrically charged particle might be able to interact with just one quark inside a proton. Such experiments have been done, and they show that even though

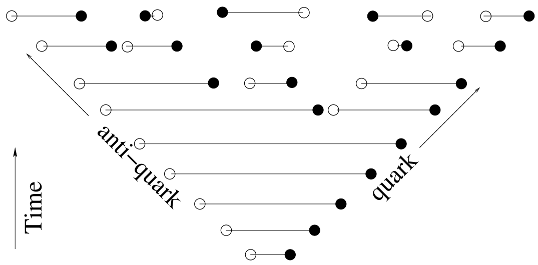

Figure 1: The figure shows a schematic "time sequence" of the hadronisation process in the Lund model. A quark anti-quark pair, formed for instance after the annihilation of an electron and a positron, move away from each other and stretch a string between them. After a sufficient amount of energy is stored in the string, new quark anti-quark pairs form out of the energy of the string.

we do not find free quarks, these particles occur as constituents of composite objects. If an electron can sense a quark inside a proton, could it not strike that quark with a lot of energy so that it is separated from the rest of the proton ? While that seems to be possible, i.e. the proton does not always survive such a collision, we still don't see any free quarks. If a quark is struck off a proton, what we observe is a group of several hadrons, rather than free quarks.

There are other situations in which quarks are produced. For instance if electrons collide with their anti-particles positrons, the two may annihilate each other and through an intermediate photon or "Z" particle produce a quark–anti-quark ($q\overline{q}$) pair. In all such cases however, the final state particles are always hadrons. If a quark is struck from a proton or a ($q\overline{q}$) pair is produced from electron positron annihilation, the moving colour charges will radiate gluons leading to a parton cascade. There is a mechanism in nature which somehow combines all those coloured particles to make a group of colourless hadrons. That process is referred to as "hadronisation".

One of the most widely used techniques in physics, the perturbation theory, is unsuitable for a description of hadronisation. This is because at the length and energy scales at which hadronisation takes place, the coupling constant of the strong interaction is large, and the perturbation series do not converge. Although it is not possible to describe hadronisation from first principles, it is possible to make physically well motivated assumptions and model the process. One such hadronisation model is the Lund string fragmentation model. The Lund model assumes that the "field lines" of the colour force do not spread out in space like the electric field. The field is assumed to be collimated in a flux tube, called the string, extending from a coloured particle to an anti-coloured particle. The field has a uniform energy density which is quite large. Therefore, if the partons in a $q\overline{q}$ pair, formed in an electron positron annihilation experiment for instance, move away from each other, they might lose a sufficient amount of energy to the string between them for a new $q\overline{q}$ pair to be generated from the string energy. This process breaks the string into two pieces in the Lund model. After a series of such string breakups, the system consists of a number of small oscillating objects, each with a coloured and an anti-coloured particle connected by a small string between them, as illustrated in Fig.1. Such systems are used as rough pictures of hadrons in the model.

Using basic symmetry assumptions one could derive a stochastic process describing the formation of hadrons in this model. Computer simulations based on this model have shown that this semiclassical model describes experimental data very well. A part of the work in this thesis involved one such implementation of the Lund model.

A Short Synopsis of this Dissertation

To be concise, this thesis develops and investigates an alternative approach to the Lund hadronisation model for multi-gluon strings.

String fragmentation for simple $q\overline{q}$ strings, often referred to as "flat" strings, is theoretically well understood. The model builds upon clear assumptions based on our understanding of strong interactions, and leads to a satisfactory description of multi-particle production. The relative probability, for the production of a multi-particle state in the model, is the phase space for the final state multiplied by an exponential suppression factor for the area traced by the string through space–time before it decays into hadrons. This result, known as the area law, is intuitively very appealing, and has several analogues in other dynamical situations.

The world surfaces of multi-gluon strings are complicated curved surfaces in space–time. The standard treatment of the fragmentation of multi-gluon strings, is built upon an extrapolation of certain relations between dynamical variables, which are derived in the context of fragmentation of flat strings. Such a treatment is very successful in describing experimental data, although these relations represent an exponential area suppression, only when the string is flat. It is therefore interesting to ask if a strict adherence to the physically well motivated area law could differ in its predictions.

An alternative fragmentation procedure, which implements the area law for multi-gluon strings, is developed in this thesis. The new procedure associates well defined planar "plaquettes" with the formation of each particle. The plaquettes serve to partition the total area used in the area law between different hadrons. The procedure has been implemented in a Monte Carlo ALFS, which has been used to study the properties of final state hadrons obtained in this method. It is found that the inclusive single particle distributions from ALFS are in agreement with those obtained from Pythia.

The new formulation for the fragmentation of gluonic strings has been used herein, to generalise a model for the Bose-Einstein correlations in the Lund model. The generalisation is possible because of the properties of QCD parton cascades and our fragmentation procedure. Our finding to date however, is that although the extension of the Bose-Einstein model has many attractive theoretical features, the total correlation strength obtained in this method is too small to describe experimental data.

The fragmentation procedure has also been extended to include certain complications which arise when the invariant mass of the decaying string is small. The Monte Carlo Alfs has accordingly grown to accommodate this. As this is a new development, the implications of this procedure for small energy systems are currently under investigation. Treatment of low energy systems is relevant not only for situations with small total initial energy, but also for higher energies, through the treatment of the limited remaining system at the end of a hadronisation cascade.

Analytical results are usually important for a physical understanding of the dynamics, but computer simulations are also frequently very valuable, or even necessary. The results obtainable from the Monte Carlo Alfs may be very valuable for the interpretation of experimental data. The results are expected to differ from the traditional Monte Carlo Pythia, in particular for the fragmentation of low energy systems and at higher energies for particle correlations, including correlations between identical particles due to Bose-Einstein statistics.

The Papers

The papers constituting the major part of this thesis will be presented in their logical order, rather than the chronological order of their publication. In paper-I, described below, the problem of formulating the area law on a general multi-gluon string is addressed. Several alternative strategies were examined and rejected in favour of one approach along the boundary curve of the string world surface. The second paper in this thesis, the last in the chronological order, extends the fragmentation process developed in paper-I. In addition it introduces a Monte Carlo implementation called Alfs.

Study of this new approach towards string fragmentation lead to the ideas for the next two papers. We found that it is possible to group the final state of hadrons obtained from Alfs into groups, so that within each group the hadron energy–momenta were aligned in a plane in the Minkowski space within small transverse fluctuations. We named these structures as “Coherence Chains”, and found that there is very little difference in the distribution of the number of hadrons in a coherence chain, between events with different cms energy, thrust, total lambda measure etc. To understand the reasons behind the occurrence of such features, we undertook an investigation of QCD parton cascades, which appears as Paper-III. The existence of coherence chains, and their stability with respect to changes in the global event properties, is an attractive base for an analysis of Bose-Einstein correlations on multi-gluon events. An effort in that direction appears as Paper-IV.

Paper I

In this paper we made a detailed investigation of the fragmentation of a multi-gluon Lund string. Using the description of the string surface in terms of its boundary curve called the "directrix", we formulated string fragmentation according to the area law for a general multi-gluon state. It turned out that a description of the fragmentation process on the string surface is possible, but rather cumbersome. An alternative process, which could be defined along the directrix, is intuitively a lot more tractable. For this process the area in the Lund model area law appeared as the area between the directrix and the space-time curve obtained by placing the hadron energy momentum vectors one after the other in rank order. Each event is thus weighted with respect to a well defined area characterising it. We found that for a consistent formulation near the bends of the directrix, it is necessary to introduce small deformations on the string state around such corners. These deformations are small compared to a resolution scale determined by the hadron masses and should therefore not be important. This procedure will be referred to as "gluon corner crossing".

We showed that the fragmentation process defined along the directrix, has a continuum limit when the hadron mass becomes small. The differential equations for this continuum limit were very similar to those derived in connection with the λ-measure, which is a generalisation of the available rapidity range for hadron formation from multi-gluon strings.

Paper II

The string fragmentation scenario developed in paper-I is extended to incorporate the generation of transverse momentum during the string breakup process, as well as some effects of limited available phase space at small cms energies.

The fragmentation process along the directrix is interpreted as the construction of a series of planar "Plaquettes" along the directrix. These plaquettes partition the area between the directrix and the hadronic curve into planar quadrangular regions corresponding to the formation of individual hadrons.

The gluon corner crossing procedure in paper-I, which involves a local modification of the directrix around the gluon corners, invariably results in adjacent plaquettes with different planes at every gluon corner. For the vertices at the junction of such plaquettes, there is only one unique direction for the transverse momentum fluctuations. This constraint is so severe that it rules out most procedures for the assignment of fragmentation transverse momenta for iterative algorithms.

If the invariant mass of the string is comparable to the hadronic mass scale, the fragmentation function is not energy independent. Further, in such a situation, the distribution of the fragmentation variable z is coupled to the quark flavours and hadronisation transverse momenta. Corrections due to a limited available phase space at the end of the iterative process, and for systems with very small invariant masses, were introduced into our model in this paper. A formulation is provided in which detailed calculations of phase space integrals can be performed and conveniently incorporated into the Monte Carlo implementation.

Another purpose of this paper is to introduce the Monte Carlo implementation for the model called ALFS. The user interface for ALFS is summarised along with a brief description of the internal structure.

Paper III

Part of the name of this dissertation is because of the work in this paper. Parton cascades are simplified treatments of multiple gluon emission in perturbative QCD. The result of a parton cascade is the input to a hadronisation model. Our aim was to understand the properties observed among the hadronisation products obtained in ALFS. The Lund colour dipole model is the framework for most of this paper. A few comparisons were also made with the parton cascade in PYTHIA concerning the main properties.

The number of gluons emitted with transverse momenta above a certain given cut-off showed an interesting linear correlation with the gluon emission phase space at that value. This was understood as the effect of uncorrelated contributions to the phase space from all the colour dipoles present. Further, the distribution of these contributions from individual dipoles is rather insensitive to the cms energy of the event, as well as the event structure parametrised by variables like the thrust and the total phase space in all dipoles.

The distribution is also surprisingly insensitive to the value of the ordering variable or the cut-off scale of the parton cascade, in an interesting range for the value of the parameter, just above the scale where non-perturbative hadronisation effects are believed to set in.

The available rapidity range for the emission of gluons in a dipole is a function of the transverse momentum of the emitted gluon. Therefore the phase space variable varies with the changes in the value of the ordering variable. Several factors contribute to the changes in the total number of dipoles with a certain size, when the ordering variable decreases. One contribution is a trivial scaling because of the definition of the size in terms of the rapidity range.

Dipoles of larger size may decay such that one of the daughter dipoles falls into the bin of dipole sizes under consideration. Dipoles in the bin might also decay to smaller dipoles and hence move out of the bin. There is an increased emission probability at smaller cut-off scales, due to the running coupling in QCD. We found that these contributions balance each other to produce the stable results mentioned above.

Paper IV

The Lund model area law has an algebraic form that is similar to quantum mechanical transition probabilities, i.e. the final state phase space multiplied by a factor characterising the event. One could motivate a possible quantum mechanical amplitude characterising an underlying physical process which would give rise to the area law. One of the consequences of such an amplitude is that the probability for the formation of identical bosons with small momentum separation is enhanced, due to interference of contributions to the amplitude from permuted configurations of identical particles in the final state. Such an effect is well known in multi-particle production, and is called the Bose-Einstein effect. In the framework of the Lund hadronisation model, such a description of the BEC, based on an amplitude corresponding to the area law is very natural. A formulation applicable to flat strings had been developed earlier by B. Andersson and M. Ringnér.

Since the hadronisation picture in ALFS adhered to the area law in a tractable way for multi-gluon strings, it is well suited for an extension of the Lund picture for BEC. Paper-IV describes such an extension. We find that the permutations of identical particles in the final state for multi-gluon strings are severely constrained. As a first approximation therefore, we considered permutations within the aforementioned coherence chains. This results in the factorisation of the event weight, and a consistent formulation. Even though the event weight showed a multiplicity dependence, we showed that because of the stability properties of the coherence chains, the fragmentation model with Bose-Einstein weights could be re-tuned so that the multiplicity distributions are restored for all event structures. The resulting Bose-Einstein signal however, appears to be too small to be a complete description of the experimentally observed correlations. This suggests that further inputs are required for a proper description of the phenomenon.

Acknowledgements

I would like to express my gratitude towards the late Prof. Bo Andersson for constantly challenging me with new ideas for two and a half years. I am grateful to Prof. Gösta Gustafson for teaching me so much while we cooperated on our projects over the last one year. I gratefully acknowledge the help I received from the senior members of the department, Torbjörn Sjöstrand and Leif Lönnblad. It has also been a great pleasure collaborating with Fredrik Söderberg during these years. Much of the work in this thesis would not have been possible without the insights derived from numerous fruitful discussions with these persons.

I thank all my colleagues for creating such a great work environment at the department and being such funny and interesting people after office hours. It has been a pleasure sharing the office with Stefan, Gabriela and Malin at different times. Finally, my sincere thanks to the meteorological department for the wonderful weather in Lund during the last one month before I finished writing this thesis.

The Lund Fragmentation Process for a Multi-gluon String According to the Area Law

Paper I

LU TP 01-22
June 2001

The Lund Fragmentation Process for a Multi-gluon String According to the Area Law

Bo Andersson[1]
Sandipan Mohanty[2]
Fredrik Söderberg[3]
Department of Theoretical Physics, Lund University,
Sölvegatan 14A, S-223 62 Lund, Sweden

Abstract
The Lund Area Law describes the probability for the production of a set of colourless hadrons from an initial set of partons, in the Lund string fragmentation model. It was derived from classical probability concepts but has later been interpreted as the result of gauge invariance in terms of the Wilson gauge loop integrals. In this paper *we will present a general method to implement the Area Law for a multi-gluon string state.* In this case the world surface of the massless relativistic string is a geometrically bent $(1+1)$-dimensional surface embedded in the $(1+3)$-dimensional Minkowski space. The partonic states are in general given by a perturbative QCD cascade and are consequently defined only down to a cutoff in the energy momentum fluctuations. *We will show that our method defines the states down to the hadronic mass scale inside an analytically calculable scenario.*

We will then show that there is a differential version of our process which is closely related to the generalised rapidity range λ, which has been used as a measure on the partonic states. We identify λ as the area spanned between *the directrix curve* (the curve given by the parton energy momentum vectors laid out in colour order, which determines the string surface) and the average curve (to be called the $\mathcal{P}$-curve) of the stochastic X-curves (curves obtained when the hadronic energy-momentum vectors are laid out in rank order). Finally *we show that from the X-curve corresponding to a particular stochastic fragmentation situation it is possible to reproduce the directrix curve* (up to one starting vector and a set of sign choices, one for each hadron). This relationship provides an analytical formulation of the notion of Parton-Hadron Duality. The whole effort is made in order to get a new handle to treat the transition region between where we expect perturbative QCD to work and where the hadronic features become noticeable.

[1]bo@thep.lu.se
[2]sandipan@thep.lu.se
[3]fredrik@thep.lu.se

1.1 Introduction

The Lund String Fragmentation Model was developed many years ago, [1, 3], and as implemented in the well-known Monte Carlo simulation program JETSET, [4], it has been very successful in reproducing experimental data from high energy multi-particle processes.

The model is based upon a few general assumptions: (i) the final state particles stem from the breakup of a string-like force field spanned between the coloured constituents, (ii) there is causality and Lorentz invariance and (iii) the production of the particles can be described in terms of a stochastic process which obeys a saturation assumption. We have, in a recent paper [5], re-derived the major result for the (1+1)-dimensional model, which is applicable for events with a quark (q, a colour-3) and an anti-quark ($\bar{q}$, a colour-$\bar{3}$) at the endpoints of the string but with no interior gluonic (g, colour-8) excitations. The result is that the (non-normalised) probability for the production of an n-particle final state of hadrons with energy momenta $\{p_j\}$ and masses $\{m_j\}$ is given by the Lund Area Law:

$$dP_n(\{p_j\}; P_{tot}) = \prod_{j=1}^{n} N_j d^2 p_j \delta(p_j^2 - m_j^2) \delta(\sum_{j=1}^{n} p_j - P_{tot}) \exp(-bA) \tag{1.1}$$

where A is the area spanned by the string "before" the breakup, cf. Fig.1.1, P_{tot} is the total energy-momentum of the state and $\{N_j\}$ and b are parameters related to the density of hadronic states and the breakup properties of the string field, respectively.

The result in Eq. (1.1) is evidently similar to a quantum mechanical transition probability. It is the final state phase space multiplied by a squared matrix element, which in this case would correspond to the negative area exponential. In [5] we have shown that it is possible to "diagonalise" the model, i.e. to express the result in Eq. (1.1) as a product of (diagonal) transition operators (in quantum mechanical language it would correspond to density operators). It turns out that in this way the dynamics can be described in terms of $(1 + 1)$-dimensional (space-like) harmonic oscillators.

Shortly after the original derivation of the Area Law, [1], Sjöstrand, [6], provided an implementation of the model applicable also for multi-gluon states, i.e. when the string surface is no longer flat but geometrically bent due to the internal excitations. Sjöstrand's method is to project the positions of the breakup points (the vertices) from the (flat) $(1+1)$-dimensional model as given by Eq. (1.1) onto the surface of the bent string. The projection is done so that the proper times of the vertices and the squared masses of the particles produced between them are the same. Unfortunately this method does not fulfil the Area Law on the bent surface because it is a geometrical fact that the

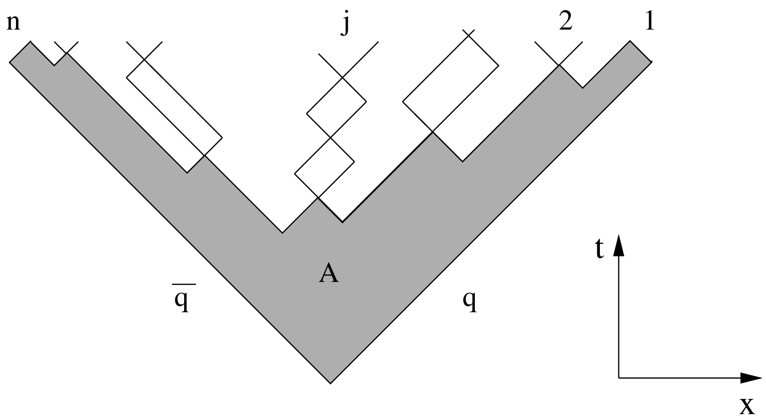

Figure 1.1: A high-energy string breakup.

areas "below the vertices" are not invariant under such a projection from a flat to a bent surface.

Although the Area Law is not fulfilled on an event to event basis by the method in [6] we will show that it is fulfilled in an average sense, i.e. the predicted inclusive distributions are little affected by the differences. It is well-known that the experimental results for these distributions are well described by JETSET even up to the largest available energies of today.

The intention of this note is to implement another method for particle production in multi-gluon states which fulfils the Area Law at every single step in the production process. We will find that it is necessary to tackle a set of problems in the definition of the states which we apply the process to. We note that the states defined by perturbation theory are resolved only to the scale of some virtuality cutoff. We will find that our method provides a set of excitations on the hadronic mass scale, in the string field. We will investigate the properties of these "soft hadronisation gluons" in future work.

The states of the massless relativistic string fulfil a minimum principle, i.e. the surface spanned in spacetime by the string during its motion is a minimal surface. This means on the one hand, that the states should be stable against small-scale variations and on the other hand that the surface is fully determined by the boundary curve. In this case the boundary curve corresponds to the orbit of one of the endpoints, conventionally chosen as the q-endpoint. Therefore, the process we are going to define is a process along this curve, to be called the *directrix curve*, which is completely defined by the perturbative cascade. In this paper we will treat the partons as massless, although both the process and the directrix curve can be defined for a general case with massive quarks.

One property which can be derived from Eq. (1.1) is that the average decay region is a typical hyperbola. On the average, the final state hadrons in our process will be produced in the same way, albeit this time along a set of connected hyperbolae. In [2] we have defined such an average curve and we will, in this paper, call it the $\mathcal{X}$-curve. Just as a simple hyperbola has a length proportional to the hyperbolic angle that it spans (this corresponds to the available rapidity range along the mean decay region, in a two-jet system of hadrons) the $\mathcal{X}$-curve has a length corresponding to a generalised rapidity range, usually called the λ measure, [2, 3]. The $\mathcal{X}$-curve is defined in terms of differential equations and we will show the close relationship between the $\mathcal{X}$-curve and our process in the limit of a vanishing hadron mass.

There are several reasons to undertake this investigation. One is to compare the precise implementation of the Area Law to the approximate process in [6]. We will do this both in this paper and in future publications.

Another reason is to get a handle on the general structure of fragmentation, in particular to be able to treat also the multi-gluon fragmentation states by the analytical methods introduced in [5]. This is of particular interest for the transition region, i.e. the region in between where we expect perturbation theory to work and where we know that the non-perturbative fragmentation sets in.

A final reason is to investigate the stability of the states in QCD under fragmentation, i.e. given a multi-gluon state defined according to the rules of perturbation theory (with cut-offs as mentioned above) to find out to what extent it can be modified so that the observable results after fragmentation are still in agreement with the experiments. In the Lund interpretation of fragmentation where the particles stem from the energy of the force field it is tacitly assumed that modifications of the perturbative state below and up to the scale of the hadronic masses should have no effects. We will find that it is necessary to take into account the coherence properties of the radiation in any modification.

Although the methods presented in this paper are applicable to any multi-gluon state, for definiteness we will concentrate on the states obtained in e^+e^--annihilation processes where we expect an original colour singlet $(q\bar{q})$-state to form and start to go apart, producing a set of bremsstrahlung gluons inside an essentially point-like region. We will also be satisfied to treat a single kind of hadron with mass m. Finally, in this paper we will not introduce gaussian transverse momentum fluctuations (which we expect in a tunneling scenario [3]) in the fragmentation process. We will investigate the influence of such fluctuations in a future publication.

In Section 1.2, we provide a set of necessary formulae from the $(1 + 1)$-dimensional Lund Model. In Section 1.3, we consider the motion of strings containing internal excitations. We also provide a description of the coherence properties of QCD and some necessary formulae to understand the $\mathcal{X}$-curve. In Section 1.4, we define the properties of the string breakup in general. We find that the most general implementation of the Area Law leads to a highly intractable process and therefore in Section 1.5 we define another approach which mends all the problems with the earlier one. In particular, in Section 1.5.3 we show a close relationship between a differential version of this process and the $\mathcal{X}$-curve. In Section 1.6, we present a set of results from our method, followed by some concluding remarks on future work in Section 1.7.

1.2 Some results from the $(1+1)$-dimensional model

1.2.1 The Area Law

The Lund Model contains a non-trivial interpretation of the QCD force-field in terms of the massless relativistic string with the quarks (q) and the anti-quarks ($\bar{q}$) at the endpoints and the gluons (g) as internal excitations on the string field. It is assumed that the force field can break up into smaller parts in the fragmentation process by the production of new ($q\bar{q}$)-states (i.e. new endpoints). A q from one such breakup point ("vertex"), together with a $\bar{q}$ from an adjacent vertex and the field between them, can form a hadron on mass shell.

For the simple case when there are no gluons, the string field only corresponds to a constant force field (with a phenomenological size $\kappa \simeq 1GeV/fm$) spanned between the original $q\bar{q}$-pair. In a semi-classical picture, conservation of energy-momentum allows the creation of a new massless pair at some point along the field. The pair will then go apart along opposite light-cones, using up the energy in the field in between (in this way the confined fields will always end on the charges). In order that the hadron produced between two adjacent vertices should have a positive squared mass, it is necessary that the vertices are placed in a space-like manner with respect to each other. Consequently, time-ordering will be a frame-dependent statement (in any Lorentz frame the slowest particles will be the first to be produced, thereby fulfilling the requirements in a Landau-Pomeranchuk formation time scenario). It is possible to order the production process instead, along the light-cones and introduce the notion of *rank* so that the first rank hadron along the original q-light-cone will contain that q together with a $\bar{q}$ from the first vertex along the light-cone, the second rank hadron a q from the first vertex and a $\bar{q}$ from the next etc.; cf. Fig.1.1. Rank ordering is a frame independent procedure. It is of course possible to introduce a rank-ordering also from the end containing the original $\bar{q}$. One obtains , [1, 3, 5], the unique process described by Eq. (1.1)

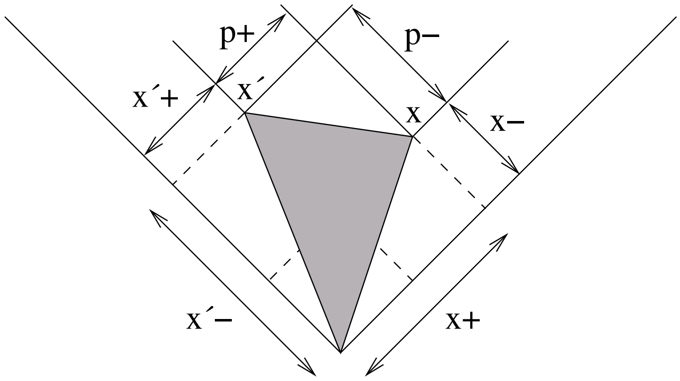

Figure 1.2: Two adjacent vertices of the string breakup process.

from these observations and an assumption that the breakup process obeys a saturation assumption, i.e. that after many steps when we are far from the endpoints the proper times of the vertices will be distributed according to an energy-independent distribution.

A particular feature is that if a particle with energy-momentum $p = (p_+, p_-)$ and with squared mass $m^2 = p^2 = p_+ p_-$ is produced between the two vertices with $x = (x_+, x_-)$ and $x' = (x'_+, x'_-)$ then we have (cf. Fig.1.2):

$$\begin{aligned} p_+ &= \kappa(x_+ - x'_+) \equiv q_+ - q'_+ \\ p_- &= \kappa(x'_- - x_-) \equiv q_- - q'_- \end{aligned} \tag{1.2}$$

Thus we find that on a flat string surface the difference between the vertex points will fulfil :

$$(x - x')^2 = -m^2/\kappa^2 \tag{1.3}$$

Eq. (1.2) implies that the $(1+1)$-dimensional Lund Fragmentation Model may also be described by means of a multi-peripheral chain diagram as in Fig.1.3 or in an energy-momentum space picture as in Fig.1.4.

This is used in [5] in order to subdivide the Area Law process into steps in between the vertices. The energy-momentum conserving δ-distribution in Eq. (1.1) can be "solved" by introducing the momentum transfers $\{q_j\}$ instead of the hadron momenta $\{p_j\}$. Then the mass-shell condition means that the hyperbolic angle between the vertices and the size of the area slit, exhibited in Fig.1.2 are fixed by the squared sizes $q^2 = -\Gamma$, $(q')^2 = -\Gamma'$ and $(q - q')^2 = m^2$.

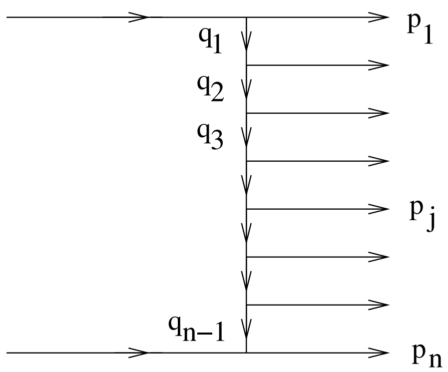

Figure 1.3: A ladder diagram describing multi-particle production.

The result is that Eq. (1.1) can be rewritten as a product of steps between the $\{\Gamma_j\}$:

$$\begin{aligned} dP_n(\{p_j\}, P_{tot}) &= \prod K(\Gamma_j, \Gamma_{j-1}, m^2) d\Gamma_j \\ K(\Gamma, \Gamma', m^2) &= N \frac{\exp(-\frac{b}{2}\sqrt{\lambda(\Gamma, \Gamma', -m^2)})}{\sqrt{\lambda(\Gamma, \Gamma', -m^2)}} \\ \lambda(a, b, c) &= a^2 + b^2 + c^2 - 2ab - 2ac - 2bc \end{aligned} \tag{1.4}$$

It is a remarkable fact that the transfer operators K can be diagonalised in terms of the eigenfunctions of the harmonic oscillator (those which are boost-invariant in a $(1+1)$-dimensional space-like Minkowski space. in a two-dimensional Euclidean space they correspond to a vanishing angular momentum) $g_n(\Gamma)$ with the eigenvalues solely determined by the squared mass of the hadrons produced in between:

$$K(\Gamma, \Gamma', m^2) = \sum_{n=0}^{\infty} g_n(\Gamma) \lambda_n(m^2) g_n(\Gamma') \tag{1.5}$$

The eigenvalues λ_n are analytic continuations of the harmonic oscillator eigenfunctions to time-like values of the argument, [5]. Useful representations of K and the eigenvalues λ_n are :

$$\begin{aligned} K(\Gamma, \Gamma', m^2) &= \int_0^1 \frac{dz}{z} \exp(-\frac{b}{2}(z\Gamma + \frac{m^2}{z}))\delta(\Gamma' - (1-z)(\Gamma + \frac{m^2}{z})) \\ \lambda_n(m^2) &= N \exp(\frac{bm^2}{2}) \int_0^1 \frac{dz}{z}(1-z)^n \exp(-\frac{bm^2}{z}) \end{aligned} \tag{1.6}$$

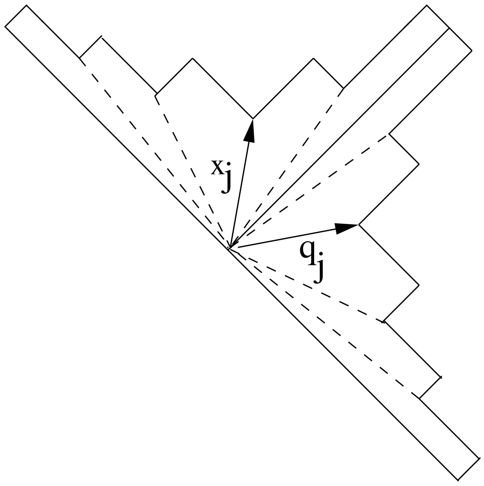

Figure 1.4: The energy-momentum space picture (q_j) and the spacetime picture (x_j) respectively.

We have introduced the positive light-cone fraction of the produced hadron z defined by $(x_+ - x'_+) = zx_+$. It is straight forward algebra to prove that the shaded area, exhibited in Fig.1.2 is given by the exponent $\frac{1}{2}(z\Gamma + \frac{m^2}{z})$ in the representation of the kernel K. We also note that the area obtained by summing the areas of the regions marked I, II and III in Fig.1.5 is equal to twice this area and that m^2/z equals the sum of the areas of regions I and II. There is a simple relationship between the two adjacent values of Γ in the representation of K:

$$\Gamma' = (1-z)(\Gamma + \frac{m^2}{z}) \tag{1.7}$$

Finally we note the identity (in easily understood notation) :

$$(I)(III) = (II)(IV) \tag{1.8}$$

Eq. (1.8), just as Eq. (1.3), is only valid for a flat string surface and a particular consequence is that the region IV is non-vanishing for the $(1+1)$-dimensional model. As the area of the region IV is proportional to $(1-z)$, the variable z must always be smaller than unity, i.e. there is a built in requirement that a typical step of the process can never use up all the available light-cone energy-momentum.

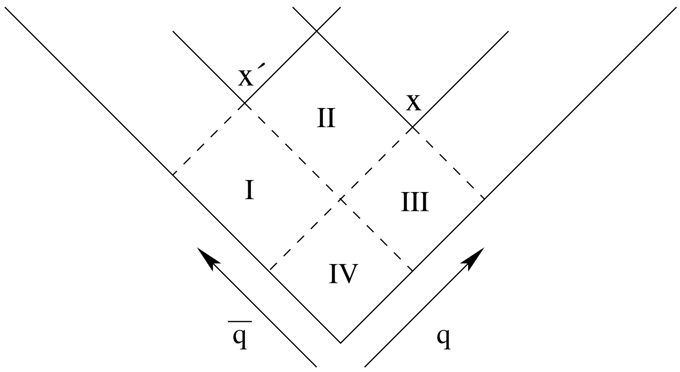

Figure 1.5: The figure shows the two vertices and the regions I, II, III and IV described in the text.

Such a requirement also comes out of the following argument. Suppose that we would integrate dP_n in Eq. (1.1) over all possible energy momenta and then sum over all multiplicities. Due to Lorentz invariance, we will obtain a function $R(s)$ which can only depend upon the total squared energy-momentum $s = P_{tot}^2$. If we pick out the dependence on the first particle and sum and integrate over all the rest we obtain an integral equation for the function R :

$$R(s) = (B.T) + \int_0^1 N \frac{dz}{z} \exp(-b\frac{m^2}{z}) R(s')$$
$$s' = (1-z)(s - \frac{m^2}{z}) \qquad (1.9)$$

where $(B.T)$ stands for "boundary condition term" and the variable s' is equal to the squared mass of all the remaining particles if the first hadron takes the light-cone fraction z (we note the similarity to the Eq. (1.7)). The integral equation (1.9) has an asymptotic solution $R \propto s^a$ (with the parameter a being a function of N and bm^2 ,cf. [5]) with the requirement :

$$\int_0^1 N \frac{dz}{z} (1-z)^a \exp(-b\frac{m^2}{z}) = 1 \qquad (1.10)$$

Consequently while the exclusive formula for the production of a particular hadron with the light-cone fraction z is given by the Area Law, the inclusive probability to produce this hadron (irrespective of what comes after it in the process) must be weighted with $R(s')/R(s) \simeq (1-z)^a$. Therefore, the well-known Lund fragmentation formula is given by the integrand in Eq. (1.10) and there is a power suppression for large values of the fragmentation variable.

The formulae presented above correspond to an ordering along the positive light-cone, i.e. the variable z is defined as the positive light-cone momentum fraction of the particle. It is possible to redefine everything in terms of an ordering along the negative light-cone, i.e. to introduce the corresponding negative light-cone component ζ by writing $(x'_- - x_-) = \zeta x'_-$. It is straightforward to prove that

$$\zeta = \frac{m^2}{m^2 + z\Gamma} \quad \text{and} \quad z = \frac{m^2}{m^2 + \zeta\Gamma'} \tag{1.11}$$

and from this we find that the integrand in the representation of the kernel K can be reformulated from $(z, \Gamma) \to (\zeta, \Gamma')$ to exhibit the symmetry between the descriptions along the positive and the negative light-cone directions

$$\begin{aligned} &\frac{dz}{z}\delta(\Gamma' - (1-z)(\Gamma + \frac{m^2}{z}))\exp(-\frac{b}{2}(z\Gamma + \frac{m^2}{z})) \to \\ &\quad \frac{d\zeta}{\zeta}\delta(\Gamma - (1-\zeta)(\Gamma' + \frac{m^2}{\zeta}))\exp(-\frac{b}{2}(\zeta\Gamma' + \frac{m^2}{\zeta})) \end{aligned} \tag{1.12}$$

1.3 The description of a multi-gluon string state

The dynamics of the massless relativistic string is based upon the principle that *the surface spanned by the string during its motion is a minimal surface.* This means that *the surface is completely determined by its boundary.* In the Lund Model the string is used as a model for the confined colour force field in QCD and the above property then has the further important implication that the dynamics will be infrared stable, i.e. *all predictable features from the decay of the force field should be stable against minor deformations of the boundary.*

For an open string a single wave moves across the spacetime surface and bounces at the endpoints. *The wave motion is determined by a (four-)vector-valued shape function, which we will call the directrix, $\mathcal{A}$.* Thus a point on the string, parametrised by the amount of energy σ, between the point and (for definiteness) the q-endpoint is, at the time t, at the position

$$x(\sigma, t) = \frac{1}{2}(\mathcal{A}(t + \frac{\sigma}{\kappa}) + \mathcal{A}(t - \frac{\sigma}{\kappa})) \tag{1.13}$$

We will from now on put the string constant κ equal to unity in order to simplify the formulae.

While the tension $\vec{T} = \partial\vec{x}/\partial\sigma$ is directed along the string, the velocity $\vec{v} = \partial\vec{x}/\partial t$ is directed transversely so that $\vec{T} \cdot \vec{v} = 0$. The definition of σ also implies that $\vec{T}^2 + \vec{v}^2 = 1$ (all the three-vector relations are valid in the local rest-frame). Together this means that the directrix function has an everywhere light-like tangent

$$\left(\frac{d\vec{\mathcal{A}}}{d\xi}\right)^2 = 1 = \left(\frac{d\mathcal{A}_0}{d\xi}\right)^2 \tag{1.14}$$

The tension must vanish at the endpoints ($\sigma = 0$ and $\sigma = E_{tot}$) and this implies that the directrix must be a periodic function with the property

$$\mathcal{A}(\xi + 2E_{tot}) = \mathcal{A}(\xi) + 2P_{tot} \tag{1.15}$$

where P_{tot} (E_{tot}) is the total energy-momentum (energy) of the state. While according to Eq. (1.13), the directrix $\mathcal{A}(t)$ describes the motion of the q-end, from Eq. (1.15) it is evident that

$$\mathcal{A}_{\bar{q}}(t) = \mathcal{A}(t + E_{tot}) - P_{tot} \tag{1.16}$$

will describe the motion of the $\bar{q}$-end. Finally, if the string starts out from a point (at the time $t = 0$) then we must have the symmetry :

$$\mathcal{A}(\xi) = -\mathcal{A}(-\xi) \tag{1.17}$$

Using the Lund interpretation of the gluons as internal excitations on the string it is easy to construct the first half period of the directrix curve: it starts with the quark energy-momentum k_1 and then the gluon energy-momenta $\{k_j\}$ are laid out in colour order and it ends with the $\bar{q}$ energy-momentum k_n, for a string with $(n-2)$ gluons. In this way the q-endpoint will be acted upon by the colour-ordered excitations as they arrive in turn. From Eqs. (1.15) and (1.17) it follows that we obtain the directrix of the second half period by reversing the order, starting with the $\bar{q}$ energy-momentum and ending with the q energy-momentum (besides the translation this is the way the $\bar{q}$-endpoint will move according to Eq. (1.16)).

The energy-momentum content in the string at a certain time t, between the point σ and the q-end is given by :

$$\int_0^\sigma d\sigma' \frac{\partial x}{\partial t} = \frac{1}{2}(\mathcal{A}(t+\sigma) - \mathcal{A}(t-\sigma)) \tag{1.18}$$

1.3.1 The coherence conditions in QCD

The properties of the directrices which are described above are common to all states of the massless relativistic string. On the other hand the use of the string as a model for the force fields of QCD may single out a particular class of all possible states. We will briefly discuss *the conditions which correspond to the coherence conditions of bremsstrahlung radiation in a gauge field theory.*

Multi-gluon radiation is in general described by means of perturbative cascade models. In order to consider the properties of the states, we will make use of the ideas behind the Lund Dipole Model. To see the emergence of a multi-gluon state we start out with the following two basic results from QCD bremsstrahlung, (cf. [3, 7, 8]).

B1 The original $(q\bar{q})$-state emits bremsstrahlung radiation according to the ordinary dipole formula, i.e. there is an inclusive density of gluon quanta which is flat in rapidity y and the logarithm of the squared transverse momentum $\kappa = \log(k_\perp^2)$ with a density given by the coupling, $\bar{\alpha} \equiv C\alpha_s/2\pi$:

$$dn = \bar{\alpha} d\kappa dy \tag{1.19}$$

B2 After the first ("hardest") gluon (g_1) is emitted there are two dipoles available, one between the (qg_1) and one between the $(g_1\bar{q})$ with squared masses $s_{12} \equiv (k_q + k_{g_1})^2$ and $s_{23} \equiv (k_{g_1} + k_{\bar{q}})^2$. The second gluon may be emitted independently inside the angular (rapidity) range of the first or the second dipole. We note that the two dipoles (each spanned by two light-like parton energy momenta) move apart in the total cms.

After the emission of the second gluon, according to the Lund Dipole Model [8], there are three independent dipoles for further emission, and so on. The masses of the dipoles will quickly decrease and therefore also the transverse momentum size of the emitted gluons. The cascades are stopped by some "virtuality" cutoff, either in the dipole mass or in the transverse momentum. The Dipole Model is implemented in the Monte Carlo simulation program ARIADNE [9].

In terms of the directrix, the original state is described by the light-like energy momenta of the original $(q\bar{q})$-pair. After the emission of the first gluon the state, in space (in the cms), will be described by a (connected) triangle, cf. Fig.1.6, where the vectors $\vec{k}_q \equiv \vec{k}_1$ and the vectors $\vec{k}_g \equiv \vec{k}_2$ constitute one of the dipoles and the $\vec{k}_2$ and $\vec{k}_{\bar{q}} \equiv \vec{k}_3$ the second dipole, as discussed above. (We note that for light-like vectors the space part length is equal to the time component) Emission of the second gluon will then occur in between the two vectors describing the dipole and this evidently means that the second gluon vector will "cut off" one of the triangular corners, making the directrix into a quadrangle etc. (Note that already with the emission of two gluons, the vectors shown in Fig.1.6 no longer need to be in a plane)

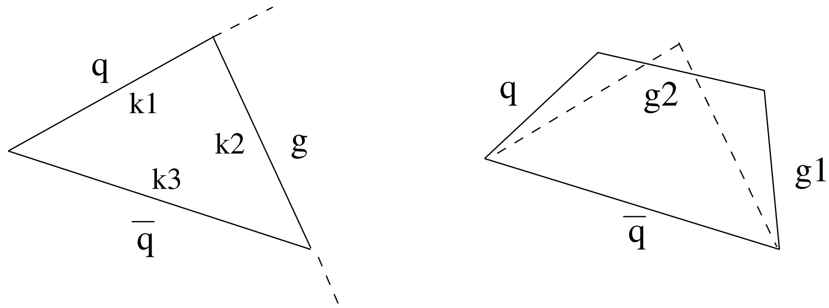

Figure 1.6: The emission of the first and the second gluon respectively.

In general, there will be an emission of a set of "hard" gluons which will determine the general shape of the directrix. The remaining emissions will then make the directrix smoother and smoother as each new emission will correspond to a gluon vector which cuts off an earlier corner. This means that the angle between the energy-momentum vectors of colour-connected partons becomes smaller (along the main directions, determined by the hard emissions) the longer the cascade continues. This is the way that the coherence properties of the bremsstrahlung radiation work, and it is sometimes referred to as the "strong angular condition". Later on, we will find that this angular condition will play an important role when we consider the deviations in the partonic states which are allowed by the fragmentation process.

1.4 The General Breakup of a String Field

We will now consider the partitioning of a general string state at a point $x(\sigma, t)$ and after that define the most general process possible for the Area Law.

According to Eq. (1.13) the breakup will occur at the middle point $\frac{1}{2}(\mathcal{A}(\xi_1)+\mathcal{A}(\xi_2))$ between two positions on the directrix, determined by $\xi_1 > \xi_2$ with $t = \frac{1}{2}(\xi_1 + \xi_2)$ and $\sigma = \frac{1}{2}(\xi_1 - \xi_2)$, cf. Fig.1.7. There will be two parts of the string left over and we will now describe their motion after the breakup.

The first part (to be denoted "(12)") can be described by the "new" directrix $\mathcal{A}_{12}(\xi) \equiv \mathcal{A}(\xi)$ for $\xi_2 \leq \xi \leq \xi_1$. It will contain the energy-momentum $P_{12} = (\mathcal{A}(\xi_1) - \mathcal{A}(\xi_2))/2$, cf. Fig.1.7, so that it can be continued as in Eq. (1.15) with $P_{tot} \to P_{12}$. Starting it out from the position $\mathcal{A}_{12}(\xi_2) \equiv \mathcal{A}(\xi_2)$, it is the "new" orbit of the (original) q-particle in the string (12). To obtain the corresponding orbit for the "new" $\bar{q}$-end we use Eq. (1.16) to obtain $\mathcal{A}_{12\bar{q}} \equiv \mathcal{A}_{12}(t + (\xi_1 - \xi_2)/2) - P_{12}$.

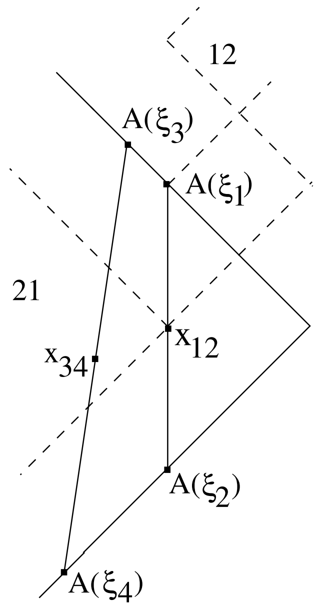

Figure 1.7: The system (12) is shown as a string piece which is moving away, while the system (21) is translated to x_{12}. The second break-up point x_{34} is the middle point between $A(\xi_3)$ and $A(\xi_4)$. In this way, the particle produced in between x_{12} and x_{34} can be taken either as the second particle in the break-up of the original system or the first in the system (21).

If we start at the "breakup" time $t = \frac{1}{2}(\xi_1 + \xi_2)$, it will evidently behave just as if we had adjoined the directrix $\mathcal{A}_{12}$ to the point $x(\sigma, t)$ (note that $\mathcal{A}_{12}(\xi_1) = 2P_{12} + \mathcal{A}_{12}(\xi_2)$).

The second part (denoted "(21)") can be described as the remainder, i.e. $\mathcal{A}_{21} = \mathcal{A}(\xi)$ with $\xi_1 \leq \xi \leq 2E_{tot} + \xi_2$ (noting that the original directrix is continued according to Eq. (1.15)) . The directrix $\mathcal{A}_{21}$ contains the energy $P_{21} = P_{tot} - P_{12}$ and is continued accordingly. To find the orbit of the produced q-end in the part (21) we adjoin the directrix $\mathcal{A}_{21}$ to the point $x(\sigma, t)$ starting it at $\xi = \xi_1$. The (original) $\bar{q}$ will again move according to Eq. (1.16).

The most noticeable property is that for a multi-gluon force field the directrices of the two new string parts will not fulfil Eq. (1.17). This implies that the endpoints of the new strings never meet but instead turn around each other so that each of the two states will contain angular momentum.

It is only in the $(1+1)$*-dimensional case that the two new string parts will have the same properties as the original string* (though they will be scaled down in size and have different rest-frames due to the momentum transfer at the breakup). The conclusion is that *the final state in a multi-gluon string fragmentation in general depends upon the ordering of the different breakups.*

1.4.1 A general process based upon the Area Law

We may nevertheless devise a string breaking process on a "frozen" string surface, i.e. under the assumption that the string surface is once and for all a given device (this is also the way Sjöstrand treated the problem exhibited above). Assume that the system (12) is a hadron on the mass-shell, produced as the "first" hadron along the original q-direction (i.e. the point $\mathcal{A}(\xi_2)$ is along the q energy-momentum vector and $\mathcal{A}(\xi_1)$ on the other side of the corner in the directrix between the q and the first gluon). Then we may choose two new points $\xi_3 > \xi_1$ and $\xi_4 < \xi_2$ to obtain the second rank hadron (34) with energy-momentum $p_{34} = \frac{1}{2}(\mathcal{A}(\xi_3) - \mathcal{A}(\xi_1) + \mathcal{A}(\xi_2) - \mathcal{A}(\xi_4))$ with the production vertex at $x_{34} = \frac{1}{2}(\mathcal{A}(\xi_3) + \mathcal{A}(\xi_4))$. We may evidently continue this process across the string surface and we note that at every step it is only necessary to choose two numbers: $(\delta\xi)_+ = \xi_3 - \xi_1$ and $(\delta\xi)_- = \xi_2 - \xi_4$. They must be chosen so that the corresponding p_{34} is the energy-momentum of a particle on the mass-shell. It is necessary to have a second condition, however, and we may then use the Area Law.

For the $(1+1)$-dimensional model the numbers $(\delta\xi)_\pm$ evidently correspond to the light-cone coordinates z and ζ in Section 1.2. The indices $\pm$ can be given a further meaning for the general directrix. According to Eq. (1.13) there is a left-moving and a right-moving wave spanning the string surface and according to Eq. (1.15) the fixed phase parts (from now on we will call them "grains") "stream" across and bounce back (thereby turning from left- to right-movers) at the q and $\bar{q}$ ends.

We may describe the situation in a (σ, t)-plane, cf. Fig.1.8, with the right- and left moving grains moving along fixed "light-cone lines". The whole string is, at the time $t = 0$, gathered into a single point at the origin. The boundary values at $\sigma = 0$ and $\sigma = E_{tot}$ are the directrix $\mathcal{A}(t)$ and the orbit of the $\bar{q}$, i.e. $\mathcal{A}_{\bar{q}}(t)$, respectively. A breakup point $x \equiv x_{12}$ is reached by the meeting of the left-moving grain indexed ξ_1 and the "right-mover" ξ_2 and the breakup at x_{34} by the left-mover ξ_3 and right-mover ξ_4. The energy-momentum p_{34}, streaming into the hadron produced between x_{12} and x_{34}, is evidently $\frac{1}{2}(\mathcal{A}(\xi_3) - \mathcal{A}(\xi_1))$ from the left and $\frac{1}{2}(\mathcal{A}(\xi_2) - \mathcal{A}(\xi_4))$ from the right. If we use $\pm$ as indices for the left- and the right-movers respectively we obtain a useful parametrisation.

With regard to surface areas there is an obvious (scalar) surface element defined by the surface spanned by the (incremental) grains coming from the

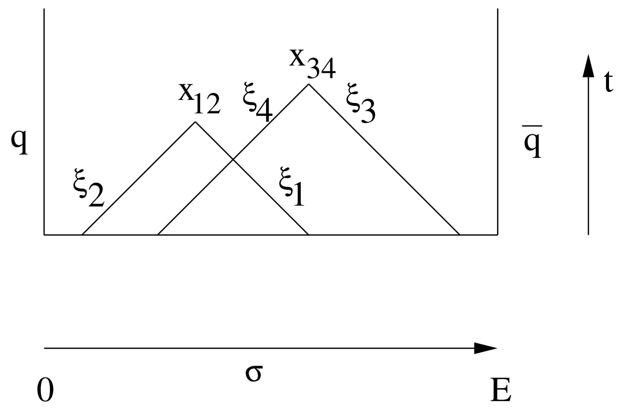

Figure 1.8: The break-up points and the corresponding right and left-moving grains in the (σ,t)-plane, as described in the text.

left and the right.

$$dA \propto d\mathcal{A}_+ \cdot d\mathcal{A}_- \tag{1.20}$$

Using this we may easily calculate the area "below the vertices" x_{12} and x_{34} (cf. Fig.1.8) as they are defined above. They are the correspondence to the squared proper times Γ considered in Section 1.2 (in the Fig. 1.5 they would correspond to the areas $I + IV$ and $III + IV$).

$$\Gamma_{12} = x_{12}^2 \quad \text{and} \quad \Gamma_{34} = x_{34}^2 \tag{1.21}$$

So, for the vertices shown in Fig.1.8, these areas are just the squared proper times of the vertices. But we note that they can not be expressed as the products of light-cone components or even in terms of products of sets of left- and right-movers solely, for general multi-gluon strings.

The area below the vertices (if we neglect the squared mass term in the Area Law, which can evidently be included in the normalisation constants N in Eq. (1.1)) can be expressed as

$$A_{1234} = x_{12}^2 + x_{34}^2 - x_{14}^2 \tag{1.22}$$

(this is the correspondence to the area called $I + III + IV$ in connection with Eq. (1.8)). We note that the area corresponding to IV, i.e. x_{14}^2 in Eq. (1.22), may vanish in this case, i.e. the left-mover indexed 1 and the right-mover indexed 4 may meet "before" $t = 0$. This means that the condition in Eq (1.8) can not be met for the general situation.

We may nevertheless include these considerations to devise an exact version of the Area Law in Eq. (1.1). We write, in an obvious way, the differentials $d^2p \rightarrow (dp_+ \cdot dp_-)$ and include the mass-shell condition by a δ-distribution as in Eq. (1.1). The result is, however, very complex to treat and for our purposes there are three shortcomings:

1 If we treat the process in an iterative way, at every step, just as we mentioned above, there are two numbers $(\delta\xi)_\pm$ to be solved for. One is fixed by the mass-shell condition and the other can be fixed by the area exponential; but the distribution functions are very complex (cf. the remarks under 2 below). In principle everything can be done by Monte Carlo simulation methods but even with very fast computers and the best possible computer routines this model will always be much slower than a process where there is only one number to be solved for, at every step.

2 Due to the complexity of the formulae there is no way we can obtain useful analytical tools to study the behaviour of the correspondences to the transition operators as in e.g. Eq. (1.5). This also implies that there is no way that we can define the total integral and sum over the produced hadronic states (as we could do for the $(1+1)$-dimensional model in Eqs. (1.9) and (1.10)) so as to be able to obtain the correct weighting in every step of an inclusive cascade.

3 Although this implementation of the Area Law is an "exact" procedure, fulfilling at every step the mass-shell condition and taking the "true" area below the vertices into account, it nevertheless starts out from the assumption that the partonic state is so well defined that there are reasons to implement an "exact" theoretical fragmentation procedure on it. This is in general not the case, i.e. the partonic state defined by perturbation theory is only well-defined down to some virtuality cut-off as we have discussed before.

We use quotation-marks on the word "exact" in order to indicate that the use of a "frozen surface" is in itself an assumption introduced to mend the problems obtained from the use of classical physics and neglect of the subsequent angular momentum production. In the third item above, we are coming back to the statement at the beginning of the section, that infrared stability should imply that minor deformations of the boundary (in this case changes in the partonic state as defined by the directrix $\mathcal{A}$ up to the order of the hadronic mass scales) should not be noticeable in the results. In the next section we will define a procedure which will mend all the three shortcomings mentioned above.

1.5 The Lund String Fragmentation as a process along the directrix

In this section, we will consider a fragmentation process which is defined along the directrix and does not suffer from the three problems considered at the end of Section 1.4.1. In order to exhibit the idea we will start with the $(1+1)$-dimensional model and rewrite it in a useful way. After that we will extend it to the general case. In particular, we will allow modifications of the order of the hadronic mass-scale in the directrix in accordance with the discussion under point 3 above.

1.5.1 The directrix process for the $(1+1)$-dimensional case

In this case the directrix contains only two directions, given by the $\bar{q}$ energy-momentum vector (to be called $\mathcal{A}_+$ in accordance with the notation introduced in Section 1.4.1) and the q energy-momentum ($\mathcal{A}_-$). A vertex point x_j, obtained after the production of j hadrons from the q-side, $p_1, \ldots, p_j$ is then described (with respect to the origin) by

$$x_j = \frac{1}{2}(\mathcal{A}_{+j} + \mathcal{A}_{-j}) \tag{1.23}$$

We also know that

$$\sum_1^j p_\ell = \frac{1}{2}(\mathcal{A}_{+j} - \mathcal{A}_{-j}) \tag{1.24}$$

Using the symmetry of a directrix passing through a single point (Eq. (1.17)) we may find another point on the directrix with the property

$$\mathcal{A}_{-j} \equiv \mathcal{A}_-(\xi_j) = -\mathcal{A}_-(-\xi_j) \equiv -\mathcal{B}_{-j} \tag{1.25}$$

We will from now on drop the indices $\pm$ on $\mathcal{A}_+$ and $\mathcal{B}_-$ but we note that they do describe points on the same directrix in accordance with the left- and right-mover notation in Section 1.4.1. While $\mathcal{A}_-$ goes "backward" for increasing j-values, $\mathcal{B}$ follows the q-direction.

We may now consider the hadron energy momenta to define a curve from the origin "along the directrix" such that after j steps it has reached the point

$$\sum_1^j p_\ell \equiv X_j = \frac{1}{2}(\mathcal{A}_j + \mathcal{B}_j) \tag{1.26}$$

while the difference between the point $\mathcal{A}_j$ on the directrix and X_j is given by x_j in Eq. (1.23). The production of a new particle p_{j+1} then corresponds to

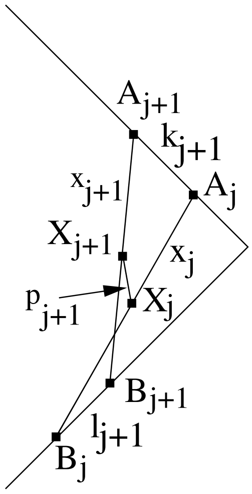

Figure 1.9: A description of the fragmentation process along the directrix with notations according to the text.

choosing two new points X_{j+1} and $\mathcal{A}_{j+1}$ (along the directrix) such that, cf. Fig.1.9

$$X_{j+1} - X_j = p_{j+1} \quad \text{and} \quad \mathcal{A}_{j+1} - \mathcal{A}_j \equiv k_{j+1} \tag{1.27}$$

We also obtain a new "vertex" vector x_{j+1} by the identity (cf. Fig.1.9):

$$p_{j+1} + x_{j+1} = x_j + k_{j+1} \tag{1.28}$$

In this way the vertex vector fulfils $x_{j+1} = \mathcal{A}_{j+1} - X_{j+1}$ just as $x_j = \mathcal{A}_j - X_j$. We have then arranged it so that the hadrons are produced along a curve, the X-curve, from the origin and the vertex vectors are the connectors for this curve going from the produced particle to the directrix. Before we consider the Area Law in this situation we note the symmetry between a reversed process and the process described above, i.e. when we go from X_j to X_{j+1} producing p_{j+1} by the use of a part k_{j+1} of the directrix along $\mathcal{A}$.

To see the reverse process we note that the vector x_j can just as well be reached by taking the difference between the point X_j on the hadron curve, Eq. (1.26), and "the backward point" on the directrix $\mathcal{B}_j$.

$$x_j = \frac{1}{2}(\mathcal{A}_j - \mathcal{B}_j) = \mathcal{A}_j - X_j = X_j - \mathcal{B}_j \tag{1.29}$$

Using this we could evidently consider the production of the particle p_{j+1} as a step from $\mathcal{B}_j$ to $\mathcal{B}_{j+1} = \mathcal{B}_j + \ell_j$ (cf. Eq. (1.27)) such that we have in correspondence to Eq. (1.28) and Fig.1.9

$$p_{j+1} + x_j = x_{j+1} + \ell_{j+1} \tag{1.30}$$

In order to formalise the determination of the particle energy momentum p, we may then in "the k-process" (along $\mathcal{A}$) assume that we know the starting vertex vector x, connected to a point $\mathcal{A}_P$. We may then choose a piece k along $\mathcal{A}$ (of a size to be determined) and then define the other light-cone direction in the plane determined by (x, k) by

$$\hat{\ell} = x - k\frac{x^2}{2xk} \tag{1.31}$$

The vector p will be described in terms of $(k, \hat{\ell})$ as

$$p = z\hat{\ell} + \frac{k}{2} = zx + \frac{k}{2}(1 - \frac{zx^2}{xk}) \tag{1.32}$$

with the requirement that the particle should be on the mass-shell

$$p^2 = m^2 = zkx \quad \text{i.e.} \quad kx = \frac{m^2}{z} \tag{1.33}$$

From Eq. (1.28) we obtain the new vertex vector x' by

$$\begin{aligned} x' &= (1-z)x + \frac{k}{2}(1 + \frac{zx^2}{xk}) \\ (x')^2 &= (1-z)(x^2 + xk) = (1-z)(x^2 + \frac{m^2}{z}) \end{aligned} \tag{1.34}$$

In Fig.1.10 we show both the production as described in Section 1.2 and the k-process described above. In particular we note the two areas exhibited. It is straightforward to prove that

$$A = A_r + \Gamma' - \Gamma \tag{1.35}$$

with the obvious definition of e.g. $\Gamma = x^2$. The Area Law in Eq. (1.1) will be fulfilled both by the use of the area in Fig.1.1 and the area in between the directrix and the hadronic curve (the X-curve) if we choose the variable z from the fragmentation function in Eq. (1.10) and apply it as in Eqs. (1.32)-(1.34). This is so because the difference between the areas A and A_r for the single step exhibited above will vanish when we consider the whole process.

It is also obvious that we may define an ℓ-process similar to the k-process we have discussed above. We just write $z\hat{\ell} = \frac{1}{2}\ell$ and introduce the variable ζ such that $\frac{1}{2}k = \zeta\hat{k}$ with ζ chosen such that $m^2/\zeta = \ell x'$. Actually we obtain the same process (although "in the opposite order") under the assumption that we

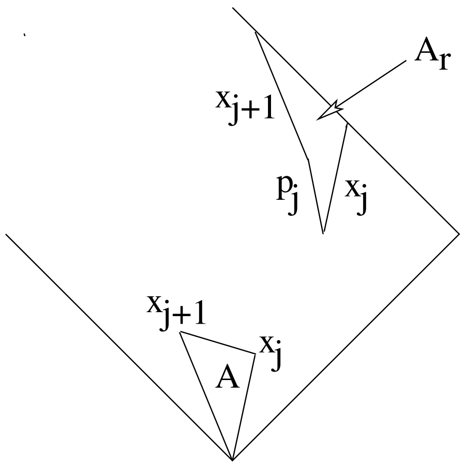

Figure 1.10: The figure shows both the production as described in Section 1.2 and the k-process described in the text.

start at x' and chose ℓ along the $\mathcal{B}$-part of the directrix with the variable ζ in accordance with Eq. (1.11). In this way the "backward" variable ζ evidently obeys the same distribution as the "forward" variable z and the Area Law is fulfilled.

We have reached a situation where a particle production step starts from a knowledge of a vector x connected to a light-cone-direction. Then we choose a light-like vector k such that Eq. (1.33) is fulfilled with a z-value stochastically chosen from the fragmentation function in Eq. (1.10). After that we construct the particle energy-momentum and a new vector x' according to Eqs. (1.32) and (1.34). We may start out choosing the "first" x-vector (x_0) equal to the q (light-cone) energy-momentum and then the $(1 + 1)$-dimensional model is defined.

1.5.2 The directrix process around a gluon corner

For a multi-gluon directrix however, we will reach situations when there are "corners", i.e. where the directrix changes direction between two colourconnected partons. Thus besides the vertex vector x, there will be a remaining light-cone vector (to the corner) c and a chosen number z such that

$$cx < \frac{m^2}{z} \tag{1.36}$$

We will now consider ways to pass over such a corner. Assuming that the directrix continues on the other side of the corner we may choose a light-cone vector k which fulfils Eq. (1.33) (we note that according to Eq. (1.36) k can not be chosen along c) and another light-cone vector c' such that

$$k + c' = c + \hat{Q} \equiv Q \tag{1.37}$$

with $\hat{Q}$, a vector pointing from the corner to a new point on the directrix, and Q describing that point from the point on the directrix where the vertex vector x is connected.

We note that with this definition the suggested way to pass the corner corresponds to an exchange of one "dipole", $c + \hat{Q}$ in the process for another $k + c'$, i.e. to make a detour onto a "new" directrix which is "close" to the original one. The choice of the new dipole corresponds to a definition of what we will mean by the allowed "minor deviations" of the original perturbative state.

In order to investigate what can be allowed under these conditions we will exhibit a few possible choices to fulfil Eq. (1.37). We will then find that all possible choices are not allowed if we would like to obtain reasonable results for the final state hadron distributions. A first set of possibilities is to choose c' as a new light-like connector that will bring us "closer" (than the vector c) to the original directrix in the next production step. One may then hope that after another step in the process the new connector becomes even "smaller" so that we are back at the original directrix after a few steps.

- C1 The vector k can be chosen in the plane spanned by the vertex vector x and the directrix Q (then both c' and k are fully determined).

- C2 A more general choice is to take the vector k in the three-space spanned by x, Q and the remainder vector c. In this case it is necessary to provide a second condition to determine k and c'. In the rest-frame of the vertex vector x the space parts of the vectors $\vec{c}$ and $\vec{\hat{Q}}$ span a triangle with the vector $\vec{Q}$ as baseline, cf. Fig.1.11. (For the case exhibited we assume that also $\hat{Q}$ is light-like. The situation can be easily generalised to the situation when there are one or more "corners" also on $\hat{Q}$.) The remaining degree of freedom will then be fixed by an angular condition. One such condition is indicated in the Fig.1.11. The two triangles $(\vec{c}, \vec{\hat{Q}}, \vec{Q})$ and $(\vec{c'}, \vec{k}, \vec{Q})$ in this construction are chosen congruent. This is a kind of minimal choice for the size of Q in this three-space. It is not difficult to see that in general the new connector will be smoothly connected to the original directrix.

For the case defined by the condition C1 we obtain that k and c' will be

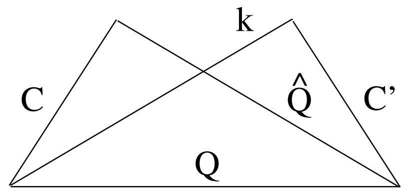

Figure 1.11: A possible construction (C2) for passing a gluon corner. The figure shows the space parts of the vectors, in the rest-frame of the vertex vector x, as described in the text.

directed along the two light-cone directions in the plane spanned by (x, Q):

$$k = \frac{Q}{2} + \frac{((Qx)Q - Q^2 x)}{2\sqrt{(Qx)^2 - Q^2 x^2}} \quad \text{and} \quad c' = Q - k \tag{1.38}$$

(In Fig.1.11 they would be directed along the $\vec{Q}$-direction with the lengths $(Q_0 \pm |\vec{Q}|)/2$, respectively). The vector Q contains one degree of freedom which can be fixed by multiplying with x in Eq. (1.38), and using Eq. (1.33).

This means on the one hand that the situation corresponds to using up the smallest possible segment of the directrix in the construction according to Eq. (1.37). On the other hand we will obtain a very sharp "bend" on the new directrix segment, defined by the dipole (kc'). While the first result is desirable from an economy point of view, the second implies that we will break the coherence conditions for the directrix (the angular ordering) as discussed in Section 1.3.1.

The fragmentation distributions obtained with this choice are not very encouraging. After we "pass" the gluon corner the density of hadrons is much higher than the density before the corner. *We find that even for a small gluonic excitation a break of coherence may result in the production of too many hadrons over a large rapidity range.*

One might hope that the situation may be mended by a suitable angular choice. This is so for the situation described in C2 for a large part of the events and for simple gluonic configurations. In Fig.1.18 we show a Monte Carlo simulation of the (inclusive) final state hadron rapidities in a state containing a single gluon placed at the centre with a transverse momentum of 15 GeV. Even though for most fragmentation events the choice C2 performs well, on the level of a few percent it does happen that the directions of the connecting c' and the new vertex x' are such that we obtain a situation close to the one for C1. The new directrix (possibly after a few further steps in the process) will all the time come closer to the original one; but at the same time we obtain a sharp bend farther and farther away from the original gluon corner with each step. This causes too many particles to be produced over a large rapidity range (cf. Fig.1.18).

It is possible to make further changes in the procedure with more sophisticated angular choices, but we will instead go over to another and more successful choice, which we will call C3.

C3 A natural choice for the vector c' is to make it into the k-vector for the next particle production in the process, i.e. chose a new stochastic value z' and put $c' = k'$ with

$$k'x' = \frac{m^{2\,\prime}}{z} \tag{1.39}$$

in terms of the new vertex vector x' determined from (z, k, x) according to Eq. (1.34). In this way we are evidently getting back to the original directrix as fast as possible.

We may define the vector k still in the space spanned by (c, x, Q):

$$k = \alpha c + \beta x + \gamma Q \tag{1.40}$$

We obtain a solution for the coefficients (α, β, γ) from the requirements

$$\begin{aligned} k^2 &= 0 \\ kx &= \frac{m^2}{z} \quad \text{and} \quad kQ = \frac{1}{2}Q^2 \end{aligned} \tag{1.41}$$

(these conditions also imply that k' is light-like), and an equation for the vector Q along the directrix using Eqs. (1.41) and

$$\frac{m^2}{z'} = k'x' = (Q - k)((1 - z)x + \frac{k}{2}(1 + \frac{zx^2}{kx})) \tag{1.42}$$

In the fragmentation distribution there is a factor $(1 - z)^a$ (stemming from the density of states according to the discussion around Eq. (1.10). This implies that we may not use up all the energy-momentum along one of the light-cone directions in a single step. Small values of z correspond to $\zeta \simeq 1$ according to Eq. (1.11), i.e. to using up almost all the energy-momentum along the other light-cone direction in a step. Such values are suppressed by the area exponential in the distribution. Nevertheless it may happen that we obtain a very small z-value ($z \leq 0.1$), corresponding to a large (but not infinitely large) area. Sometimes for the general multi-gluon directrix however, there might be no possibility to accommodate such a large area due to energy-momentum conservation. Then the choice C3 can not be done. Instead of introducing a general projection of the two-particle distributions for all such cases, in the

Monte Carlo simulation we have chosen to go back to the beginning and start a new fragmentation event. Such situations, when we can not use the choice C3, are infrequent enough to let this "restart strategy" be usable.

In order to test the influence of this feature on the model we investigate the influence on the single particle and two-particle distributions below in Section 1.6 and we find them negligible. In order to show that our changes in the directrices actually are of the hadronic mass scale we have defined a local "bending parameter" closely related to the $k_\perp$ variable used in the ordering of the Lund Dipole Model, cf. Eq. (1.50)

$$k_{\perp 2}^2 = \frac{2(xk_1)(k_1k_2)}{x(k_1+k_2)+k_1k_2} \tag{1.43}$$

From the results in Section 1.6 we conclude that we are at most making local modifications on the order or below the hadronic scale in our directrices.

1.5.3 A Differential Process and its Relationship to the Generalised Rapidity

There is a direct connection between a differential version of our hadronisation process and the $\mathcal{X}$-curve that was referred to in the Introduction, [2]. In order to investigate this process we consider the limiting situation for a vanishing mass parameter. Then the distribution function will obviously develop a pole for $z \to 0$. We will assume that the model is defined by the incremental step size dz with the ratio $m/dz \to m_0$. The corresponding incremental k vector will be called $d\mathcal{A}$ and it will fulfil the mass-shell condition (we will use the notation q_P instead of x for the vertex vector in connection with the differential process)

$$q_P d\mathcal{A} = \frac{m^2}{dz} \to dz m_0^2 \tag{1.44}$$

From the model formulae for the change in q_P and the particle energy-momentum p (Eqs. (1.32) and (1.34)) we obtain the following differential equations defining a curve to be called the $\mathcal{P}$-curve

$$\begin{aligned} d\mathcal{P} &= dz q_P + \frac{d\mathcal{A}}{2}(1 - \frac{q_P^2}{m_0^2}) \\ dq_P &= -dz q_P + \frac{d\mathcal{A}}{2}(1 + \frac{q_P^2}{m_0^2}) \end{aligned} \tag{1.45}$$

Firstly we note that from the sum and differences of the Eqs. (1.45) we obtain

$$\begin{aligned} \mathcal{P} + q_P &= \mathcal{A} \\ \mathcal{P} - q_P &= \mathcal{L} \end{aligned} \tag{1.46}$$

where the vector $\mathcal{L}$ has a light-like tangent just as the directrix $\mathcal{A}$:

$$d\mathcal{L} = 2dzq_P - d\mathcal{A}\frac{q_P^2}{m_0^2} \tag{1.47}$$

In this way the $\mathcal{P}$-curve goes in between two curves with everywhere light-like tangents and the vector q_P connects to both of them.

The vector q_P is time-like and quickly approaches the length m_0. To see that we multiply the second line of Eq. (1.45) by q_P and obtain

$$dq_P^2 = dz(-q_P^2 + m_0^2) \tag{1.48}$$

This means (remembering that $dz = q_P d\mathcal{A}/m_0^2$) that we may write:

$$q_P^2 = m_0^2(1 - T_P^{-1}) \quad \text{with} \quad T_P = \exp(\int(\frac{q_P d\mathcal{A}}{m_0^2})) \tag{1.49}$$

We have then assumed that $q_P = 0$ and $T_P = 1$ at the start of the process. We note that the integrand in the exponent for T_P is an area, more precisely the area between the directrix and the $\mathcal{P}$-curve. This is very similar to the results we obtained in [2] for the generalised rapidity and we will now briefly connect to these results.

1.5.4 The $\mathcal{X}$-curve and its Properties

The distribution in Eq. (1.1) contains two terms, the phase space and the exponential area suppression. In order to obtain a large probability it is necessary for a given total energy-momentum on the one hand to make many particles on the other hand to make them in such a way that the area is small. The obvious compromise is that the decay region is around a typical hyperbola with an average squared distance to the origin $< \Gamma > \equiv \Gamma_0$. The length of the hyperbola is proportional to the available rapidity range for the final state particles, i.e. $\Delta y = \log(s/\Gamma_0)$ with s the squared cms energy.

In the Lund Model interpretation for a string with a single gluon excitation, there will be two parts of the string; one spanned between the q and the g and one between the g and the $\bar{q}$. Each of them should break up in a similar way as the single string region described by Eq. (1.1). Besides that there will be a few particles produced in the connected region around the gluon "tip", cf. Fig.1.12. If the energy-momenta of the partons are k_j, $j = 1, 2, 3$ (with indices 1 (3) for the q ($\bar{q}$)), then there will be two hyperbolic angular ranges, $(\Delta y)_{12}$ and $(\Delta y)_{23}$. The sum of these ranges is

$$\begin{aligned} \lambda = (\Delta y)_{12} + (\Delta y)_{23} &= \log(\frac{s_{12}}{2\Gamma_0}) + \log(\frac{s_{23}}{2\Gamma_0}) \\ &= \log(\frac{s}{\Gamma_0}) + \log(\frac{s_{12}s_{23}}{4\Gamma_0 s}) \end{aligned} \tag{1.50}$$

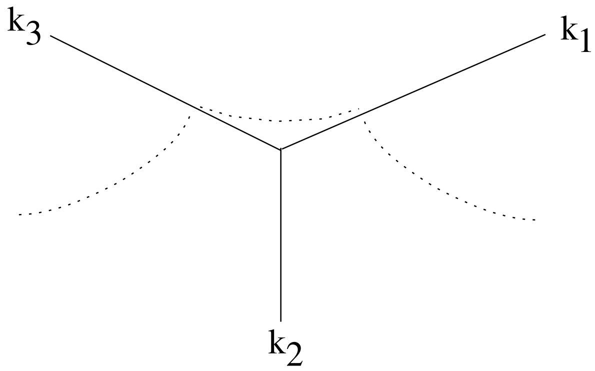

Figure 1.12: A string with a $q(k_1)$, $\bar{q}(k_3)$ and a single gluon excitation (k_2). The figure shows the connected region around the gluon "tip".

Here $s_{j\ell} = (k_j + k_\ell)^2$ and $s = s_{12} + s_{23} + s_{13}$ and the factors 2 are introduced because only half of the gluon energy-momentum goes into each string region.

The quantity $k_\perp^2 \equiv s_{12}s_{23}/s$ is a convenient (and Lorentz invariant) approximation for the transverse momentum of the emitted gluon. From Eq. (1.50) we conclude that after the emission of a single gluon the phase space is increased from the single hyperbola result above by an amount corresponding to a "sticking-out tip" of length given by the logarithm of the emitted transverse momentum. In conventional notions this corresponds to the "anomalous dimensions" of QCD, i.e. the emission of a gluon increases the region of colour flow inside which more gluons can be emitted and hadronisation can take place. The whole scenario is easily visualised and used in the Lund Dipole Model, [8], and the corresponding Monte Carlo simulation program ARIADNE, [9].

It is straightforward to see that if there are many gluons then there is a corresponding quantity, a generalised rapidity $\lambda \simeq \log(\prod s_{jj+1})$ stemming from the hyperbolae spanned between the colour-connected gluons. But we note that this is not an infrared stable definition. We will now provide a convenient generalisation.

A closer examination of the region around the tip of a gluon reveals that there is a correction corresponding to a connected hyperbola in the region (k_1, k_3) between the "endpoint" of the hyperbola in the region spanned between $(k_1, k_2/2)$ and the one spanned between $(k_2/2, k_3)$, cf. Fig.1.12. In formulae we obtain for the average hyperbolae

$$
\begin{aligned}
&(\alpha_1 k_1 + \frac{1}{2}\beta_1 k_2)^2 = \Gamma_0 \quad \text{and} \quad (\gamma_3 k_3 + \frac{1}{2}\beta_3 k_2)^2 = \Gamma_0 \\
&(\alpha_2 k_1 + \gamma_2 k_3 + \frac{1}{2}k_2)^2 = \Gamma_0
\end{aligned}
\tag{1.51}
$$

with the ranges $1 \geq \alpha_1 \geq 2\Gamma_0/s_{12}$, $2\Gamma_0/s_{12} \geq \alpha_2 \geq 0$, $2\Gamma_0/s_{12} \leq \beta_1 \leq 1$ and similarly for the other variables. The length of the two hyperbolae in the segments $(k_1, k_2/2)$ and $(k_2/2, k_3)$ are then given by Eq. (1.50) but the third hyperbola provides an extra contribution (in the appropriate limit $s_{13} \simeq s$) equal to $\log(1 + 4\Gamma_0 s/s_{12}s_{23})$. Then the total (generalised) rapidity length becomes

$$\lambda_{123} = \log(\frac{s}{\Gamma_0} + \frac{s_{12}s_{23}}{(2\Gamma_0)^2}) \tag{1.52}$$

This is evidently a nice interpolation between the situations with and without a gluon on the string and it is also an infrared stable definition of the notion of rapidity length. Eq. (1.52) is noted in [2] and led us to introduce a functional defined on a multi-gluon string directrix.

We may firstly define a set of connected integrals, [2]:

$$I_n = \int ds_{01} ds_{12} \cdots ds_{nE} \tag{1.53}$$

with the easily understood notation (cf. Eq. (1.18)) $s_{jj+1} = (\mathcal{A}(\xi_j) - \mathcal{A}(\xi_{j+1}))^2$, i.e. it is proportional to the squared mass between the points ξ_j and ξ_{j+1} along the directrix. By performing the integrals, we obtain that the argument in the logarithm in Eq. (1.52) is given by the sum $I_1/\Gamma_0 + I_2/(2\Gamma_0)^2$ and that we may in general define the functional T by :

$$T = 1 + \sum_{n=1}^{\infty} \frac{I_n}{(2m_0^2)^n} \tag{1.54}$$

as a suitable generalisation for any string state. For a finite number of partons N the terms with $n > N$ will all vanish and we also note that the highest degree term will always have the generic form :

$$2\frac{s_{12}}{4m_0^2}\frac{s_{23}}{4m_0^2} \cdots \frac{s_{N-1N}}{4m_0^2} \tag{1.55}$$

We also note that for a finite total energy E the contributions for very large degrees will become smaller and smaller compared to the scale m_0.

In order to study the functional T it is suitable to introduce a varying value ξ instead of the total energy E in the connected integrals. It is then evident that the functional $T(\xi)$ will fulfil the integral equation :

$$T(\xi) = 1 + \int_0^{\xi} \frac{ds(\xi, \xi')}{2m_0^2} T(\xi') \tag{1.56}$$

We will also introduce the vector-valued function $q_T(\xi)$ together with T so that we have

$$q_{T\mu}(\xi) = \frac{\int_0^{\xi} d\mathcal{A}_\mu(\xi') T(\xi')}{T(\xi)}$$

$$T(\xi) = 1 + \int_0^{\xi} \frac{q_T(\xi')d\mathcal{A}(\xi')}{m_0^2} T(\xi') \tag{1.57}$$

By differentiation and integration we obtain the results

$$\begin{aligned} T = \exp(\int_0^{\xi} \frac{q_T(\xi')d\mathcal{A}(\xi')}{m_0^2}) &\equiv \exp(\lambda(\xi)) \\ q_T^2(\xi) &= m_0^2(1 - T^{-2}(\xi)) \end{aligned} \tag{1.58}$$

The generalised rapidity λ corresponds to the result in Eq. (1.52) for the simple case described above and it provides an infrared stable definition for any multi-gluon state. Further the vector q_T is time-like and will quickly approach the finite length m_0.

1.5.5 The Correspondence between the $\mathcal{X}$-curve and the $\mathcal{P}$- curve

The similarity between these results and the results obtained for the $\mathcal{P}$-curve in Eqs. (1.48) and (1.49) are obvious (besides the power in T^{-1}) and there is a correspondence to the Eqs. (1.45) and (1.46) also. The interpretation of the $\mathcal{X}$-curve (as worked out in [2], cf. also [3]) is that there is a vector valued function $\mathcal{X}_\mu(\lambda)$ conveniently labelled by λ such that

$$\begin{aligned} \mathcal{X} + q_T &= \mathcal{A} \\ \frac{d\mathcal{X}}{d\lambda} &= q_T \\ \frac{dq_T}{d\lambda} &= -q_T + \frac{d\mathcal{A}}{d\lambda} \end{aligned} \tag{1.59}$$

i.e. the vector q_T is the tangent to the curve defined by $\mathcal{X}$ such that it reaches to the directrix. There is no direct correspondence to the $\mathcal{L}$-curve (unless the vectors q has reached its asymptotic length m_0).

It is useful to calculate the results from the differential equations for the case when there is a finite length light-like vector k_j in the directrix. By direct integration we find that if we have the vector q_{Tj} then "after" application of the parton energy-momentum k_j we obtain the vector q_{Tj+1} and will take a step along the $\mathcal{X}$-curve equal to $\delta\mathcal{X}_j$

$$\begin{aligned} q_{Tj+1} &= \gamma_j q_{Tj} + \frac{(1+\gamma_j)}{2} k_j \\ \delta\mathcal{X}_j &= (q_{Tj} + \frac{1}{2}k_j)(1-\gamma_j) \\ \gamma_j &= \frac{1}{1 + \frac{q_{Tj}k_j}{m_0^2}} \end{aligned} \tag{1.60}$$

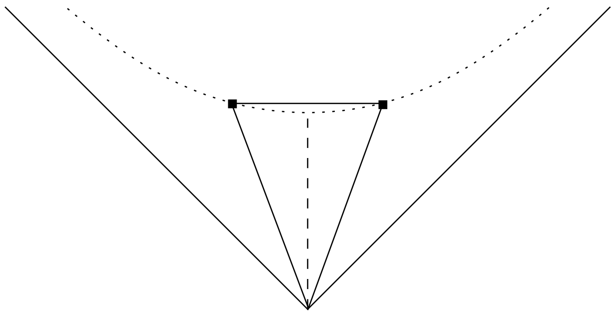

Figure 1.13: Two vertices placed symmetrically (around the rapidity y=0) at $m_0(\cosh(\delta y/2), \sinh(\delta y/2))$ and $m_0(\cosh(\delta y/2), -\sinh(\delta y/2))$ respectively, with a distance $2m_0\sinh(\delta y/2))$.

(we also note that the products of the γ_j is equal to T^{-1}). The formulae corresponding to these results for the $\mathcal{P}$-curve are

$$\begin{aligned} q'_P &= \gamma q_P + \frac{(1+\frac{q_P^2\gamma}{m_0^2})}{2}k \\ \delta\mathcal{P} &= (1-\gamma)q_P + \frac{(1-\frac{q_P^2\gamma}{m_0^2})}{2}k \\ \delta\mathcal{L} \equiv \ell &= 2(1-\gamma)q_P - \frac{q_P^2\gamma}{m_0^2}k \\ \gamma &= \frac{1}{1+\frac{q_Pk}{m_0^2}} \quad \text{and} \quad (T_P)^{-1} = \prod \gamma_j \end{aligned} \tag{1.61}$$

This means that while the length of a step along the $\mathcal{X}$-curve depends upon q_T^2 the corresponding step length along the $\mathcal{P}$-curve is

$$(\delta\mathcal{P})^2 \equiv M_j^2 = \frac{(1-\gamma_j)^2m_0^2}{\gamma_j} \tag{1.62}$$

This has a very simple meaning for a step length M_j along a hyperbola with the parameter m_0, cf. Fig.1.13. If the vertices are placed symmetrically around the rapidity $y=0$ at the positions $m_0(\cosh(\delta y/2), \pm\sinh(\delta y/2))$ then the step length is evidently $2m_0\sinh(\delta y/2))$ which should be compared to M_j. Then if we square them and define $\gamma_j \equiv (1-z_j) = \exp(-\delta y)$ the relationship in Eq. (1.62) will ensue.

The identification of γ and $(1-z)$ is actually a very general feature of the process(we will come back to this aspect in the future). At this point we only note that if the lengths (proper-times) of the two adjacent vertices are equal $\Gamma = \Gamma' = m_0^2 \equiv < \Gamma >$ then from Eq. (1.7) we obtain

$$m_0^2 = \frac{(1-z)m^2}{z^2} \tag{1.63}$$

which evidently coincides with the result in Eq. (1.62). Therefore, for this particular value of z, the fragmentation process will all the time proceed along the connected hyperbolae. It is in this way that the $\mathcal{P}$-curve can be considered the average of the hadronic X-curve.

In order to provide a precise relationship between the vectors q_P and q_T as well as the functionals T_P and T we make use of an interesting relationship for the $\mathcal{X}$-curve which is derived in [2]. If we define the $(1+4)$-dimensional vector $(Q_\mu \equiv T q_{T\mu}/m_0, T)$ (which has a length in the $(1+4)$ dimensional Minkowski metric equal to $Q^2 - T^2 = -1$) then the differential equation for q_T can be rewritten as

$$dT = Qd\mathcal{A} \quad \text{and} \quad dQ = TdA \tag{1.64}$$

i.e. as a group of special rotations in this space (corresponding to a subgroup of SO(1,4)) which are defined by the incremental changes along the directrix curve. The corresponding relationship for the $\mathcal{P}$-curve is, from the Eqs. (1.44) and (1.45) :

$$d(q_P T_P) = d\mathcal{A}(T_P - \frac{1}{2}) \quad \text{and} \quad dT_P = q_P d\mathcal{A} T_P \tag{1.65}$$

so that the (1+4)-dimensional vector $(2q_P T_P, 2T_P - 1)$ has both the same length and fulfils the same differential equations with respect to incremental changes along the directrix as (Q, T). In [2] we characterised the different directrices by means of the eigenvalues of the transfer matrix along the directrix and we found a simple and useful method to relate them to the generalised rapidity $\lambda = \log(T)$. We will come back to this formalism in a future publication and show the significance of the extended space.

In conclusion we have found a differential version of our stochastic process which corresponds to a curve of connected hyperbolae along the directrix function. The area in between the curve and the directrix (scaled by the single parameter m_0^2) has the interpretation of a generalised rapidity measure for the multi-gluon case. It is also related to a group of rotations with the incremental steps along the directrix as the generators. The curve may be interpreted as the average hadronic curve stemming from the hadronisation of the given directrix.

1.5.6 The Reverse Problem, to Find the Directrix from the Hadronic Curve

We will end this section by solving the reverse problem to the hadronisation process, i.e. to exhibit to what extent we can trace the directrix from a knowledge of the hadronic curve, which we will call the X-curve in accordance with the notation introduced in Section 1.5.1.

We will then assume that the X-curve is defined by the hadronic energy momenta $\{p_j\}$, ordered and laid out according to rank. (Note that this can not be done for a real event obtained from an experiment, since in general, rank is not an observable.) We will concentrate on the production of the hadron p_j, produced between the vertex vectors x_{j-1} and x_j with the directrix segment k_j, and an appropriately distributed stochastic number z_j. According to Eq. (1.28), in order to construct k_j it is sufficient to know p_j and the difference vector

$$(x_j - x_{j-1}) = \epsilon_j \hat{p}_j \tag{1.66}$$

It is straightforward to solve for $\hat{p}_j$ in terms of p_j and x_{j-1}

$$\hat{p}_j = \frac{(x_{j-1}p_j)p_j - p_j^2 x_{j-1}}{\sqrt{(p_j x_{j-1})^2 - p_j^2 x_{j-1}^2}} \tag{1.67}$$

The sign ϵ_j should be positive or negative depending upon whether m^2/z_j is larger or smaller than $z_j x_{j-1}^2$ (it is useful to note that $2(p_j x_{j-1}) = (m^2/z_j + z_j x_{j-1}^2)$). Therefore if we prescribe the first vertex vector x_0 (this is always chosen in our process as the original q energy-momentum vector) then the directrix vectors as well as the vertices are determined recursively up to a sign:

$$\begin{aligned} k_j &= p_j + \epsilon_j \hat{p}_j \\ x_j &= x_{j-1} + \epsilon_j \hat{p}_j \end{aligned} \tag{1.68}$$

It is evident that the other sign will determine the corresponding ℓ_j. We note however, that neither the necessary rank ordering of the hadrons, nor the colour ordering of the directrix gluons, are experimental observables. Therefore in this form the result has solely a theoretical meaning. It is also necessary to take the possible transverse fluctuations in the fragmentation process (mentioned before as stemming from tunnelling) into account before any observables can be presented.

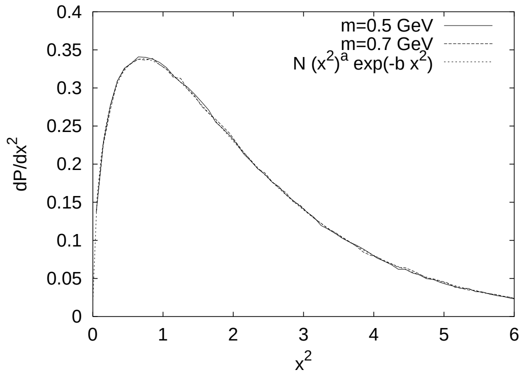

Figure 1.14: The x^2 distribution of the production vertices in our method for different values of the hadron mass, together with a plot of the Γ distribution in Eq.(1.69) with a=0.5 and b=0.7.

1.6 Results

In the previous section, we have proposed a method of fragmenting a multi-gluon string based upon the Area Law. It can be described as an iterative stochastic process along the directrix curve, which fulfils the Area Law at every step. We have discussed a few different approaches for passing a gluon corner, cf section 1.5.2, and from among these we have picked a preferred one. In this section we present a few basic results from this preferred solution and we also compare it with JETSET and the other approaches we have discussed.

We start with comparing the distribution of x^2 from our model with the distribution of the proper time of the break-up points derived inside the $(1+1)$-dimensional model [3].

$$H(\Gamma) = N\Gamma^a exp(-b\Gamma) \tag{1.69}$$

The result is presented in Fig.1.14. As mentioned in the discussion at the end of section 1.5.2, sometimes certain values of z can not be accommodated when we pass the corner according to choice C3. Our Monte Carlo simulation program handles this by starting a new event from the beginning whenever this occurs. One may then expect that this might cause changes in the z-distribution and also in the Γ-distribution that we obtain. This is, however, not the case as can be seen from Fig.1.14 and Fig.1.15. Further these distributions are as they should be according to the Lund Model formulae. The Γ-distribution is completely independent of the mass value used just as in the standard, $1+1$-dimensional Lund Model.

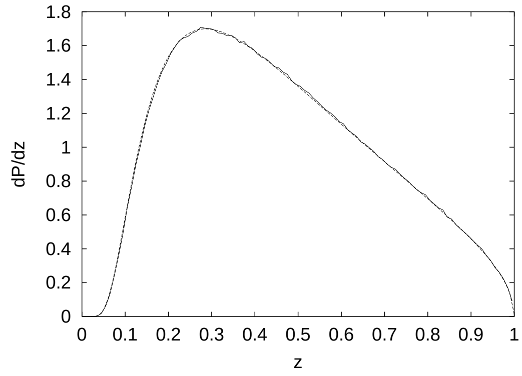

Figure 1.15: z values used in particle production in our method (solid line) compared to the Lund fragmentation function f(z)(dotted line). Though z value generation is according to the distribution f(z), not every value produced is used. This plot shows however, that the rejection of z values in the present method is unbiased.

To examine further effects in connection with our "restart strategy", we define the following measure Δy, of the correlation between two adjacent particles in the production process

$$\Delta y = ln(\frac{z_1}{z_2(1-z_1)}) \tag{1.70}$$

It corresponds to the difference in rapidity between the particles in the $(1+1)$-dimensional model. This distribution would be altered if we rejected particular correlations between successive values of z (e.x. a large value followed by a small value etc) more often than others.

In Fig.1.16 we compare our result with the result one obtains using only the Lund symmetric fragmentation function. There is no noticeable difference between the two curves, suggesting that the restart procedure (involving possible rejection of some z values) is effectively insensitive to such correlations between adjacent values.

In Fig.1.17 we show the distribution of our "local bending" parameter, $k_{\perp 2}^2$, defined in Eq.(1.43). This figure illustrates that the modifications of the directrix that we make when we apply our method are of the order of the hadronic mass scale. For values of $k_{\perp 2}^2 > m^2$ there is a fall off faster than a Gaussian.

In the left-hand side plot of Fig.1.18 we summarise the rapidity distributions obtained using the different approaches for passing a gluon corner, C2

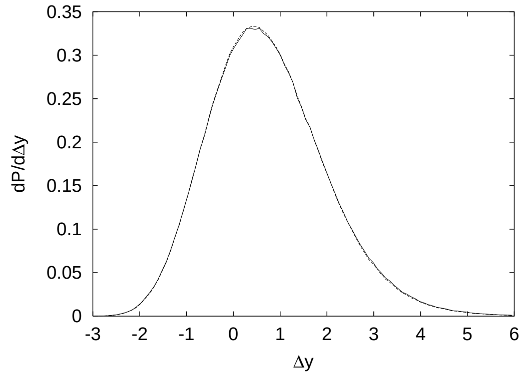

Figure 1.16: The Δy distribution, defined in Eq.(1.70), from our method (solid line) compared with the distribution obtained using only the Lund symmetric fragmentation function (dashed line).

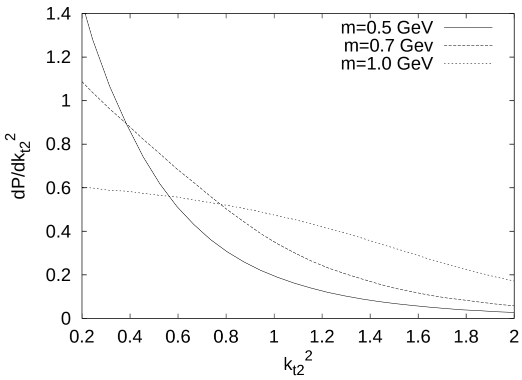

Figure 1.17: Plot of $\frac{dP}{d(k_{\perp 2}^2)}$ vs $k_{\perp 2}^2$ measured in $(GeV)^2$. Modifications of the directrix are on the scale of hadronic mass.

and C3 described in section 1.5.2, and compare them to a curve produced using PYTHIA in one simple situation: a perturbative string state consisting of a quark, an anti-quark and a single gluon. We conclude that modifying the directrix leads to the production of too many particles over a large range of rapidity if the modifications are not "smooth". In the right-hand side of Fig.1.18 we show a few rapidity distributions obtained from using our preferred method for different energies of the gluon. In Fig.(1.19) we show an example of in-

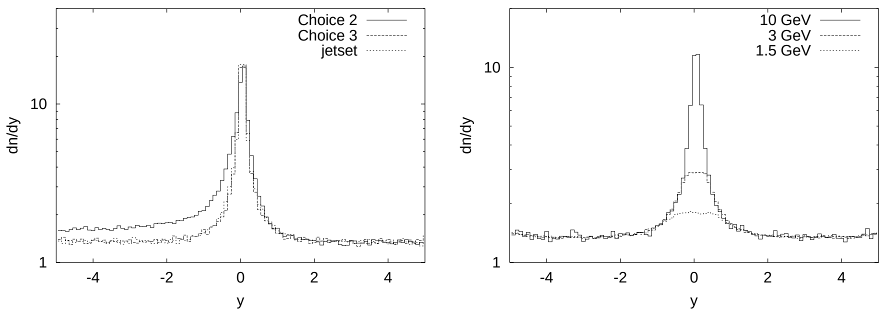

Figure 1.18: The figure to the left shows rapidity distributions for different choices for the vector k. The figure to the right shows rapidity distributions for a 3 jet event, obtained with the preferred method (C3), for different gluon energies. Note that the y axis is plotted on a log scale here.

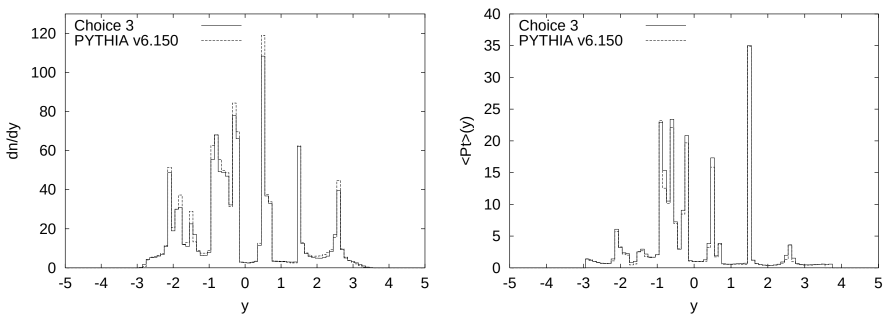

Figure 1.19: The rapidity distribution (left) and mean $|p_\perp^{hadrons}|$ (GeV) as a function of rapidity (right), for a string state of λ measure 70 (which is above the average λ for the energy and $p_\perp^{cut}$ used for this plot: $\sqrt{s}$ = 2000 GeV , $p_\perp^{cut} = 2GeV$) generated by ARIADNE, fragmented using our method (solid curve) and PYTHIA (dashed curve).

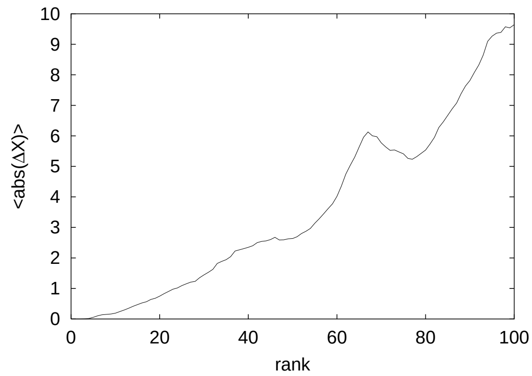

Figure 1.20: Comparison of JETSET and our method on an event to event basis: We plot here the average of the absolute value of the difference (GeV) between the hadronic curves for the same partonic event used in Fig.(1.19), obtained from the two programs as a function of rank, where for every event the particles of a certain rank were produced using exactly the same value of z in the two alternative procedures.

clusive rapidity distributions obtained by JETSET/PYTHIA and our method. For the comparison, we have used an arbitrarily chosen partonic event taken from ARIADNE. A close examination will show that in general there is a small multiplicity difference in the gluon jets. We have traced that to the fact that the two to three particles with the largest energy-momenta in the jets are faster according to our method compared to JETSET. It is impossible to compare to experimental data because firstly in this case we have only made use of a single partonic event. And secondly, at present we have not introduced the "fragmentation transverse momenta". Nevertheless we conclude that the inclusive distributions are very similar.

But we are definitely not dealing with the same particles on an event to event basis. To show this, we compare the two procedures on an exclusive, event to event basis in Fig.1.20. For this plot we devised a procedure to use exactly the same values of z for particle production in both programs. Since both our procedure, and PYTHIA might need to reject some sequences from time to time, we took only those events where no such rejection was required by either program. We have plotted the distribution of the absolute value of the difference of the two hadronic curves, $\sqrt{|\sum_{j=1}^{n}(p_{C3})_j - \sum_{j=1}^{n}(p_{PYTHIA})_j|^2}$, as a function of rank. The curve clearly shows that the hadronic curves obtained from the two programs are different. The absolute value prevents cancellation of the differences which would occur in an average over a large number of events, as we find from the comparison of the inclusive distributions.

1.7 Concluding Remarks

We have presented a precise method to implement the Lund Area Law (Eq. (1.1)) to fragment a multi-gluon string state. The final state hadrons are produced in an iterative stochastic process. The energy-momentum vectors $\{p_j\}$ can be laid out in rank order as a curve, the X-curve, with a vertex vector at every point connecting to the directrix curve. The directrix corresponds to the parton energy momentum vectors laid out in colour order. It describes on the one hand the orbit of a (massless) q-particle connected to a string and on the other hand the whole string surface.

It is possible to describe the whole process by analytical means, in particular in terms of a transfer matrix formalism similar to the one used for the $(1+1)$-dimensional model in [5]. This time it is necessary to make use of a $(1+3)$-dimensional framework. We will investigate this problem in the future.

In this paper, we have neglected the possibility of introducing transverse fluctuations in the hadronisation process. Such fluctuations are introduced on the basis of tunnelling arguments in the $(1+1)$-dimensional model. We feel that they are necessary for a consistent quantum mechanical treatment (there is no way to localise the string surface area better than what is allowed by Heisenberg's indeterminacy relations). We will examine the effects of such transverse fluctuations on our results in the future.

The directrix curve is in general given by a perturbative cascade (although in some cases precise matrix elements are also available). This means that the partonic states we are fragmenting, are resolved only down to some cutoff, usually in virtuality or in terms of the smallest allowed partonic excitations. String dynamics is infrared stable in the sense that minor modifications of the directrix only have a local influence, due to the minimal nature of the string world surface. We have made use of this freedom in the fragmentation process and in this way the partonic states will be defined down to the hadronic mass-scale. We will investigate the properties of the soft gluons thus introduced into the partonic state, in the future.

We have shown that the fragmentation process, with step size equal to the hadronic mass can be defined also in the limit of a vanishing mass in terms of a differential process. The corresponding solution, the $\mathcal{P}$-curve, is stretched in between two curves, the original directrix, $\mathcal{A}$, and another curve, the $\mathcal{L}$-curve, also with a light-like tangent. The correspondence to the vertex vectors for the fragmentation process are connectors to the $\mathcal{P}$-curve reaching out to the

$\mathcal{A}$ and the $\mathcal{L}$-curves. The area in between the $\mathcal{P}$-curve and the directrix $\mathcal{A}$ corresponds to a generalised rapidity variable in the same way as the average hyperbola defines rapidity for the $(1+1)$-dimensional model. There is an interesting relationship to the group of rotations in a $(1+4)$-dimensional space which we will investigate further in the future.

We have also shown that there is a duality (with properties similar to the Parton-Hadron Duality introduced by the St. Petersburg group [10]) between hadronic X-curve, defined by our process and the original directrix. We note, however, that the hadrons produced in our process always stem from the energy-momenta of two or more partons. The vertex vectors x_j contain the "memory" of the earlier partons. It is nevertheless possible to reconstruct the directrix from the X-curve, although the relationship contains a large number of degrees of freedom (the number of degrees of freedom increases further if we introduce transverse momentum fluctuations in the fragmentation process). We will investigate these properties in the future.

The process we have defined has also been implemented into a Monte Carlo simulation program. Due to the way it is constructed it is fairly direct to include also the multi-particle production features of the original JETSET, i.e. to include probabilities for different $(q\bar{q})$-flavours, different kinds of mesons, the decay of resonances etc. This is necessary for a comparison with experimental data.

1.8 Acknowledgements

We would like to thank G. Gustafson for extensive discussions and T. Sjöstrand and L. Lönnblad for a lot of help both with the material and in particular with the way the Monte Carlo programs JETSET and ARIADNE work.

References

[1] B. Andersson, G. Gustafson and B. Söderberg, Z. Phys. **C20**, 317 (1983).

[2] B. Andersson, G. Gustafson and B. Söderberg, Nucl. Phys. **B264**, 29 (1986).

[3] B. Andersson, The Lund Model, (Cambridge University Press 1998).

[4] T. Sjöstrand, Computer Physics Commun. **82**, 74 (1994).

[5] B. Andersson and F. Söderberg, Eur. Phys. J. **C16**, 303 (2000).

[6] T. Sjöstrand, Nucl. Phys. **B248**, 469 (1984).

[7] Ya.I. Azimov et al., Phys. Lett.**B165**, 147 (1985). Yu.L. Dokshitzer, V.A. Khoze and S.I.Troyan, in A.H. Mueller ed., Perturbative QCD, p.241, World Scientific.

[8] G. Gustafson and U.Pettersson, Nucl. Phys. **B306**, 746 (1988).

[9] L. Lönnblad, Ariadne v 4.10, Computer Physics Commun. **71** (1992) 15.

[10] Yu.L. Dokshitzer and S.I.Troyan, Proceedings of the XIX Winter School of the LNPI, **1**, 144 (1984). Ya.I. Azimov, Yu.L. Dokshitzer, V.A. Khoze and S.I. Troyan, Z. Phys. **C27**, 6 (1985).

ALFS: A New String Fragmentation MC Based on the Lund Model

Paper II

LU TP 03-09
June 2001

ALFS: A New String Fragmentation MC Based on the Lund Model

Sandipan Mohanty[1]
Department of Theoretical Physics, Lund University,
Sölvegatan 14A, S-223 62 Lund, Sweden

Abstract
A string fragmentation procedure for multi-gluon strings satisfying the Lund model area law was developed in [1]. In this note, the model will be extended to incorporate hadronisation transverse momenta and effects of limited available phase space for strings with small cms energies. A Monte Carlo implementation of the model Alfs is presented. The model has been summarised and formulated in a way to emphasise the physical ideas. This paper can also be used as a reference for the description of program elements presented in the second part of the paper.

[1] sandipan@thep.lu.se

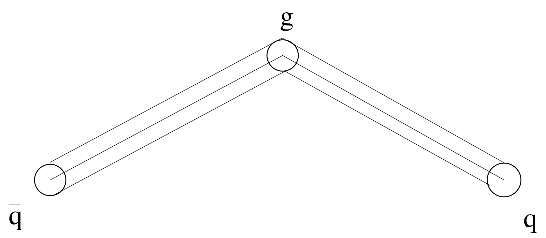

Figure 2.1: Quarks and anti-quarks appear as end points of the string while the gluons appear as internal excitations, effectively being attached to two string pieces.

2.1 The Lund String Fragmentation Model Revisited

The central concept in the Lund hadronisation model [2, 3] is that of a string, or a colour flux tube connecting partons in a colour singlet system. Each quark and anti-quark is thought to be connected to exactly one other parton by a string, while each gluon is connected to two other partons, cf. Fig.2.1. The string exerts a constant attractive force on its endpoints, which is either parallel or anti-parallel to the direction of motion of the endpoints. The string has a constant energy per unit length in any small segment of the string, in the rest frame of the segment. This constant is known as the string constant κ with a value about 1 GeV/fm. Unless otherwise mentioned, throughout this paper, space-time variables will be specified scaled with the string constant, so that both lengths and energies will be measured in the units of GeV.

Mesons: Consider a system with just a quark (q) and an anti-quark ($\overline{\mathrm{q}}$) with a straight string connecting them. In the attractive force field of the string, the pair executes a periodic motion, called a yoyo-mode. The Lund model associates such a picture with a meson. The squared mass of the meson would be the squared energy–momentum content in the q, the $\overline{\mathrm{q}}$ and the string connecting them. The q and the $\overline{\mathrm{q}}$ could have equal and opposite transverse momentum in the rest-frame of this system.

It is important to note that a yoyo-mode is only mapped to, or associated with, a certain hadron, not identified with it. If the q has transverse momentum relative to the string in the rest frame of the system, the angular momentum content of the system is non-zero. If a yoyo-mode is identified with a meson, such an angular momentum would be an orbital angular momentum of the system, and should be quantised, should manifest itself in the magnetic moments and so on. The average magnitude of this angular momentum is of the order

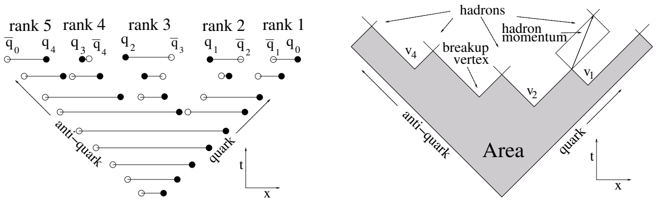

Figure 2.2: On the left is a sequence of "snapshots" of a high energy string stretched between a $q_0\overline{q}_0$ pair. The string breaks through the formation of $q\overline{q}$ pairs at many "vertices", and the resulting small mass systems called yoyo-modes are projected on to hadron states. On the right is the same figure showing the area traced by the string before its decay, which is used in the Lund model probability for the process.

of 0.1 $\hbar$, and could be interpreted as a probability of about 10% for the mesons to be $L = 1$ mesons. However, such mesons are almost always very wide resonances, which decay into ρ, π or other $L = 0$ mesons, and make little difference to the final state. The usual treatment in the model therefore, ignores their production. All yoyo-mode states with the same q and $\overline{q}$ flavours and the same total energy–momentum are mapped to the same meson state. This means that the only properties the meson inherits from the yoyo-mode are the spin, the flavours and the total energy–momentum. No constraints are applied to the other properties of the yoyo-modes which do not manifest themselves in the meson state.

Having made the distinction between the yoyo-modes and the hadrons, I will now use the words interchangeably, where a distinction is not necessary.

Baryons: The simplest possible way to incorporate baryon production in the Lund model is by allowing systems of two quarks, called diquarks (qq) to form in the intermediate stages during hadronisation. In order to combine with one more quark and form colour singlet systems, the diquarks need to have the same colour as an anti-quark. One can then construct q-qq yoyo-modes like the usual q-$\overline{q}$ yoyo-modes considered above. Such a yoyo-mode could then be mapped onto a baryon state. There are more sophisticated pictures for baryon production in the Lund string picture, eg. the pop-corn mechanism [6], which, as of now, have not been incorporated into the hadronisation scenario and the Monte Carlo ALFS being presented here.

String Breaking: Consider a q_0-$\overline{q}_0$ system formed, for instance, in a high energy e^+e^- annihilation event. The pair would stretch a string between them, depositing their energy in the string. When sufficient energy is stored in the string, new q-$\overline{q}$ pairs might be created from the string energy. Such pair production breaks the string, as the force field disappears between the newly produced pair. The breaking of the string through pair production is qualitatively similar to the cancellation of the electric field in a parallel plate capacitor through the introduction of two new capacitor plates of opposite polarity inside the field.

Breaking of a string by pair production will be referred to as a "breakup-vertex", or simply a vertex. Thus, "vertex location" would refer to the space time location of such an event, "vertex flavour" would refer to the quark flavour produced, etc.

Consider a situation where a set of breakup-vertices have formed on the string, cf. Fig.2.2. The q_0 would no longer be connected to $\overline{\mathrm{q}}_0$ by a string. No matter what the time ordering of the vertices is, there will be a unique anti-quark which will be connected to q_0 by the string. The vertex at which that anti-quark is produced will be called v_1, and the newly produced pair $\mathrm{q}_1\overline{\mathrm{q}}_1$. Similarly, there will be a unique anti-quark connected to q_1, and the vertex corresponding to that will be called v_2, and so on.

Formation of a set of breakup vertices would leave a set of $\mathrm{q}\overline{\mathrm{q}}$ string systems with relatively small invariant masses. These are thought of as the yoyo-modes[2] of the discussion above. In the Lund model, one considers only those vertices which give rise to yoyo-modes which can be mapped onto physical hadron states. This means that the vertices have to be placed on the string in such a way that the total energy–momentum included in a yoyo-mode between two vertices corresponds to the known mass of a hadron with the relevant flavours. This leads to a constraint on the space time locations x_α and $x_{\alpha+1}$, of the two vertices v_α and $v_{\alpha+1}$:

$$(x_{\alpha+1} - x_\alpha)^2 = -m_{\perp\alpha}^2 \tag{2.1}$$

Just like the vertices, one could introduce a system of enumerating the yoyo-modes, or equivalently, the hadrons emerging from the string decay. The hadron formed out of q_0 and $\overline{\mathrm{q}}_1$ is said to have "rank" 1. Similarly, the hadron $(\mathrm{q}_1, \overline{\mathrm{q}}_2)$ has rank 2 and so on. If n hadrons form from the decay of the string, they could be numbered from 1 to n (by their ranks), or, equivalently from 0 to $n-1$. Conforming to the indexing conventions for arrays in the programming language used for the Monte Carlo, a numbering starting from 0 will be used in this paper. The first rank hadron will be referred to as having a "rank index" 0, or just index 0.

Since the production vertices obey the constraint in Eqn.(2.1), they are separated by space-like intervals, and their time ordering is frame dependent. The rank ordering on the other hand is a Lorentz-invariant ordering, which is also equivalent to an ordering along the (positive) light-cone for a simple

[2]In the usual definition of the yoyo-mode, the q and $\overline{\mathrm{q}}$ do not have any transverse momentum. The expression is used here to also refer to the small pieces of string formed when a string fragments, which are projected onto hadron states.

$q\overline{q}$ string. The words "before", "after" are often used in the sense of such an ordering in the context of string fragmentation, as opposed to a their usual meanings.

For the string to break up into n hadrons, $n-1$ vertices are required. Since all but the pair $q_0\overline{q}_0$ are associated with a vertex, from the point of view of notation, it is convenient to introduce fictitious vertices v_0 and v_n containing the q_0 and $\overline{q}_0$ respectively. The location associated with these vertices will be the turning points of q_0 and $\overline{q}_0$. In this system of enumeration, the hadron h_α will be produced from q_α and $\overline{q}_{\alpha+1}$ and the string between them, or in other words, "between" vertices v_α and $v_{\alpha+1}$.

Since the new q-$\overline{q}$ pairs are produced from the string, the production points are well localised within the transverse size of the string. One would therefore expect, from the uncertainty principle, that the pair would be generated with some transverse momentum relative to the string. Pair production has been modelled as a tunnelling across a potential barrier in [5]. The result is that the probability for the production of a q-$\overline{q}$ pair with quark mass μ is

$$dP \propto d^2k_\perp \exp(-\frac{\mu_\perp^2}{2\sigma_q^2}), \quad \text{with } \mu_\perp^2 = \mu^2 + k_\perp^2 \quad \text{and } 2\sigma_q^2 = \frac{\kappa}{\pi} \tag{2.2}$$

This has two consequences:

- The heavier a quark flavour, the less likely it is to be produced during the string decay. The branching ratio for the newly generated quark flavours between u, d, s and c quarks calculated from the above is approximately $1 : 1 : 0.3 : 10^{-11}$. One can conclude that only u, d, s quarks are generated during string decay.
- The distribution of the transverse momenta carried by the pair is a Gaussian with a width independent of the quark flavour produced.

A hadron receives transverse momentum from both the vertices involved in its formation, and thus obtains a Gaussian distribution with width $\sigma = \sqrt{2}\sigma_q$. Because of the generation of transverse momentum in the pair production process the energy momenta of the fragmentation products are not exactly aligned with those of q_0 or $\overline{q}_0$. This contributes towards the reduction of the thrust of the event. The contribution from this "hadronisation transverse momentum" dominates over the transverse momentum due to gluon radiation at small cms energies, while gluon radiation is the major contribution at higher energies, with the transition occurring at about 30-50 GeV. The phenomenological value for the width σ, about 0.36 GeV, is a bit higher than what is indicated by its expected relation with the string constant. This is usually interpreted as an effect of radiation of soft gluons below the cut-off in the parton cascade.

A typical string fragmentation event could be visualised as shown in Fig.2.2. The pair $q_0\overline{q}_0$ moves away from the origin along the z-axis, stretching a string.

The string sweeps a region in the zt-plane in space–time with q_0 and $\overline{\mathrm{q}}_0$ moving along the positive and negative light-cone directions respectively. The partons in the newly formed $\mathrm{q}\overline{\mathrm{q}}$ pairs are drawn away from each other by the string, so that the string field vanishes in the forward light-cone of a production vertex. The probability in the Lund model, for the production of a set of yoyo-modes with energy–momenta $\{p_\alpha\}$ and masses $\{m_\alpha\}$, cf. Fig.2.2, is given by the following result, known as the area law:

$$dP_n(\{p_\alpha\};P_{tot}) \ \propto \ d\overline{P}_n(\{p_\alpha\};P_{tot}) = \tag{2.3}$$
$$= \left(\prod_{\alpha=0}^{n-1} N_\alpha d^4p_\alpha \delta(p_\alpha^2 - m_\alpha^2)\right) \delta(\sum_{\alpha'=0}^{n-1} p_{\alpha'} - P_{\mathrm{tot}}) \exp(-bA) \exp(-\frac{1}{2\sigma_{\mathrm{q}}^2}\sum_{\beta=0}^{n} k_{\perp\beta}^2)$$

In this expression, A is the area swept by the string before it decays due to pair production as shown in Fig.2.2, and the parameter b has a phenomenological value[3] of about 0.6 GeV^{-2}. The exponential suppression favours production of vertices close to the light-cones, which leads to fewer particles and hence less available phase space. The competition between the exponential suppression with area and the size of the phase space leads to a hyperbolic average production region, and also to a rough correlation between the rapidity of a particle and the mean hyperbolic angles of its production vertices. A Gaussian suppression factor for the hadronisation transverse momenta produced at each of the vertices also appears in the expression.

It should be noticed that the expression in Eqn.(2.3) has not been given an overall normalisation. The phase space integrals are defined as the integrals of the above expression over all particle properties. Since all details about the particles are summed over, Lorenz invariance implies that the functions depends only on the invariant mass of the system and the flavours of the endpoint $\mathrm{q}\overline{\mathrm{q}}$ pair:

$$g_n(s) = \int_{\text{all particle properties}} d\overline{P}_n \tag{2.4}$$

$g_n(s)$ represents the relative probability or density for the production of all possible n particle states from a system with invariant mass s. The (normalised) probability for the decay into exactly n particles is then:

$$\overline{g}_n(s) \equiv \frac{g_n(s)}{\sum_l g_l(s)} \quad = \quad \frac{g_n(s)}{g(s)} \tag{2.5}$$

[3]The conventional tuning of the b parameter, which yields the value given here, refers to an area calculated using light-cone coordinates which is twice the true space-time area.

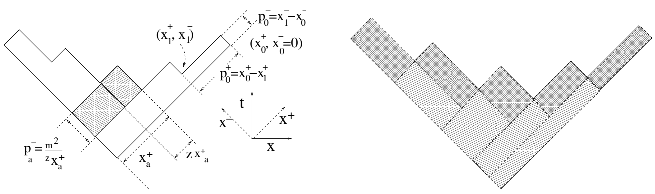

Figure 2.3: On the left, the light-cone components of the energy–momenta of particles with index 0 and α are shown. Their relation to the light-cone components of the space–time locations of the production vertices is also exhibited. The shaded area on the left hand side is an area characterising the production of the particle with index α. In the figure to the right, the entire area under the string is partitioned with similar contributions from all the hadrons.

For any finite s the $g_l(s)$ in the sum above is zero for l above a certain maximum value. The true or normalised probability for one particular n particle state should then be evaluated as:

$$dP_n(s) = \frac{g_n(s)}{g(s)} \cdot \frac{d\overline{P}_n}{g_n(s)} \tag{2.6}$$

By partitioning the area A into contributions associated with the production of individual particles, the above results could be formulated in terms of an iterative scheme. There is no unique prescription for the partitioning, and several methods will be outlined below.

The first such scheme will be in terms of the light-cone coordinates and energy momenta. If (x_1^+, x_1^-) are the light-cone coordinates of the location of vertex v_1, the total energy–momentum carried by the hadron h_0 is given by $(x_0^+ - x_1^+, x_1^-) + p_{\perp 1}$ (cf.Fig.2.3). Similarly for the hadron h_α, we have

$$\begin{aligned} p_\alpha^+ &= x_\alpha^+ - x_{\alpha+1}^+ = -\Delta x_\alpha^+ \\ p_\alpha^- &= x_{\alpha+1}^- - x_\alpha^- = \Delta x_\alpha^- \\ p_\alpha \cdot \Delta x_\alpha &= 0 \\ p_{\perp\alpha} &= k_{\perp\alpha+1} - k_{\perp\alpha} \end{aligned} \tag{2.7}$$

As in Eqn.(2.2) $k_{\perp\alpha}$ denotes the transverse momentum produced at vertex v_α carried by the quark q_α. The transverse momentum of the anti-quark $\overline{\mathrm{q}}_\alpha$ will then be $-k_{\perp\alpha}$, if transverse momentum is assumed to be balanced at every vertex. While this is the usual assumption, it is possible to consider alternative scenarios in which some of the transverse momentum is balanced in neighbouring vertices [7].

From Eqn.(2.7) it is easily seen that the total positive and negative light-cone components of the hadrons h_0 to $h_{\alpha-1}$ are

$$\sum_{\beta=0}^{\alpha-1} p_\beta^+ = x_0^+ - x_\alpha^+ \tag{2.8}$$

$$\sum_{\beta=0}^{\alpha-1} p_\beta^- = x_\alpha^- \tag{2.9}$$

Therefore, the available energy–momentum along the remaining positive light-cone direction after the production of h_0 to $h_{\alpha-1}$, from which the hadron h_α could take its share, is x_α^+. If the particle takes a fraction z_α of this available positive light-cone momentum, the negative light-cone component of its momentum would be given by $\frac{m_{\perp\alpha}^2}{zx_\alpha^+}$, and the shaded area in Fig.2.3 would be $\frac{m_{\perp\alpha}^2}{z}$, in terms of the transverse mass $m_{\perp\alpha}$. This is one possible area which can be associated with the production of the particle h_α. The total area A is partitioned into rectangular regions corresponding to the formation of individual hadrons as shown in Fig.2.3. The proper-time Γ of adjacent vertices v_α and $v_{\alpha+1}$ satisfies the following relation:

$$\Gamma_{\alpha+1} = (1 - z_\alpha)(\Gamma_\alpha + \frac{m_{\perp\alpha}^2}{z_\alpha}) \tag{2.10}$$

The particle production "step" in which the particle h_α is produced consists of the generation of the vertex quark flavour and transverse momentum $k_{\perp\alpha}$, selecting a type of hadron consistent with the flavours at the two vertices, according to their respective probabilities, and selection of a value for z_α, which fixes the light-cone momentum components for the particle and the location of vertex $v_{\alpha+1}$. If s_α is the invariant mass of the system before the production of h_α (so that s_0 refers to the invariant mass of the system $\mathrm{q}_0\overline{\mathrm{q}}_0$), the distribution of the variable z_α can be found from Eqn.(2.6) and Eqn.(2.3):

$$\begin{aligned} \frac{dP}{dz}dz &= \frac{dz}{z}\exp(-b\frac{m_{\perp\alpha}^2}{z}) \cdot \frac{g(s_{\alpha+1})}{g(s_\alpha)} \\ s_{\alpha+1} &= (1-z)\cdot(s_\alpha - \frac{m_{\perp\alpha}^2}{z}) \end{aligned} \tag{2.11}$$

One could use the above as an integral equation for the function $g(s)$:

$$g(s) \quad = \quad N\int_0^1 \frac{dz}{z}\exp(-b\frac{m_{\perp\alpha}^2}{z})\cdot g((1-z)\cdot(s-\frac{m_{\perp\alpha}^2}{z})) \qquad (2.12)$$

For large s, this equation has solutions of the form $g(s) \propto\ s^a$ which, when combined with Eqn.(2.11) gives

$$\frac{dP}{dz} = f(z) = N\frac{(1-z)^a}{z}\exp(-b\frac{m_{\perp\alpha}^2}{z}) \qquad (2.13)$$

This is known as the Lund symmetric fragmentation function. To satisfy Eqn.(2.12), the value of the power a must depend on N and b in such a way that the distribution $\frac{dP}{dz}$ is properly normalised. In arriving at the above result, effects of different possible quark flavours generated at the vertices, different hadron masses, transverse momentum etc have all been neglected. None of these factors seems to affect the resulting distributions if the invariant mass of the decaying string is large. In a generalisation to account for different quark flavours, the power a in the function $g(s)$ could in principle depend on the flavour of the produced quark. Phenomenologically this dependence is weak for large s, and it is possible to describe experimental data with a single value for a, with the exception of diquark production in connection with baryon production. Therefore, an implementation of the Lund model based on the generation of light cone momentum fraction z from the distribution in Eqn.(2.13), would be consistent with the area law and the available phase space of Eqn.(2.3), in all but the situations with very small invariant masses, of the order of a few GeV, for flat string systems.

To complete the discussion of the iterative procedure for string fragmentation we consider what happens when the invariant mass of the remaining system is small, so that the power like behaviour $g(s) \propto s^a$ is not a good approximation. At the end of the cascade the mass may even only be sufficient for the production of one or two particles, in which case $g(s)$ is a sum of just a few terms. The error from using the asymptotic result in Eqn.(2.13) is particularly large for reactions where the total initial energy is small, e.g. in low energy e^+e^--annihilation or in several neutrino scattering experiments. The error may also be important in reactions at higher energies, if one is interested not only in inclusive distributions, but also in particle correlations.

For a multi-gluon string, the string surface is not planar, and the above process needs to be generalised. However, the basic assumptions in the Lund model do not lead to a unique prescription, and additional assumptions have to be made. In PYTHIA [8], the relation between the proper-times of adjacent vertices in Eqn.(2.10) is assumed to be true for multi-gluon strings. In the resulting procedure, the quantity $\frac{m_\alpha^2}{z_\alpha}$ does not represent an area associated with the production of the particle h_α on the curved world surface of the string.

The Monte Carlo introduced in this paper addresses these issues. The method that will be described in section 2.2 associates a simple and well defined area for the production of every particle, and the relation between this area and the particle energy–momentum is uniform throughout the event, both for flat strings and for multi-gluon strings. For small cms energies the new Monte Carlo also takes into account some of the complications arising from the non-trivial behaviour of the functions $g(s)$, which have been neglected in earlier MC implementations.

2.2 String Fragmentation in ALFS

In [1], we developed an alternative procedure for implementing the Lund model area law for multi-gluon strings. We showed the relationship of this procedure with a continuous four-vector valued curve called the $\mathcal{X}$-curve, defined on the partonic state. The $\mathcal{X}$-curve will be very briefly introduced in section 2.2.2. The fragmentation procedure of [1], can be alternatively introduced as a discretized version of the differential equations describing the $\mathcal{X}$-curve[4], as will be done in section 2.2.3.

In section 2.2.4, the procedure developed in [1] will be extended to incorporate effects of transverse momentum generation at the breakup vertices. In section 2.2.5, the treatment of limited available phase space for the hadrons at small invariant masses will be discussed. Section 2.2.6 is a brief mention of an implementation of Bose-Einstein correlations in this model. Section 2.2.7 summarises the model in the way it is implemented in ALFS.

With the treatment of multi-gluon strings in mind, the useful concept a "directrix" will be introduced in section 2.2.1.

2.2.1 The Directrix

The area A of Eqn.(2.3) corresponds to a total event weight, which can be separated into contributions associated with the individual hadrons in different ways. One method was presented in the previous section. In this section another method will be presented which will be applicable to the general case of multi-gluon strings.

The action describing the motion of the string in space–time is the free string action, with the consequence that the string traces a minimal area world

[4]The $\mathcal{X}$-curve is not a straight-forward continuum limit of the discrete process. That limit leads to another curve which we called the $\mathcal{P}$-curve in [1]. However, the relationship between the $\mathcal{X}$-curve and our formulation of the hadronisation iterations is close enough for it to be useful as a starting point.

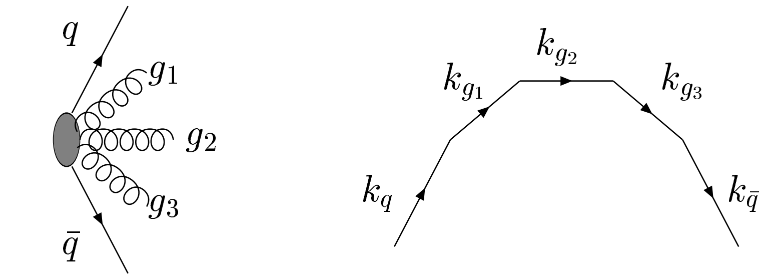

Figure 2.4: The directrix for a multi-gluon state is obtained by placing the parton energy momentum vectors next to each other in colour order. The figure shows only half of the directrix. The other half is obtained by continuing the arrangement shown with the same vectors in the reverse order, i.e. k_{q},k_{g1},k_{g2},k_{g3}, $k_{\overline{\mathrm{q}}}$ followed by $k_{\overline{\mathrm{q}}}$,$k_{g3}$,$k_{g2}$,$k_{g1}$ and k_{q}.

surface. Since the quark and anti-quark appear as end points of the string, a string connected to such a parton will be an open string and the surface traced by it will be bounded by the trajectories of the quark and the anti-quark. Further, a minimal surface with a boundary is completely determined by the specification of its boundary, called the "directrix". An arbitrary point on the surface is determined by the directrix $\mathcal{A}(\xi)$ as :

$$X(t,\zeta) = \frac{1}{2}\left[\mathcal{A}(t+\zeta) + \mathcal{A}(t-\zeta)\right] \tag{2.14}$$

The four-vector valued function $\mathcal{A}(\xi)$ has a light-like tangent and the parameter ζ for a point on the string is defined as the energy contained in the string between that point and the quark endpoint.

The action principle thus determines the string motion and the world surface, once the state of the string is specified at any instant of time. The simplest cases are those in which there is an instant of time when the spatial extent of the string could be taken to be zero, eg. a string formed in e^+e^- annihilation. For such a system, the directrix satisfies $\mathcal{A}(\xi) = -\mathcal{A}(-\xi)$. A complete specification of the state can be made with the energy momenta of the partons formed in the annihilation event and the subsequent gluon radiation, and colour connection information. The directrix, which describes the string surface stretched by such a colour singlet system, consists of the energy momentum vectors of the partons placed one after the other in colour order, as shown in Fig.2.4.

The concept of a directrix is especially useful while examining properties of multi-gluon strings. It is a function with a single parameter describing the complicated surfaces traced by multi-gluon strings. Visualising the surface

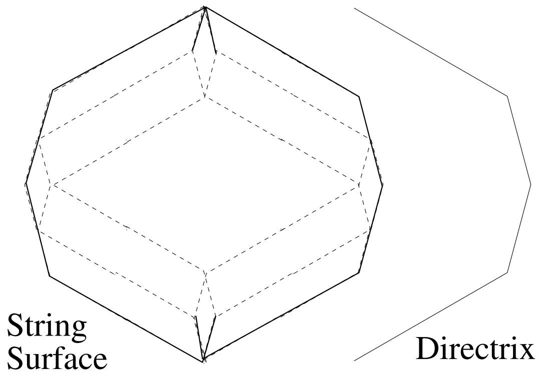

Figure 2.5: World surfaces of multi-gluon strings consist of a complicated structure of a large number of planar regions. However, since they are minimal area surfaces, their boundaries, i.e., the directrix curves contain all the information about the surfaces.

traced by a two gluon state as shown in Fig.2.5 is a lot more challenging than just visualising the directrix which consists of only the boundary, and contains the same information.

2.2.2 The λ-measure and the $\mathcal{X}$-curve

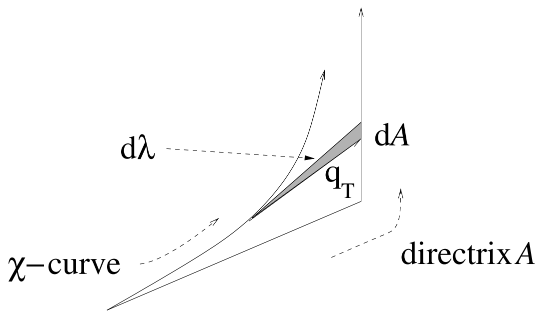

Figure 2.6: The $\mathcal{X}$-curve is a continuous curve which can be defined for a given directrix. The λ-measure, which is proportional to the area between the $\mathcal{X}$-curve and the directrix, is a generalisation of the rapidity range available for hadron formation.

A generalisation of the concept of the rapidity range available to hadrons, called the λ-measure, was developed as a function of the directrix. In [13], we have discussed the properties of this measure, its interpretation as a rapidity range and its connection with a phase space measure for parton cascades. Only a set of defining equations will be recalled in the following, as the iterative particle production steps in ALFS bear a close resemblance.

Let a directrix $\mathcal{A}(\xi)$ for a state be specified, and define a four vector valued function $q_T(\xi)$, and the measure $\lambda(\xi)$ through the following differential equations and initial conditions:

$$\begin{aligned} d\lambda &= \frac{q_T \cdot d\mathcal{A}}{m_0^2} \\ dq_T &= d\mathcal{A} - \frac{q_T \cdot d\mathcal{A}}{m_0^2} q_T \\ q_T(0) &= 0\ , \quad \lambda(0) = 0 \end{aligned} \tag{2.15}$$

The parameter m_0^2 in Eqn.(2.15) is normally chosen as the mean proper-time of the vertex locations of section 2.1. The quantity $d\lambda$ appears as the area between the vector $q_T(\xi)$ and the incremental step $d\mathcal{A}$ along the directrix, cf Fig.2.6. Defining another trajectory $\mathcal{X}(\xi)$ in space–time through

$$d\mathcal{X} = d\mathcal{A} - dq_T = \frac{(q_T \cdot d\mathcal{A})}{m_0^2} q_T\ , \quad \mathcal{X}(0) = 0 \tag{2.16}$$

we could identify the λ-measure as (being proportional to) the area between the directrix and the $\mathcal{X}$-curve, cf Fig.2.6.

It can be seen from Eqn.(2.15) that λ remains equal to zero until ξ becomes large enough so that the directrix changes direction. Therefore, one could equivalently use the initial condition on q_T as

$$q_T(e_{\rm q}) = \mathcal{A}_{\rm q} \ \text{ and } \ \lambda(e_{\rm q}) = 0 \tag{2.17}$$

where $\mathcal{A}_{\rm q}$ is the energy–momentum vector of the quark and e_q is its energy component. With these initial conditions, Eqn.(2.15) will result in the same value for the area.

2.2.3 Fragmentation procedure in ALFS as discrete steps along the directrix

Similar to the manner in which the directrix was constructed from parton energy–momenta in Fig.2.4, we construct a curve to be called the “hadronic curve”, or the X-curve, by placing the hadron energy momentum vectors one after the other in rank order. For flat strings, it can be shown that the area

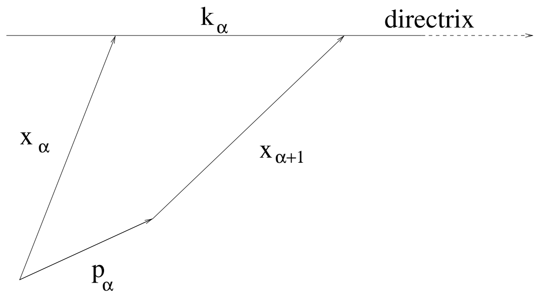

Figure 2.7: Production of every hadron in the fragmentation model in ALFS is associated with a well defined planar region called a "Plaquette" bounded by two vertices involved in the formation of the plaquette, the particle energy–momentum vector, and a section of the directrix, referred to as the k-vector for the plaquette in the text.

between the directrix and the hadronic curve could be used equivalently as the area shown in Fig.2.2, in the area law. The fragmentation event of the string thus corresponds to the determination of a stochastic X-curve, such that the area between the directrix and the X-curve is exponentially suppressed as in Eqn.(2.3).

An iterative process for the determination of the X-curve can be formulated involving finite steps along the directrix, which obey relations that are very similar to those mentioned in section 2.2.2, in connection with the $\mathcal{X}$-curve. In this process, a finite length step along the directrix will result in a change in an abstract four-vector, to be called[5] a "vertex vector" x_α, which would form our analogy to the vectors q_T of section 2.2.2. We can write a difference equation for the evolution of vertex vectors as (with a finite light-like segment along the directrix $\Delta\mathcal{A}$ denoted k):

$$x_{\alpha+1} - x_\alpha = z'_\alpha k_\alpha - z_\alpha x_\alpha \tag{2.18}$$

Comparison with Eqn.(2.15) shows the similarity between the vertex vectors and the q_T vectors; but we have deferred the determination of the constants used in the linear combination, for later. The constants in Eqn.(2.15) were inspired by the fact that $q_T \cdot d\mathcal{A}$ is an infinitesimal area associated with the incremental step, and the choice in Eqn.(2.15) also makes the q_T vectors tangent to the $\mathcal{X}$-curve at every point.

[5]The reason for the notation "vertex vector" is the fact that for a straight string they correspond exactly to the vertex locations of section 2.1. This exact correspondence is however lost for general string states.

With this difference equation for the vectors x_α, the step along the X-curve, can be written in complete analogy with Eqn.(2.16) (writing p for ΔX)

$$p_\alpha = k_\alpha - (x_{\alpha+1} - x_\alpha) = (1 - z'_\alpha)k_\alpha + z_\alpha x_\alpha \tag{2.19}$$

So far, in this approach, the size of the step along the directrix k and the variables (z, z') have been treated as independent quantities. Since the vector k is a section of the directrix, it is light-like, but its length in a given frame has to be determined. There are two constraints among the three quantities, which can be expressed in many alternative consistent ways. Since the segments along the X-curve represent particle energy–momenta, the $\sqrt{p_\alpha^2}$ equals the (transverse) mass of the particle. For the second constraint, one can make a comparison with Eqn.(2.7) and demand that the vertex vectors defined here, just like the vertex locations on the string in Eqn.(2.7) obey the relation that the difference between adjacent vertex vectors x_α, $x_{\alpha+1}$ is orthogonal to the momentum p_α in between. This gives (treating z as the only remaining free variable):

$$\begin{aligned}
p_{l\alpha} \cdot k_\alpha &= m_{\perp\alpha}^2 \\
x_\alpha \cdot k_\alpha &= \frac{m_{\perp\alpha}^2}{z_\alpha} \\
p_{l\alpha} = z_\alpha x_\alpha &+ \frac{1}{2}(1 - \frac{z_\alpha^2 x_\alpha^2}{m_{\perp\alpha}^2})k_\alpha \\
x_{\alpha+1} = (1 - z_\alpha)x_\alpha &+ \frac{1}{2}(1 + \frac{z_\alpha^2 x_\alpha^2}{m_{\perp\alpha}^2})k_\alpha
\end{aligned} \tag{2.20}$$

In Eqn.(2.20) I have introduced subscripts l to denote the in-plane or "longitudinal" momentum of the particles, since the X-curve was concerned with the in-plane kinematics. As mentioned earlier, the production of a particle in the Lund model also involves generation of transverse momentum at the two string breakup vertices involved in the production, so that $p_\alpha = p_{l\alpha} + p_{\perp\alpha} = p_{l\alpha} + k_{\perp\alpha+1} - k_{\perp\alpha}$. The hadronisation transverse momentum is orthogonal to the local world surface of the string, on which the area law calculations are performed for the longitudinal parts. In the scenario described above, we should therefore associate transverse momenta with each vertex, so that it is orthogonal to the vectors x_α and k_α which define the local planar region around the directrix.

One discrete step in the above process can be summarised as the creation of a finite segment along the X-curve and a new vertex vector $x_{\alpha+1}$ from a given vector x_α and a step along the directrix. From Eqn.(2.20) it is seen that these four vectors are in the same plane, and satisfy the relation in Eqn.(2.19):

$$x_\alpha + k_\alpha = p_{l\alpha} + x_{\alpha+1} \tag{2.21}$$

We have used the name "Plaquette" to represent the planar area bounded by these four vectors which are involved in the discretized steps discussed above. Figure 2.7, shows the construction for a typical plaquette. This concept will be used frequently in the description of the hadronisation model in ALFS. A plaquette is formed between two vertices containing the energy momentum vector of the hadron and a section of the directrix, and is associated with the production of a particle.

The area of a plaquette as in Fig.2.7 can be shown to be

$$A_{\text{plaquette}} = \frac{1}{2}\left(\frac{m_{\perp\alpha}^2}{z_\alpha} + \frac{1}{2}(x_{\alpha+1}^2 - x_\alpha^2) - \frac{1}{2}m_{\perp\alpha}^2\right) \tag{2.22}$$

The total area contained in all plaquettes is analogous to the area swept by the q_T curve, i.e. the λ measure, since the contributions from intermediate vertices in Eqn.(2.22) cancel and $\frac{m_{\perp\alpha}^2}{z_\alpha} = x_\alpha \cdot k_\alpha$. Since we construct the directrix as a sequence of light-like vectors, if the last plaquette in a series ends with its ending vertex vector parallel to the last vector of the directrix, the total area of all the plaquettes will be

$$A_{\text{total}} = \frac{1}{2}\sum_0^{n-1}\left[\frac{m_{\perp\alpha}^2}{z_\alpha} + \frac{1}{2}m_{\perp\alpha}^2\right] \tag{2.23}$$

Using Eqn.(2.11) to generate stochastic values of z, one can then construct a procedure in which the events would be weighted according the Eqn.(2.3). The above process is exactly equivalent to the process outlined in section 2.1 for strings without gluons. However, this formulation is easily extended to the case of multi-gluon strings. The quantities $\frac{m_\perp^2}{z}$ retain the same relation to the area of a plaquette as in Eqn.(2.22) so that the same form of weighting may be used. One would expect that the functions $g(s)$ in Eqn.(2.11) would get modified in the presence of gluons; but as pointed out earlier, for large invariant mass strings, these phase space integrals are quite insensitive to the kinematic details. However, the Monte Carlo ALFS is designed to accommodate a possibility of different weighting schemes for gluonic strings, for instance by treating the λ-measure as the relevant variable instead of the invariant mass. For low invariant string masses when the simple power dependence $g(s) \propto s^a$ is not a good description, there are very few gluons present to complicate the calculations. Thus it is sufficient to have a more detailed calculation of low energy phase space for flat strings.

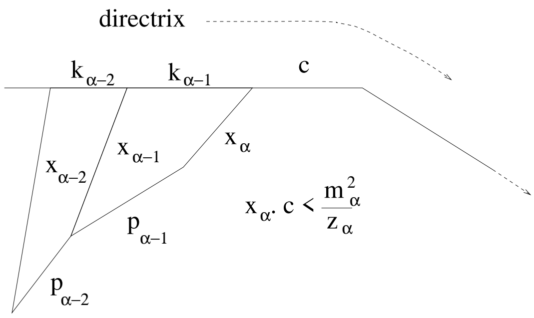

Figure 2.8: An iterative procedure with finite steps along the directrix is bound to come to a situation where a regular step is not feasible. In the situation shown here, $x_\alpha \cdot c < \frac{m_{\perp\alpha}^2}{z_\alpha}$. Since k_α is required to satisfy $x_\alpha \cdot k_\alpha = \frac{m_{\perp\alpha}^2}{z_\alpha}$, k_α can not be chosen as a fraction of c or along the directrix, like the two regular steps shown.

2.2.4 Gluon Corners

Unlike the infinitesimal steps used to build the $\mathcal{X}$-curve, the finite steps in the plaquette building process face a problem at gluon "corners". It is illustrated in Fig.(2.8). The situation shown has α plaquettes constructed from sections of the directrix. A value of z_α has been chosen, but the remaining straight part of the directrix c, in front of x_α, is such that $\frac{m_{\perp\alpha}^2}{z_\alpha} > x_\alpha \cdot c$. Thus it is impossible to use a part of c as the incremental step for the discrete process. Taking a segment along the directrix which is longer than c, would make it time-like, and not appropriate to be the k-vector of a plaquette. If a time-like vector is used as k, most of the equations normally valid for plaquettes, like Eqn.(2.20) and Eqn.(2.22), are not satisfied.

Various possible solutions to the problem were examined in [1], and one was picked as the most successful. This process, however, did not treat hadronisation transverse momenta. In this section the gluon corner procedure of [1] will be extended to handle these transverse momenta.

The problem has its origins in the iterative procedure. In such a procedure, particle properties are calculated in their rank order, and the iterative sequence with finite size steps fails around the gluon corners. It should be recalled however, that the infinitely thin string in the Lund model must be an approximation. The hadronisation process implies that the string state can only be determined with a finite resolution. The solution to the gluon corner problem makes use of this idea.

Consider an imaginary situation where two plaquettes P_α and $P_{\alpha+1}$ have

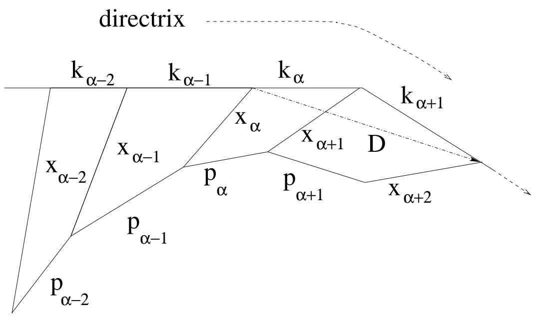

Figure 2.9: An imaginary situation in which the stochastic z_α value is such that the k-vector of one plaquette ends exactly at a corner, so that the next plaquette is constructed along the next straight part of the directrix. The vector D shown here, satisfies Eqn.(2.24).

been constructed such that the directrix changes direction exactly between them, cf. Fig.2.9. The two directrix sections in the plaquettes, k_α and $k_{\alpha+1}$ are then not parallel. Their sum, $D = k_\alpha + k_{\alpha+1}$, represents a combined step along the directrix. Using Eqn.(2.20), for the vectors of the two plaquettes, it can be seen that D satisfies the relation

$$\frac{1}{4}(1+\frac{z_\alpha^2 x_\alpha^2}{m_{\perp\alpha}^2})D^2 + (1-z_\alpha)x_\alpha \cdot D = \frac{m_{\perp\alpha+1}^2}{z_{\alpha+1}} + (1-z_\alpha)\frac{m_{\perp\alpha}^2}{z_\alpha} \qquad (2.24)$$

Now consider a realistic situation as mentioned at the beginning of this section. It is not possible to choose the vector k_α equal to c, which would correspond to the above imaginary situation. We can then find a slightly deformed directrix in the following way. Using the notation $\mathcal{A}_\alpha \equiv \mathcal{A}(\xi_\alpha)$ (cf. Fig.2.10), to represent the point on the directrix where the vertex v_α is connected to the directrix, we can find a point $\mathcal{A}_{\alpha+2} = \mathcal{A}_\alpha + D$, such that D satisfies the Eqn.(2.24). The vector D can then be written as the sum of two light-like pieces k_α and $k_{\alpha+1}$, which are not segments of the initial directrix. These pieces can define a modified directrix between the points $\mathcal{A}_\alpha$ and $\mathcal{A}_{\alpha+2}$, passing through the point $\mathcal{A}'_{\alpha+1} = \mathcal{A}_\alpha + k_\alpha$, which is not on the original directrix.

In [1], we first made use of Eqn.(2.24) to determine the combined step along the directrix around a gluon corner for two plaquettes, and then made use of properties of plaquettes to determine k_α and $k_{\alpha+1}$. However, our solution presented there, was without considering hadronisation transverse momenta.

In Fig.2.10, the above two step procedure around the gluon corner of Fig.2.8 is illustrated. The plaquettes $P_{\alpha-1}$, P_α are not in the same plane in space–time. The transverse momentum created at vertex v_α has to be orthogonal

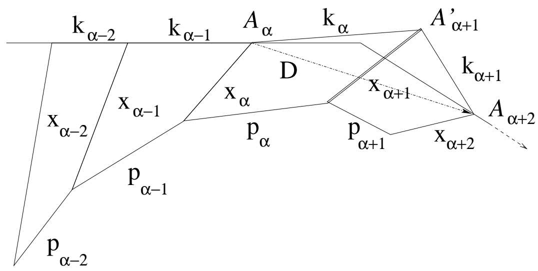

Figure 2.10: It is possible to find a solution to the Eqn.(2.20) around gluon corners, if k-vectors are allowed to have small transverse components relative to the local planar regions on the string around a corner.

to both these plaquettes. There is only one unique direction in space–time which can satisfy this requirement. Similarly, the transverse momentum at the vertices $v_{\alpha+1}$ and $v_{\alpha+2}$ would have their directions completely fixed because of the plaquettes they are connected to.

This creates complications for the iterative fragmentation procedure, because transverse momentum information for plaquette P_α has to be generated before $m^2_{\perp\alpha}$ can be calculated, which appears in Eqn.(2.13) for the distribution of z_α. If z_α is such that a gluon corner is crossed, the resulting planes of the plaquettes will be different from the preceeding planes. As mentioned earlier, this would leave one unique direction for the transverse momentum at each vertex involved in the corner crossing process, and that direction might be different from the direction initially generated.

This can be partially addressed by the observation that the transverse mass of a hadron depends only on the angles (in the rest frame of the corresponding plaquette) between the momenta of the newly produced $q\overline{q}$ pairs at adjacent vertices. Only the magnitude of the transverse momentum and the above mentioned relative angle need to be generated initially. After the k-vectors for the plaquettes have been determined, an overall rotation may be applied to all the vertex transverse momenta, if that can make these transverse momenta orthogonal to the plaquette planes. This proves to be insufficient, however, since for states with two or more gluons, it can be shown that the transverse momentum directions will conflict irreconcilably for plaquettes between two gluon corners. This is because an overall rotation of all transverse momenta between two gluons would conflict with the fixed direction of transverse momentum at the vertices involved in crossing either one gluon or the other.

If the transverse momentum at vertices like $v_{\alpha+2}$ in Fig.2.10, which occur at the end of the gluon corner crossing procedure, are set to zero, an overall rotation of transverse momenta in all plaquettes between two gluon corners could be

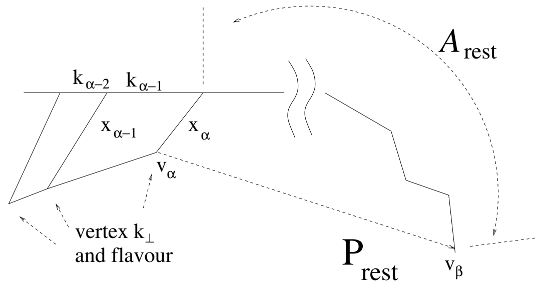

Figure 2.11: The string remainder consists of the unused portion of the directrix denoted as $\mathcal{A}_{\mathrm{rest}}$, the vertex v_α consisting of the location x_α, transverse momentum $k_{\perp\alpha}$ and quark flavour generated at that vertex, as well as the flavour of the parton corresponding to the last segment of the directrix.

used to find consistent directions for all transverse momenta. This would mean that at every gluon corner, one of the plaquettes would statistically receive less transverse momentum than the rest of the plaquettes. However, in our solution for the gluon corners in [1], we noted that our procedure introduces an extra transverse momentum for the particles around the gluon corners, due to the fact that k_α and $k_{\alpha+1}$ can not be chosen in the local string plane. This extra transverse momentum is of the same order of magnitude as ordinary vertex transverse momenta, and therefore compensates for the zero vertex transverse momentum mentioned above.

In this way, expressions for the vectors k_α and $k_{\alpha+1}$ can be derived by taking into account all the constraints imposed by the Eqn.(2.20) and the angles between the transverse momentum directions at the two vertices v_α and $v_{\alpha+1}$.

2.2.5 Treatment of Finite Available Phase Space in ALFS

Consider a situation like the one shown in Fig.2.11, where a series of plaquettes have been formed with the last calculated vertex being v_α. The fictitious vertex containing the end point anti-quark for the system is denoted by v_β. The energy–momentum available for the formation of new plaquettes is $x_\alpha + \mathcal{A}_{\mathrm{rest}}$. The flavours, transverse momenta and the energy–momentum contained in the system between v_α and v_β are available for the construction of the rest of the plaquettes in the event. This set of properties will be referred to as the "string remainder".

In the current version of ALFS, the treatment of the phase space is based on Eqn.(2.11). The random variables z and $k_\perp$, described earlier, define a step in the iteration process, together with the probabilities for the production of particular quark flavours, and the corresponding probabilities for hadron flavours. Eqn.(2.11) is interpreted as a weighting of an "a priori" probability distribution of the random variables with a phase space factor. In general, the phase space factors could depend on all the properties in the string remainder. In the following, it will be implicit that $g(s)$ is not just a function of s, but also of quark flavours and transverse momenta at the vertices α and β. However they will be disregarded in the formulae to keep the notation simple.

The distribution of z without the phase space weighting is

$$\bar{f}(z) \propto \frac{1}{z}\exp(-b\frac{m_{\perp}^2}{z}) \tag{2.25}$$

For large s, the distributions of flavour and transverse momentum are independent of each other and of z. Therefore, above a certain cut-off, they are generated with their independent distributions while z is weighted assuming $g(s) \propto s^a$, so that the treatment is identical to one using Eqn.(2.13) when $\frac{m_{\perp}^2}{z}$ is small compared to s.

The asymptotic solution of Eqn.(2.12) can not be expected to apply for small values of s. In fact, if s is of the order of a hadron mass, $g(s)$ defined in Eqn.(2.5) would have only one or two non-zero terms, as the states with more particles can not contribute because of the δ functions in Eqn.(2.3). The functions $g_l(s)$ can be related to each other using Eqn.(2.3) and Eqn.(2.4) with an equation very similar to Eqn.(2.12) :

$$g_n(s) \quad = \quad N\int_0^1 \frac{dz}{z}\exp(-b\frac{m_{\perp\alpha}^2}{z})\cdot g_{n-1}((1-z)\cdot(s-\frac{m_{\perp\alpha}^2}{z})) \tag{2.26}$$

From Eqn.(2.3) and Eqn.(2.4) one can write, $g_1(s) = N\exp(-bm_{\perp 1}^2)\delta(s - m_1^2)$, for one hadron flavour. From this, using Eqn.(2.26), one can derive an equation for $g_2(s)$ (without including transverse momenta):

$$g_2(s) = N^2\Theta(\sqrt{s}-m_1-m_2)\frac{2\exp(-\frac{b(s+m_2^2-m_1^2)}{2})\cosh(\frac{b}{2}\sqrt{\lambda(s,m_1^2,m_2^2)})}{\sqrt{\lambda(s,m_1^2,m_2^2)}} \tag{2.27}$$

$$\text{where } \lambda(x,y,z) \equiv x^2+y^2+z^2-2xy-2yz-2zx$$

The above expression should be integrated with respect to transverse momenta and summed over flavours to yield the full $g_2(s)$, as well as $g_3(s)$, $g_4(s)$... Unfortunately the integrals can not be expressed in closed form. Besides, finding their value for all possible flavour combinations and then using the result to find a more general distribution for the variable z is not a suitable strategy for a Monte Carlo. There might be Monte Carlo methods to approximate the effect of a detailed calculation of $g(s)$ for small values of s.

For values of s of the order of a few GeV, the contribution to $g(s)$ from $g_2(s)$ might be significant. Therefore the expression in Eqn.(2.27) is evaluated for all possible flavour combinations for the branching of the string remainder into two particles. Contributions from multi-particle modes are approximated by a power law as before. Branching fraction into one particular two particle mode is calculated as the ratio of $g_2(s)$ for that particular flavour and transverse momentum combination and the approximate parametrisation of $g(s)$. This branching fraction is used to decide between two particle and multi-particle modes. If a multi-particle mode is chosen, a z value is chosen from Eqn.(2.25) and weighted with the approximate $g(s)$ for the string remainder that would be left when the step is completed. In practice, in order to avoid infinite loops during computations, if a large number of z values selected with the distribution in Eqn.(2.25) are rejected, it is necessary to look for two particle modes. The treatment is very approximate, but the Monte Carlo presented here offers a framework in which more careful estimations of the phase space functions $g(s)$ can be incorporated into the model with ease. Different choices for parametrisations are currently under investigation.

2.2.6 Bose Einstein Correlations

One of the features of the hadronisation model presented here is that it associates a well defined, planar structure with the production of every hadron, even for gluonic strings. This allows a generalisation [11] of a coherent interference based model [9, 10] for Bose Einstein correlations to include multi-gluon strings. It turns out that the hadrons generated using this model, from string states obtained from parton showers in ARIADNE [12] and PYTHIA can be subdivided into groups called "Coherence Chains", such that the energy momenta of the hadrons in a group lie in a plane, up to small transverse fluctuations of the order of hadronisation transverse momenta. We discussed the origin and some interesting properties of the coherence chains in [11].

The interpretation of the area law in Eqn.(2.3) as the final state phase space multiplied by a transition rate inspires a form for an underlying quantum mechanical amplitude. Such an amplitude implies interference effects between different contributions to the amplitude, which are allowed when the final state contains identical particles. The different contributions are obtained from different permutations of the identical particles in the final state. The interference effect can be introduced into the Monte Carlo through an event weight. We showed that for a multi-gluon string the event weight factorises into contributions from coherence chains. Stability properties of the coherence chains gave many attractive features to the Bose Einstein model. Our investigation in [11] though, concludes that the correlation strength obtained in this method is insufficient to account for the experimentally observed correlation effects, suggesting contributions from other effects.

2.2.7 Summary of the hadronisation model

String fragmentation in this model can be schematically summarised in terms of three "decay modes" for a string remainder as follows (denoting a string remainder and a plaquette starting at vertex v_α by R_α and P_α respectively)

$$\begin{aligned} \text{mode 1}: R_\alpha &\rightarrow P_\alpha + R_{\alpha+1} \\ \text{mode 2}: R_\alpha &\rightarrow P_\alpha + P_{\alpha+1} + R_{\alpha+2} \\ \text{mode 3}: R_\alpha &\rightarrow P_\alpha + P_{\alpha+1} \end{aligned} \tag{2.28}$$

Mode 1 refers to the usual construction of a plaquette along a light-like segment of a directrix described in section 2.2.3. Mode 2 refers to the corner crossing procedure described in section 2.2.4. Mode 3 is the decay of the remainder into two particles for small invariant masses of the remainder, to finish the fragmentation iterations, as described in section 2.2.5.

At the start of the iterations, the entire string is thought of as the remainder. Branching probability for mode 3 is neglected for large invariant masses, and mode 2 is only used near gluon corners, when mode 1 fails. Properties of the plaquettes generated depend upon the distributions of a set of random variables like z as in Eqn.(2.25), $k_\perp$ and flavours as in Eqn.(2.2), as well as a phase space weight which depends on the properties of the string remainders before and after the step. For smaller invariant masses the same phase space factors are used to decide if mode 3 should be used to end the iterations.

The particles generated here stem directly from the decay of strings and are called primary hadrons. Many of these are normally short lived resonances. The decay of resonances is not described in the string language. The Monte Carlo implementation of this model can optionally use an external routine to perform calculations pertaining to such decays.

2.3 ALFS: The MC Implementation

In this section I will introduce a Monte Carlo implementation of the ideas presented or summarised here. ALFS stands for "Area Law Fragmentation of Strings", since originally that was the sole purpose of the project. The programming language used for ALFS is C++, although the main utilities can be used inside a Fortran program. The details of such interfacing between C++ and Fortran codes will not be mentioned here, as they tend to be system specific.

In keeping with the object oriented programming approach, ALFS has been written to expressly represent the ideas in the preceding sections. The key concepts in connection with this approach to hadronisation, like the directrix, the vertex, the plaquette, the string remainder etc., are represented as separate classes. These elements are combined precisely in the vein of the method described in section 2.2 in some "process" classes. Setting up parameters, receiving and sending out information to an external event generator, and regulating various actions in connection with string fragmentation is taken care of, through an interface class called the Hadronizer.

2.3.1 Installation

ALFS can be downloaded from "http://www.thep.lu.se/∼sandipan/ALFS/", as a tar archive. The current version ALFS uses many utilities in the CLHEP package as its base, and hence requires that CLHEP be installed. Small adjustments might have to be made in the Makefile for ALFS to set the choice of compilers, path for CLHEP, installation directory for ALFS etc.

ALFS can be installed as a stand alone hadronisation program, processing partons received from an abstract interface and returning the hadrons to the abstract interface. A typical use, though, would involve another event generator to simulate the hard subprocess and the parton shower before hadronisation is invoked. The interface between ALFS and the external event generator is not a part of the core utilities of ALFS. Simple interface classes can be written in the lines of the interface to PYTHIA, which is provided with ALFS by default, in the directory `ALFS/Interface/PY6Wrap`. If PYTHIA, or any event generator using the PYTHIA event record is to be used in conjunction with ALFS, the PYTHIA interface routines should be compiled. Since these interface routines use other utilities in ALFS, they should be linked before the main ALFS library while creating executable programs.

2.3.2 Interface

ALFS is designed to receive partons from an abstract interface, hadronise them, and return the hadronisation products back to the abstract interface. This abstract interface class called `ERInterfaceBase` is described below.

The organisation of the external event generator is regarded as unknown, but by writing a simple interface class inheriting from ERInterfaceBase, one can perform hadronisation with ALFS once the partons are specified by another program. I have provided two examples of such classes in `Interface/BasicERInterface`, `Interface/PY6Wrap/PY6ERInterface`.

Once an interface class is defined, one can associate an object of that class with the Hadronizer, like for instance

```
Hadronizer alfs;
```

`PY6ERInterface intf;`
`alfs.SetIOInterface(&intf);`
The strategy for generation of flavours, the mass spectrum of the hadrons, the model for transverse momentum generation could all be changed to conform to an external program, so that effectively ALFS would only handle the hadronisation kinematics, as illustrated in the following example program. More examples for usage are provided in the directory `ALFS/Examples`.

2.3.3 An Example Program

The following example program `example1.cc` creates a multiplicity distribution from a $u\overline{u}$ string at 50 GeV, using Pythia routines for the selection of flavours and hadron mass spectrum:

```
#include "ALFS/Interface/Hadronizer.h"
#include "ALFS/Interface/BasicERInterface.h"
#include "ALFS/Interface/PY6Wrap/PY6FlavourSelector.h"
#include "ALFS/Interface/PY6Wrap/PY6MassLookup.h"

using namespace std;
using namespace ALFS;

int main() {
  Hadronizer alfs;
  BasicERInterface intf;
  PY6FlavourSelector flselect;
  PY6MassLookup massfinder;

  alfs.SetIOInterface(&intf);
  alfs.flavourSelector(&flselect);//Uses pythia routines to generate flavours
  alfs.massLookup(&massfinder);//Retrieves hadron masses from pythia

  alfs.SetUp();//propagate parameter values to helper classes, check settings
  double ecms(50);
  Histogram MultDist(PROB_DIST,0.5,20.5,20);
  //see description of class Histogram
  ALFS_particle q(2,LorentzVector(0,0,0.5*ecms,0.5*ecms));
  ALFS_particle qbar(-2,LorentzVector(0,0,-0.5*ecms,0.5*ecms));
  //create q and qbar for the simple test

  for (int i=0;i<10000;++i) {
    intf.reset();
    intf.push_back(0,q);
    intf.push_back(0,qbar); //put q and qbar in intf as undecayed particles
    alfs.Execute(1,1);
    MultDist.put(intf.Multiplicity());
  }
  MultDist.Export("multdist.dat");
  return 0;
```

```
};
```

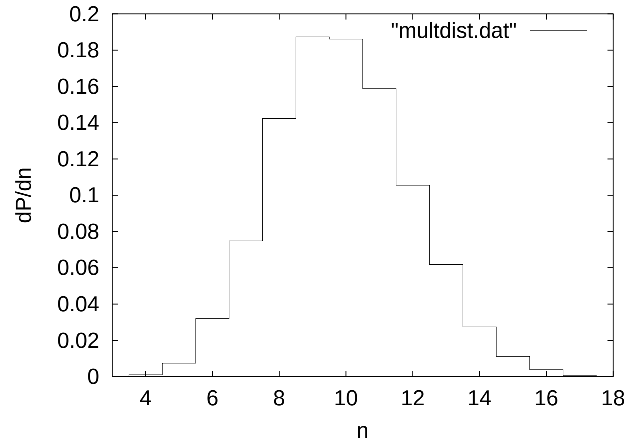

Figure 2.12: Multiplicity distribution of primary hadrons from the program `example1.cc`

The plot generated by the program is shown in Fig.2.12. The following is a description of the classes and functions the user needs to know in order to run the program.

- `Hadronizer`: An application program needs to declare an object of this class, which would perform hadronisation according to the model presented here. The following functions are available to the user.
  - `void SetIOInterface(ERInterfaceBase *eri)` : Set input of partons and output of hadrons will be handled by the interface `eri`. The application needs to define such an interface and pass its address to `Hadronizer`. If this is not done properly, ALFS will exit with error.
  - `void massLookup(MassLookup *massfinder)` : Sets the mass finding method to use the strategies specified by an object of class `MassLookup`, which is described below. The argument passed should be of a type which inherits from the base class `MassLookup`.
  - `void flavourSelector(FlavourSelector *fls)`: Sets the flavour selection methods to those in class `FlavourSelector` described below.
  - `void trmGenerator(HdnTrMomentum *hdnpt)`: If the user wishes to investigate hadronisation properties with a different model for transverse momentum generation, that model should be implemented in

a class inheriting from HdnTrMomentum and the address of an object of that class should be passed to the `Hadronizer` through this function.

- `void Execute(int i1,int i2)`: Performs hadronisation of the strings found in the input-output interface. Both integer arguments have default values 1, and can be omitted. `i1=0` would mean the program should try to proceed with hadronisation without trying to retrieve a new set of partons from the interface. This could be used for instance, to perform some calculations on the partonic level in ALFS before proceeding with hadronisation. To do this, one would use the function `Import()` to get the partonic state, perform analysis, and then call Execute with `i1=0`. If `i2=0`, `Execute` returns after hadronising the strings, without returning the hadronisation products to the external event record.
- `void Hadronize()`: May be used to perform hadronisation of the strings stored.
- `double BEEventWeight()`: Returns the Bose Einstein event weight obtained in our model for the last hadronisation event.
- `int Multiplicity()`: Multiplicity of hadrons from all strings.
- `int Multiplicity(int i)`: Multiplicity of hadrons from the i'th string.
- `NumberOfStrings()`: Number of strings retrieved from the interface.
- `LundString & String_no(int i)`: Returns a reference to the i'th LundString object in the initial state.
- `HadronizedState & HadronicSystem(int i)`: Returns a reference to a `HadronizedState`, which is a structure containing the details of the calculation of hadronic properties for the decay of the i'th string.
- `void WritePartonicState()`: Prints information about all strings.
- `void WriteHadronicState()`: Prints decay products of all strings.
- `Parameters * ParameterList()`: Returns a pointer to the parameter list used by ALFS.

• `Parameters`: All the parameters and switches used in ALFS are collected together in this class. The `Hadronizer` class declares one object of this type and its address is passed to all other classes. Interface to some of the more commonly used parameters will be given below. The class `Parameters` can read in a set of values from a file through the member function `ReadConfig(char *filename)`. It recognises keywords "opt" and "par" at the beginning of a new line. Any line beginning with any other word would be ignored as a comment. The syntax for specifying parameters and a description of the parameters can be obtained by using default configuration in a program and calling `SaveConfig(char *filename)`.

- `void a(double); double a();`: Set or retrieve the Lund model "a" parameter (see Eqn.(2.13)).
- `void b(double); double b();`: The "b" parameter in area law in Gev^{-2}.
- `void StringConstant(double); double StringConstant();`: The string constant κ in Gev^2.
- `void Sigma_Pt(double); double Sigma_Pt();`: Root mean square transverse momentum fluctuation for $q\overline{q}$ pairs.
- `void Asymptotic(double); double Asymptotic();`: Value of invariant mass above which the asymptotic behaviour of the phase space integrals $g(s)$ will be assumed to hold.

2.3.4 Interface to External Event Records

The design of the interface to external event records is based on three classes.

- `ERIterator`: An iterator for an event record is an abstract object which can loop over the entries and return information about particles, such as identification codes, masses and energy–momenta. It is meant to be used just like the iterators in the standard library container classes. The exact procedure for the retrieval of the information depends on the event record in question.
- `ERTemplate<IteratorType>`: This template is used as an abstraction of an external event record. Apart from providing simple functions for the first and last iterator positions in the event record, it can construct the strings to be used during hadronisation. The functions returning starting and ending iterators, the functions inserting entries into the external event record etc must be modified through inheritance. By contrast function for the construction of strings for ALFS in the base class can be used unchanged, as long as the iterator class for the external event generator can return the colour and energy–momentum of its entries. It is also required that the partons are arranged in their colour order in the external event record.
- `ERInterfaceBase`: This base class only serves to define the interface to the `Hadronizer`. It has three virtual functions to handle: (i) input of a partonic state from an external event generator (ii) output of the hadrons from ALFS to the external generator (iii) decay of short lived resonances (those with width larger than a specified cutoff). The virtual functions in the base class do not do anything, and must be over-ridden by inheritance. The inherited class should read in a partonic state as the initial

state in ALFS, and write the decay products back into the external event record. Unless one desires to study the Bose Einstein effects in our model, for which a symmetrised amplitude is calculated from the string decay products, one need not bother with the resonance decays while designing the interface. The two examples provided with ALFS, `BasicERInterface` and `PY6ERInterface` both use multiple inheritance, i.e., each inherits from this base class and the relevant event record class.

2.3.5 Auxiliary Utilities

Certain smaller utilities which were developed alongside ALFS as byproducts of testing the program appear in the directory `ALFS/Utils`. These utilities are not vital to the functioning of ALFS, and may be replaced by alternative utilities the user is more familiar with. The most important of such utilities will be described here.

`Histogram`: This simple histogram class provided with ALFS can meet a variety of elementary requirements in connection with taking statistics. It is constructed with a "mode", a range specified by minimum and maximum values, and the number of bins the range should be divided into. The mode is a variable of the "enumerated" type which can take the following values and meanings:

`PROB_DIST`: The data should be interpreted as a probability distribution. One can create a probability distribution for a random number x, generated in the program as follows:

```
//function body
Histogram hst(PROB_DIST, 0, 1, 100);

//loop ...
//calculations lead to a variable x whose distribution is desired
hst.put(x);
//... end of loop
hst.Export("filename");
```

In this mode, if one inputs (x, y) values in the histogram using `put(x,y)` instead of `put(x)` as above, the `Histogram` will "Export" only a probability distribution of the x values, i.e., $(x, \frac{dP}{dx})$. It can optionally normalise the distribution to a value other than 1, or for the given range. `HIST_SUM`: Export sum of y value from all trials in a bin around x. `HIST_MEAN`: Export average y value in a bin around x, i.e., $(x, < y >)$. `HIST_STDEV`: Export standard deviation of y value in a bin around x. `HIST_ERRBAR`: Export three columns with x, mean and standard deviation of y. `HIST_STATERR`: Mean and MC error-bars are exported. `HIST_RANGEBAR`: Average and the full range of y values for every bin are exported. `FUNCTION`: Single y value for every x bin, obtained for instance when algebraic operations are performed on two histograms.

Data is inserted into the histogram with the function `put(double)`, or `put(double,double)`. It is possible to define a histogram in any one mode (except `FUNCTION`) and export it in any other. An alternative normalisation procedure interpreting the y values for every entry as a weight for the corresponding x value is also provided.

2.3.6 Internal Structure of Alfs: Hadronization Concepts

The concepts involved in the model are represented by classes whose characteristics reflect the intuitive meanings. Each of the important concepts elaborated upon in the previous sections is represented by a class in Alfs. They can be found in the directory `ALFS/Hadronization/Concepts`.

- `ALFS_particle`: By particles in Alfs, one only means the final state hadrons. This is a very simple class with just a few data members to hold an identity code, the particle mass and an energy momentum four-vector, which can be conveniently reached and altered through interface functions.
- `Directix:` The concept of a directrix was described in section 2.2. Apart from methods `E()`, `P()` etc, to return the most trivial properties in connection with a collection of parton energy momenta, the directrix has member functions to evaluate its λ-measure. Since as of now, fragmentation of heavy quarks has not been carefully considered in this approach, the energy momentum vector of a bottom quark, for instance, will make one segment of the directrix into a time-like vector. This is undesirable because the property that the directrix consists of light-like segments is used in many places. The directrix class provides a self filter in member function `MakeLightLike()`, which finds a close approximation in terms of light-like vectors. The segments can be reached through the `operator[]` member function, but the directrix class also provides a `segment(int i,enum normal,reversed sd)` member function to return the i'th segment seen from the side specified by the argument sd of enumerated type. An `operator()` function is also provided, though never used in this version of Alfs, which means that an object declared to be a directrix can be used like a four-vector valued function, just like in section 2.2.
- `LundString`: The string is not regarded as a particle that decays into a bunch of hadrons. A string has a directrix associated with it, which is a very non-trivial structure. A string has a world surface, it could be open or closed; but otherwise for most practical purposes it is specified entirely by its directrix. In keeping with this idea, that the string is determined by its directrix except for the properties just mentioned, the `LundString` class is derived from the directrix class with these properties added as enhancements.

- `Vertex`: This class represents the abstract idea of a vertex, i.e. a space–time location for pair production, the flavour and the transverse momentum generated along with pair production. It is also connected to the directrix at one value of the parameter describing the directrix, often written as ξ in this paper.

- `Plaquette`: This class which represents the idea of a plaquette associated with the creation of a hadron, answers queries about the hadron, like the identity code, mass, of the hadron; and also about the variables involved in its production, like the light-cone momentum fraction z, the angle between the two transverse momenta at the attached vertices in the rest frame of the plaquette, the transverse mass, whether the hadron was produced around a gluon corner, whether it is a decay product of a resonance etc. It also performs some basic calculations about the production of the corresponding particle.

- `RemString`: Hadronisation is thought of as a series of decays of a string remainder into either of (i) one plaquette and a remainder (ii) two plaquettes and a string remainder, around gluon corners (iii) two plaquettes, to end the fragmentation iterations. These three decay modes are the most important features of the string remainder class. Besides, the ideas about the available phase space presented earlier would need an estimation of functions $g\_2(s)$ and $g(s)$ for the string remainder. As pointed out earlier, the true available phase space for small invariant masses of the remainder system might depend on the flavours at the two bounding vertices, transverse momentum content, and perhaps, the presence of gluons in the system. The phase space integral is therefore referred to as `g_tot()` for the `RemString`. So far, only very approximate calculations have been made for this function. Above a certain limit in s, the function is approximated with the power law. Even for such situations, an option is provided to calculate using the λ-measure instead of s. The calculation of `g_tot` is expected to become much more sophisticated in the future, through better approximations to the solution of Eqn.(2.12), and more detailed consideration of flavour dependence. However, it will still be a property of the `RemString`, and the hadronisation iterations only need to know that there is a way to calculate the total available phase space `g_tot`, and the phase space for a two particle decay mode. This keeps the design of hadronisation iteration procedure separate from the phase space calculations.

- `HadronizedState`: This class acts like an internal event record for ALFS. It contains information about the intermediate stages during the iterations, namely, the series of vertices and plaquettes.

2.3.7 Hadronisation Process

The classes described in the previous section form the elements, or building blocks for the program. The model is built by combining these building blocks in an appropriate way, so that they perform their intended tasks. The class `Hadronization` is such a "process" class which combines the concept classes described earlier to implement the hadronisation model.

- `Hadronization`: This class provides methods to construct a `HadronizedState` out of a `LundString`. The interface for this action is the `operator()(LundString &, HadronizedState &)`. During the iterations, it needs to generate flavours, transverse momenta for the vertices, and the random number z. These tasks are consigned to smaller helper classes, while Hadronization itself only manages the iterations and phase space weighting procedure.
- `FlavourSelector`: This is a simple base class to help select the flavours of the quark anti-quark pairs produced in the vertices and the hadrons which can be formed by combining the flavours at two vertices.
- `PY6FlavourSelector`: This class inherits from FlavourSelector and merely calls functions from Pythia6 to do its job.
- `HdnTrMomentum`: As the name suggests, this is a class which is used inside the Hadronization class to generate hadronisation transverse momenta. The usual model has no transverse momentum correlations, but it is possible to inherit from this class and implement another model for transverse momentum generation, possibly with correlations.
- `ZDistribution`: This is a random number generator class in the directory `ALFS/Random`, which returns random numbers distributed like Eqn.(2.13) or Eqn.(2.25), as demanded.

2.3.8 Bose Einstein Correlations

Though our first analysis has shown that the model yields rather low correlation strengths, the routines for the calculation of Bose Einstein weights are integral parts of ALFS, and will be presented here. Besides, while addressing the Bose Einstein Correlations, a few classes were developed which might be of more general interest. They will be described in the next subsection. The key concepts involved in our model for BEC will be mentioned here.

`CoherenceChain`: This class represents the concept of a coherence chain mentioned in section 2.2.6. It holds the data from a set of hadrons which can be thought to be in a plane, and then projects the hadron energy momenta to transverse and longitudinal parts relative to the plane. A method to calculate and return the BE weight for the coherence chain is provided.

`BEState`: The result of hadronisation, i.e., a `HadronizedState` can be divided into groups called `CoherenceChains`. The name just indicates that as far as BEC is concerned in our model, a `HadronizedState` is equivalent to a bunch of `CoherenceChains`. A `BEState` can be constructed out of a `HadronizedState`, and the constructor finds out all `CoherenceChains` in the event. A `BEWeight()` function returns the Bose Einstein weight for the `BEState`, or equivalently for our model, for the hadronisation event. This weight is calculated as the product of all the `BEWeights` from the `CoherenceChains`.

2.3.9 Generation of Permutations

Our Bose Einstein model led us into the requirement of generating permutations of a set of objects with a certain constraint. The problem and one solution will be presented here. The Bose Einstein weight for a coherence chain is found by calculating contributions to an amplitude from all possible configurations of identical particles in the final state. For example, if the final state is $\{\pi_0^+, \pi_1^-, \pi_2^+, \pi_3^0, K_4^-\}$, there is one alternative configuration $\{\pi_2^+, \pi_1^-, \pi_0^+, \pi_3^0, K_4^-\}$, which will contribute to the amplitude. This was a particularly simple event. An event with 6 π^+s and 6 π^-s and two π^0s would have about a million contributions to the amplitude. On the other hand, we found that for an event like that, the contribution to the amplitude from most of the permutations is negligible, whereas the permutations with significant contributions were not necessarily of smaller order. It is of great interest therefore to find a method which will generate only those permutations which make a significant contribution to the amplitude.

It was found that the contribution to the amplitude from a configuration was small if it assigned a new position to a particle that was very dissimilar to the original position. This qualitative idea of very dissimilar corresponded to the following quantitative definition in our case: A particle is said to have a link with the position of another particle if (i) $Q^2 = -(p_1 - p_2)^2 < Q^2_{cut}$ (ii) $(\Delta x)^2 = -(x_1 - x_2)^2 < S_{max}$. Only those permutations gave any non-negligible contributions in which particles were permuted to alternative positions which they had links with. The set of all links could be summarised in a "link matrix" L, with every element either equal to 0 or 1, such that the particle "i" has a link with position "j" if and only if $L_{ij} = 1$.

The problem can be presented in a completely general terms as follows: Consider a set of n boxes $\{B_0, B_1, B_2, ..., B_n\}$, and a set of cats $\{c_0, c_1, c_2, ..., c_n\}$. Assume that each cat has a certain number of preferred boxes, which are specified by a link matrix, i.e., cat c_i can accept box B_j if $L_{ij} = 1$, not otherwise. What are all the possible arrangements of the cats in the boxes ?

The classes `PermutationBase`, `Permutation`, `ExchangeLink`, `LinkChain` and `LCStructure` solve the above problem. These classes are templates, and are completely independent of the structure and purpose of the rest of ALFS, and can be used for any problem which can be expressed like the cat problem above. The solution in ALFS, is as follows:

1. Construct a list of linked objects and isolate objects in the original list which do not have links with any other position.
2. Out of the links found in step 1, construct a set of graphs (represented by the `LinkChain` class). Isolate all disjoint graphs, and enumerate them.
3. Build a "clock" structure with these disjoint graphs as hands. For each call to the `NextPermutation` function, advance the first graph through its permutation, while leaving every other graph as they are. When the first graph returns to the identity permutation, advance the next, and so on.

This reduces the problem to the generation of permutations of a graph with the link matrix constraint. This is handled in the `LinkChain` class. It allocates a set of allowed objects for every box. It then generates the permutations by placing each object into each box it is allowed to occupy, through a simple recursive algorithm.

The structure used to represent permutations is slightly more complex than an array of integers. When one represents a permutation with a set of integers, $\{e_0, e_1, e_2 ...\}$, the number e_i might represent one of the two things: (i) It could mean which cat occupies box B_i (ii) It could mean which box is cat c_i sleeping in. These representations are transpose of each other. The `Permutation` class in ALFS makes use of the first meaning in its `operator[ ](int)`. The set of numbers which would represent the transpose can be accessed through the member function `Transpose(int)`.

This structure is functional, though it is not elegant or efficient. The BE weight calculations in ALFS take a long time, not because it takes long to find the permutations, but because there are a large number of them. The calculations that need to be done for each permutation take a lot longer than generation of permutations, and hence making the generation of these permutation more efficient would not make the BE calculation noticeably faster. The author would nevertheless be interested in an efficient or elegant solution.

2.3.10 Summary

The documentation given here refers to the version 1.0 of ALFS. Updates are expected in the near future in connection with the treatment of low energy systems. The user interface however, is unlikely to change very quickly. Because of the extra transverse momentum generated around the gluon corners and the different treatment of phase space, the Lund model parameters such as a, b and σ should be tuned for ALFS, independent of their values used in PYTHIA. A study of the behaviour of this program in different hadronisation related situations will be presented soon.

Acknowledgements

I would like to thank Gösta Gustafson, Torbjörn Sjöstrand and Leif Lönnblad for many useful discussions. I would also like to thank Fredrik Söderberg for testing ALFS and informing me about errors.

References

[1] B. Andersson, S. Mohanty, F. Söderberg, *Eur. Phys. J.* **C21** (2001) 631.

[2] B. Andersson, G. Gustafson and B. Söderberg, *Z. Phys.* **C20** (1983) 317.

[3] B. Andersson, The Lund Model, (Cambridge University Press 1998).

[4] B. Andersson, G. Gustafson, G. Ingelman, T. Sjostrand, *Phys. Rept.* **97** (1983) 31

[5] B. Andersson, G. Gustafson and T. Sjöstrand, *Z. Phys.* **C6** (1980) 235.

[6] B. Andersson, G. Gustafson, T. Sjöstrand, *Phys. Scripta.* **32** (1985) 574.

[7] B. Andersson, G. Gustafsom, J. Samuelsson, *Z. Phys.* **C64** (1994) 653.

[8] T. Sjöstrand, P. Edén, C. Friberg, L. Lönnblad, G. Miu, S. Mrenna and E. Norrbin, *Computer Phys. Commun.* **135** (2001) 238.

[9] B. Andersson and W. Hofmann, *Phys. Lett.* **B169** (1986) 364.

[10] B. Andersson and M. Ringnér, *Nucl. Phys.* **B513** (1998) 627.

[11] S.Mohanty, F. Söderberg, LU TP 03-08

[12] L. Lönnblad, *Computer Phys. Commun.* **71** (1992) 15.

[13] B. Andersson, S. Mohanty, F. Söderberg, *Nucl. Phys.* **B646** (2002) 102.

The λ-Measure and the Generalised Dipoles in the Lund Model

Paper III

LU TP 02-13
July 2002

The λ-Measure and the Generalised Dipoles in the Lund Model

Bo Andersson
Sandipan Mohanty[1]
Fredrik Söderberg[2]
Department of Theoretical Physics, Lund University,
Sölvegatan 14A, S-223 62 Lund, Sweden

Abstract We demonstrate that the multiple gluon emission phase space in the dipole cascade model has a strong linear correlation with the number of gluons emitted. The number of gluons per unit available phase space at a certain resolution scale is found to be remarkably independent of the cms energy and global event properties like thrust, and even changes in the ordering variable or resolution scale. We show that the distribution of sizes of gluon-gluon dipoles in a parton cascade has stability properties which are sufficient to account for those of the phase space variable. We observe that certain more abstract entities, defined in the context of hadronisation and related to the gluon emission phase space, share those properties of colour dipoles and name them Generalised Dipoles. We also present an analytical model to qualitatively describe our findings.

[1]sandipan@thep.lu.se
[2]fredrik@thep.lu.se

3.1 Introduction

The phase space for multiple bremsstrahlung emission of photons in QED is entirely given by the properties of the original current. The reason is that the photon-quanta are uncharged and therefore the currents are not changed because of emission of photons (besides the recoil effects from hard emissions).

On the other hand the QCD field quanta, the gluons, are charged. Already the emission of a first QCD gluon in e^+e^--annihilation means that the original $\mathrm{q}\overline{\mathrm{q}}$ dipole is changed. It so happens that the change is (to a very good approximation) from one dipole to two independent dipoles, one between the quark (q) and the first gluon and the other between the gluon and the anti-quark ($\overline{\mathrm{q}}$). The initial dipole is at rest in the total cms whereas the two "new" dipoles move away from each other. The combined phase space for emitting from either one or the other of these dipoles is found to be larger. In rapidity space the increase can be described as an extra region of a size corresponding to the logarithm of the squared transverse momentum of the first emitted gluon.

In the Dipole Cascade Model [1], as implemented in the event generator ARIADNE [2], a second emission leads to three independent dipoles and so on. The ordering variable is an invariantly defined transverse momentum of the emitted gluons. The dipole masses decrease quickly with successive emissions.

HERWIG [3], and PYTHIA [4], subdivide the emerging dipole angular regions into independent cones for each emitting parton. One way to state the coherence conditions is that they do not permit double-counting in the emission process. HERWIG and PYTHIA implement the coherence conditions by means of angular ordering to avoid such overlaps. The ordering variable for HERWIG is just the angle (or the rapidity variable) occurring in the coherence conditions. PYTHIA uses the "virtuality" along the emission lines as an ordering variable and only afterwards introduces an angular ordering condition.

In this paper we will mainly describe the emerging features in terms of the notions of the Dipole Cascade Model (ARIADNE) and only perform a cursory comparison to similar results from PYTHIA. Some of the ideas presented here were also discussed in [20] in their preliminary form. Our aim is to investigate a set of distributions stemming from the perturbative parton cascades. We will show that the cascades result in a local structure, corresponding to sets of independent entities, which we are going to call Generalised Dipoles (*GD*s). The *GD*s are linked together along the colour lines of the QCD force field. They have a common distribution in a generalised rapidity range λ, and in the (local) transverse momentum. This structure is independent of the total cms energy, the global event variables like thrust and the number of hard emissions. Further the *GD*s show a surprisingly small scale dependence, i.e. almost the same distributions occur inside a wide range of the ordering variable.

We will concentrate upon e^+e^--annihilation events, where the gluon cascade is produced through the bremsstrahlung from an originally produced $\mathrm{q}\overline{\mathrm{q}}$

pair (although we expect that the same structures will emerge also in other dynamical situations). Such a multi-gluon state is conveniently described by means of a four-vector valued function, the directrix $\mathcal{A}_\mu$ [5]. The directrix is obtained by laying out the energy–momentum vectors, k_j, of the emitted partons in colour-order, starting with the q and ending with the $\overline{\mathrm{q}}$ (we will neglect the production of "new" $\mathrm{q}\overline{\mathrm{q}}$-pairs through the gluon splitting process). As we will use massless partons, the directrix is a curve with a tangent that is light-like everywhere.

As mentioned earlier the phase space available for gluon emission at a certain value of the ordering variable $k_\perp$ depends on the partons present and their colour order. It could, therefore, be regarded as a functional of the directrix $\mathcal{A}_\mu$. In section 3.2, we will discuss a measure of this phase space, to be called ℓ, for multiple gluon emission in perturbative QCD. An infrared stable generalisation of this phase space, involving a "resolution parameter" m_0 leads to the concept of the λ-measure [6].

The λ-measure was introduced many years ago [6], as a generalisation of the rapidity range, to describe the phase space for hadronisation. At the same time [6], a curve similar in appearance to a set of connected hyperbolae along the directrix was introduced, the $\mathcal{X}$-curve. Its length is related to λ in the same way as the "ordinary" rapidity variable measures the length of a hyperbola spanned between two light-like vectors.

The tangent vector, to be called q_T, at a point on the $\mathcal{X}$-curve that reaches out to a point on the directrix quickly reaches a constant length, $q_T^2 = m_0^2$, just like the constant distance in Minkowski metric between the light-cones and an ordinary hyperbola. The parameter m_0 is a resolution parameter for the properties of the directrix. In the context of hadronisation, it is fixed by the properties of the spectrum of hadrons produced. Thought of as a generalisation of ℓ, the λ-measure has a resolution parameter which can be directly related to the ordering variable in the perturbative cascade. When the tangent vector q_T follows the directrix it will span a surface between the directrix and the $\mathcal{X}$-curve. The λ-measure is also proportional to the area of this surface.

In the dipole model, the available phase space for gluon emission, ℓ, in the Leading Log Approximation (LLA) [7] and in the Modified Leading Log Approximation (MLLA) [7] schemes is a sum of a series of terms , $(\Delta\ell)_j$, one for each pair of consecutive vectors along the directrix [6]. These terms are contributions to the phase space from individual dipoles in the Dipole Cascade Model. We will show that the λ-measure can be similarly subdivided into a number of parts $(\Delta\lambda)_j$, one for each vector along the directrix, and that they are strongly related to the contribution from the dipoles, $(\Delta\ell)_j$. The process of subdividing λ corresponds to a partitioning of the surface mentioned above into "plaquettes"[3] that are enclosed by one "initial" q_T and one "final" q_T vector

[3] In this paper, we will use the word plaquette to denote this area even though one part

together with a hyperbolic segment of the $\mathcal{X}$-curve and the parton energy–momentum vector in between, cf. Fig 3.1 in section 3.2. It is the regularity in the $(\Delta\lambda)$ distribution that will lead to the definition of the GDs. For the surface mentioned above this regularity implies a simple general structure, which shows only a slowly varying dependence on the ordering variable.

The directrix also plays a major role in the description of the state of the massless relativistic string, which is used as a model for the QCD force fields in String Fragmentation [5]. The surface spanned by the string during one period is a minimal surface. This has two consequences. On the one hand the surface is completely determined by its boundary curve. On the other hand the surface is stable against small deformations (the model is infrared stable). In the motion of a massless relativistic string, a wave moves across the string surface bouncing at the endpoints defined by the orbits of the q and the $\overline{\text{q}}$. This means that the internal excitations (which in the Lund Model are identified as the gluons) will reach and affect the endpoints in turn, i.e. in the colour order of their emission. The corresponding orbit of the q endpoint is the directrix.

It is interesting to note that the $\mathcal{X}$-curve (or rather a close relative, called the $\mathcal{P}$-curve in [8]) and the λ-measure play a major role in the String Fragmentation process for multi-gluon string states. In the process that we devised in [8], the final state hadron energy–momenta, laid out in rank order, constitute a curve, the X-curve. The X-curve follows the directrix at a typical stochastically fluctuating distance and the area in between the two curves could be thought of as the area in the Lund Model Area law [8]. It turns out that the average X-curve is just the $\mathcal{P}$ curve with a length given by λ. The generalised dipoles to be defined in this note also play an interesting role in the fragmentation process. Just as they emerge as independent entities from the partonic cascades, they also fragment essentially independently of each other into the final state hadrons, in a fragmentation scheme along the directrix.

The λ-measure has been used in many different contexts in investigations over the years. It was quickly found, that the $\mathcal{X}$-curve shows properties of a fractal character [9] and the multi-fractal dimensions were shown to be identical to the so-called anomalous dimensions of QCD [10].

In section 3.2, we recapitulate some features of the gluon emission phase space ℓ-measure and the λ-measure with the aim of pointing out similarities and differences between the two quantities[4]. We also introduce the quantities $\Delta\lambda$ and present a geometrical interpretation for them. In section 3.3, we describe our findings and define the Generalised Dipoles. In section 3.4, we present a

of the boundary curve is a part of a hyperbola. The plaquettes defined in this paper are not related to the plaquettes used in Lattice QCD.

[4] In the past, like in the references listed in this paper, the gluon emission phase space has often been called the λ-measure. But since both this phase space and the phase space for hadronisation are relevant for this work, we make the distinction here and give them different names.

model to understand the distributions we have obtained. At the same time we will consider some earlier results and the theoretical analysis. Finally, in section 3.5 we make some concluding remarks.

3.2 The λ-Measure and The Perturbative Cascades

3.2.1 The phase space in a dipole cascade and the ℓ-Measure

The probability for the emission of gluons in the Dipole Model can be described in terms of an inclusive density of gluons (cf. [1]):

$$\mathrm{d}n = \alpha_{\mathrm{eff}} dy \frac{dk_\perp^2}{k_\perp^2} \times (\textstyle\sum_p) \tag{3.1}$$

with α_{eff} the effective running coupling and $(\sum_p)$ the polarisation sum, i.e. the coupling between the spin of the emitters and the gluon. The coherence conditions in this case are identical to energy–momentum conservation, i.e. the cms energy of the gluon cannot exceed half the total cms energy

$$k_\perp \cosh(y) \leq \frac{\sqrt{s}}{2} \tag{3.2}$$

A convenient approximation, corresponding to the Leading Log Approximation, is $|y| < \frac{1}{2}\ln(\frac{s}{k_\perp^2})$ so that the total rapidity range is $\Delta y \simeq \ln(\frac{s}{k_\perp^2})$. As we mentioned above the emission of a gluon will change the current. But it is an immense simplification that this change is simply a change from one dipole to two independent dipoles (to a very good approximation) [7, 11]. Thus the density for the emission of two gluons is factorisable, so that we obtain

$$\mathrm{d}n(\mathrm{qg_1g_2\overline{q}}) \simeq \mathrm{d}n(\mathrm{qg_1\overline{q}})\,[\mathrm{d}n(\mathrm{qg_2g_1}) + \mathrm{d}n(\mathrm{g_1g_2\overline{q}})] \tag{3.3}$$

(with a negative correction that formally is of the order of $1/N_c^2$ for a finite number of colours, but reduced further in practice due to kinematics). Eq. (3.3) is valid if the transverse momenta are ordered so that $k_{\perp 1} > k_{\perp 2}$ or else the two gluons are exchanged. While the original $(\mathrm{q\overline{q}})$ dipole is at rest in the cms the two "new" dipoles move apart. Each of them will decay in its own rest-frame with a phase space given by Eq. (3.2) and this means that the combined rapidity region for emitting the second gluon with transverse momentum $k_\perp$ is

$$\begin{aligned}(\Delta\ell)_{01} + (\Delta\ell)_{12} &= \ln\left(\frac{s_{01}}{k_\perp^2}\right) + \ln\left(\frac{s_{12}}{k_\perp^2}\right) \\ &= \ln\left(\frac{s}{k_\perp^2}\right) + \ln\left(\frac{s_{01}s_{12}}{sk_\perp^2}\right)\end{aligned} \tag{3.4}$$

The expression $\frac{s_{01}s_{12}}{s}$ is the conventionally defined invariant squared transverse momentum of the first gluon, $k_{\perp 1}^2$. Similarly, for an emission at $k_\perp^2$ from a system of n gluons, we can write the phase space as:

$$\ell = \sum_{i=0}^{n} (\Delta\ell)_{i,i+1} = \sum_{i=0}^{n} \ln(\frac{s_{i,i+1}}{k_\perp^2}) = \ln \prod_{i=0}^{n} (\frac{s_{i,i+1}}{k_\perp^2}) \tag{3.5}$$

At this point, it is necessary to differ between two definitions of the transverse momentum. The one we have used up to now is the ordering variable $k_\perp$, i.e. the value used for the emission of a gluon and defined by the partitioning of a dipole of mass M into a pair of dipoles with masses (m_1, m_2) so that $k_\perp^2 = m_1^2 m_2^2 / M^2$. There is another local variable, to be called k_t, which is defined along the directrix so that we have

$$k_{tj}^2 = \frac{(2k_{j-1}k_j)(2k_j k_{j+1})}{(2k_{j-1}k_j) + (2k_j k_{j+1}) + (2k_{j-1}k_{j+1})} \equiv \frac{s_{j-1,j}s_{j,j+1}}{s_{j-1,j,j+1}} \tag{3.6}$$

in terms of the energy–momentum vectors of the (colour) adjacent gluons.

We note that the two values of $k_\perp$ and k_t coincide for the last emitted gluon. But in general the transverse momentum k_t of a gluon may be much smaller than the $k_\perp$ value at which it was emitted, because of the recoils from subsequent emissions. In fact, in this way k_t can even become smaller than the resolution scale at which the state is being sampled. But the "emission" $k_\perp$ and the concepts of the "first emitted" gluon and the "second emitted" gluon etc are necessities of the strategies used to simulate this quantum mechanical process, and not properties of the final state of partons. When one asks what the probability is for the production of a state with a certain number of partons, where colour connected partons with transverse momenta smaller than a certain value would not be considered as resolved emissions, the only relevant transverse momentum is the k_t, which is calculated using vectors in the final state. Therefore, it is undesirable that this variable is pushed to values smaller than the resolution parameter. We have used two different methods to avoid such situations. The first is to veto such emissions along the cascade[5] and the second to change the ensuing directrix vectors so that three neighbouring light-like vectors are combined into two. All the results of this investigation are independent of the method that is used. Furthermore, such a procedure is essential for the inclusion of the second order matrix element corrections into ARIADNE [12].

[5]This feature will be made available in the next version of ARIADNE

3.2.2 The λ-measure, its properties and its connection with the ℓ-measure

When a string without gluonic excitations fragments under the usual Lund Model assumptions, hadrons are formed by breaking of the string field at "vertices" which, on the average, lie on a typical hyperbola parametrised by a squared proper time from the origin, usually called Γ_0 or m_0^2. The rapidity range available along this hyperbola is given by $\ln \frac{s}{m_0^2}$.

In the Lund Model interpretation for a string with a single gluon excitation, there will be two parts of the string; one string piece spanned between the q and the g and one between the g and the $\overline{\text{q}}$. Therefore there will be two hyperbolic angular ranges $(\Delta y)_{01}$ and $(\Delta y)_{12}$ for hadron formation. The sum of these ranges is

$$(\Delta y)_{01} + (\Delta y)_{12} = \ln(\frac{s_{01}}{2m_0^2}) + \ln(\frac{s_{12}}{2m_0^2}) = \ln(\frac{s}{m_0^2}) + \ln\left(\frac{s_{01}s_{12}}{4sm_0^2}\right) \tag{3.7}$$

We draw attention to the factor of 4 in Eq. (3.7), and its absence in Eq. (3.4). In the Lund Model, when the partons move apart stretching a string-like field between them, they lose energy–momentum to the string field. A gluon is attached to two string pieces while a quark or an anti-quark is attached to one. Therefore a gluon will lose energy–momentum twice as quickly as a quark or an anti-quark. Flat string regions will therefore be formed, bounded by the whole of quark or anti-quark momenta, but half of gluon momenta. Since hadrons form from this field, the phase space is calculated by adding up the lengths of typical hyperbolae in each of these flat string regions. For instance, the invariant mass of the region involving the quark and the gluon, for the system in Eq. (3.7), is $(k_{\text{quark}} + \frac{1}{2}k_{\text{gluon}})^2 = \frac{s_{01}}{2}$, and its contribution to the phase space for hadronisation is $\frac{s_{01}}{2m_0^2}$.

Such a factor was not necessary in Eq. (3.4). A gluon is shared between two dipoles, but both of those dipoles are modified by the emission of a single gluon from either of these dipoles. This is because the gluon in common between them would receive a recoil and that would change the invariant masses of both the dipoles. Formation of a single hadron in string fragmentation does not give recoils to the partons making up the string. Hadron formation occurs from the string, which has a spatial extent. Gluon emission, on the other hand, is a perturbative phenomenon and the new emission is thought to come directly from one or the other of the two partons making a dipole, or from the dipole as a whole regarded as a unit. Therefore, in the implementation of the dipole cascade model in Ariadne, the full gluon momentum is used for both the dipoles involving the gluon. There is no problem in conserving energy–momentum because both the dipoles can not emit "simultaneously". As soon as there is an emission from one dipole, the whole system is updated into a new chain of dipoles.

The expression in Eq. (3.7) does not make sense for soft or collinear gluons, as these would give negative contributions to the effective rapidity range. An infrared stable generalisation applicable for arbitrarily many gluons was presented in [6] and its relation to the hadronisation process was discussed in [13]. For a state with a single gluon we replace the expression in Eq. (3.7) with:

$$\ln\left(\frac{s}{m_0^2}+\frac{s_{01}s_{12}}{4m_0^4}\right) \tag{3.8}$$

This is a nicely interpolating expression between the results for a string with and without a gluon. It can be generalised to an arbitrary number of gluons by introducing the following quantities, defined as integrals along the directrix $\mathcal{A}(\xi)$ (with ξ a suitable parameter, here taken to be the energy along the directrix):

$$\begin{aligned} t_j \quad = \quad & \int_0^{E_{tot}} d\xi_1 \int_0^{\xi_1} d\xi_2 \left[\frac{d\mathcal{A}}{d\xi_1}\cdot\frac{d\mathcal{A}}{d\xi_2}\right] \int_0^{\xi_2} d\xi_3 \int_0^{\xi_3} d\xi_4 \left[\frac{d\mathcal{A}}{d\xi_3}\cdot\frac{d\mathcal{A}}{d\xi_4}\right]\cdots \\ & \cdots \int_0^{\xi_{2j-2}} d\xi_{2j-1} \int_0^{\xi_{2j-1}} d\xi_{2j} \left[\frac{d\mathcal{A}}{d\xi_{2j-1}}\cdot\frac{d\mathcal{A}}{d\xi_{2j}}\right] \end{aligned} \tag{3.9}$$

This corresponds to a $2j$-fold partitioning of the directrix into non-overlapping pieces and then to multiplying the adjacent vector differentials two by two. For a massless relativistic string, a point on the string (parametrised by the energy (σ) between the point and the quark end) at time t will be at $x(\sigma,t)$:

$$x(\sigma,t)=\frac{[\mathcal{A}(t+\sigma)+\mathcal{A}(t-\sigma)]}{2} \tag{3.10}$$

i.e. it is given by one left-moving and one right-moving vector defined by points on the directrix. As the differentials of the directrix are light-like the quantities $d\mathcal{A}(\xi)\cdot d\mathcal{A}(\xi')$ occurring in the integrals in Eq. (3.9) are surface elements on the string. The integrals in this way correspond to all the possibilities of obtaining j-fold partitionings into non-overlapping areas on the string surface.

We may then define a functional $T\equiv\exp(\lambda)$ as

$$T=1+\sum_{j=1}^{\infty}\frac{t_j}{(m_0^2)^j} \tag{3.11}$$

i.e. as the generating function of the partitioning functionals t_j in Eq. (3.9) with m_0 an energy scale to make it dimensionless. We note that the integrals t_j will vanish if $j>n+1$ where n is the number of gluons emitted. The term involving one power of m_0 is always equal to $\frac{s}{2m_0^2}$ and the last (non-vanishing) term will have the generic form

$$\frac{1}{2}\frac{s_{01}}{2m_0^2}\frac{s_{12}}{4m_0^2}\frac{s_{23}}{4m_0^2}\cdots\frac{s_{n,n+1}}{2m_0^2} \tag{3.12}$$

with $(j, j+1)$ indices of colour-consecutive partons (index 0 for the q, indices 1 .. n for gluons, and $n+1$ for the $\overline{\mathrm{q}}$). Besides the addition of 1 and a factor of 1/2 (both introduced to obtain simple factorisation properties, cf. below) the T functional in Eq. (3.11) coincides with the argument of the logarithm in Eq. (3.8).

It is useful to define a generalisation, $T(\xi)$, by exchanging the upper limit in Eq. (3.9) from E_{tot} to ξ [6]. This functional fulfils

$$T(\xi) = 1 + \int_0^{\xi}\int_0^{\xi_1}\frac{d\mathcal{A}(\xi_1)\cdot d\mathcal{A}(\xi_2)}{m_0^2}T(\xi_2) \tag{3.13}$$

and together with the four-vector valued functional ${q_T}^6$:

$$q_T(\xi) = \frac{1}{T(\xi)}\int_0^{\xi} d\mathcal{A}(\xi')T(\xi') \tag{3.14}$$

we obtain the differential equations

$$\begin{aligned} dT &= \frac{q_T d\mathcal{A}}{m_0^2}T \\ dq_T &= d\mathcal{A} - \frac{q_T d\mathcal{A}}{m_0^2}q_T \\ dq_T^2 &= 2(1-\frac{q_T^2}{m_0^2})q_T d\mathcal{A} \end{aligned} \tag{3.15}$$

They can be integrated to

$$\begin{aligned} T(\xi) &= \exp\left(\int_0^{\xi}\frac{q_T(\xi')d\mathcal{A}(\xi')}{m_0^2}\right) \\ q_T^2(\xi) &= m_0^2[1-T(\xi)^{-2}] \end{aligned} \tag{3.16}$$

Finally, we define a four-vector valued function $\mathcal{X}_\mu = \mathcal{A}_\mu - {q_T}_\mu{}^7$ so that

$$d\mathcal{X} = \frac{(q_T d\mathcal{A})}{m_0^2}q_T \tag{3.17}$$

[6] Called q in [6]
[7] Called X in [6]

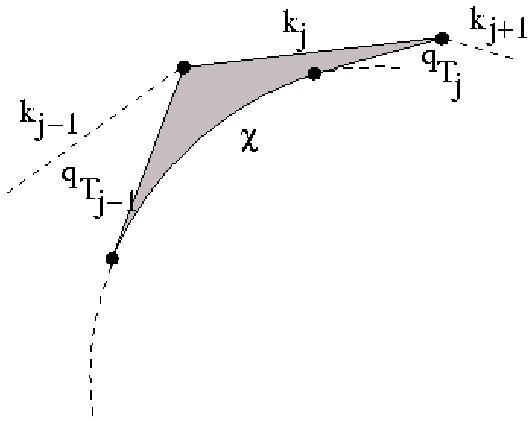

Figure 3.1: A plaquette bordered by q_{Tj}, q_{Tj+1} , k_j and a hyperbolic segment from the $\mathcal{X}$-curve, as described in the text.

i.e. the vector q_T is the tangent to the $\mathcal{X}$-curve reaching out to the directrix. From Eq. (3.16) we conclude that the functional T is the exponential of an area (note that the vector $d\mathcal{A}$ is light-like, and $q_T d\mathcal{A}$ is an area element between the directrix and the $\mathcal{X}$-curve). This area is proportional to the functional λ as mentioned in the Introduction. We also note that the vector q_T quickly reaches the length m_0. Integrating the differential equations for a directrix built up from a set of light-like vectors $\{k_j\}$ we obtain the iterative equations [6]:

$$\begin{aligned} T_{j+1} &= (1 + q_{Tj}k_{j+1}/m_0^2)T_j \equiv \frac{T_j}{\gamma_{j+1}} \\ q_{Tj+1} &= \gamma_{j+1}q_{Tj} + \frac{1+\gamma_{j+1}}{2}k_{j+1} \end{aligned} \tag{3.18}$$

The starting values are $T_0 = 1$ and $q_{T0} = k_0$.

The factorisability of the functional T means that its logarithm, λ, can be written as a sum containing one term for each k_j:

$$\lambda \equiv \sum_{j=1}^{n+1} \Delta\lambda_j = \sum_{j=1}^{n+1} \ln\left(1 + q_{Tj-1}k_j/m_0^2\right) \tag{3.19}$$

The $\Delta\lambda_j$ defined in this way is the size of a subarea just as the total λ represents the area spanned between the $\mathcal{X}$ and the directrix curves. In Fig. 3.1 we exhibit such a region bordered by the "initial" q_{Tj-1} and the "final" q_{Tj} together with a hyperbolic segment from the $\mathcal{X}$-curve and the gluon energy–momentum vector k_j from the directrix.

If we define $\gamma_0 \equiv 1$ and the vectors $k_j^{'} \equiv \frac{1}{2}k_j(1+\gamma_j)$, then it is easy to see that the vector q_{Tj} is a weighted sum of the $k_l^{'}$ vectors ($l \leq j$). The weight for any vector $k_m^{'}$ is exponentially suppressed with $\sum_{l=m}^{j-1} \Delta\lambda_{l+1}$.

To see that $\Delta\lambda_j$ as defined in Eq. (3.19) actually has the meaning of a rapidity we go to the rest frame of the vector q_{Tj-1} and assume for simplicity that it has the length m_0. Further assume that the light-like vector k_j is directed along the 3-axis with the length ω so that $\Delta\lambda_j = \ln(1+\omega/m_0)$. Then it is easy to show that the "next" q_T-vector q_{Tj} will have the light-cone coordinates along the 3-axis equal to $(m_0 \exp(\Delta\lambda_j), m_0 \exp(-\Delta\lambda_j))$, i.e. the q_T vector has been accelerated from rest to the rapidity $\Delta\lambda_j$ by "the step" k_j along the directrix. The corresponding segment of the $\mathcal{X}$-curve is a part of a hyperbola.

For sufficiently well ordered emissions and a resolution scale much smaller than the smallest transverse momentum present, the last term (Eq. (3.12)) will dominate in Eq. (3.11) and therefore $\lambda(m_0 = \frac{1}{2}k_\perp)$ will be approximately equal to $\ell(k_\perp)$ defined in Eq. (3.5).

From the definition in Eq. (3.19) it is easy to show (cf. the definition of the vectors q_{Tj} in Eq. (3.18)) that the argument in the logarithm of the $\Delta\lambda_j$ is equal to $(1+s_{j-1,j}/4m_0^2)$ plus terms down by at least a factor of γ. From the definition of the local k_t variables, Eq. (3.6), we may also conclude that

$$k_{tj}^2 < \frac{s_{j-1,j}s_{j,j+1}}{(s_{j-1,j}+s_{j,j+1})} \tag{3.20}$$

and consequently we obtain

$$\begin{aligned} \Delta\lambda_j &> \ln(\frac{s_{j-1,j}}{4m_0^2}) = \ln(\frac{s_{j-1,j}}{k_\perp^2}) \equiv \ell_{j-1,j} \\ \ln(\frac{k_{tj}^2}{k_\perp^2}) &< \min(\ell_{j-1,j}, \ell_{j,j+1}) \end{aligned} \tag{3.21}$$

This implies that there is a minimum positive value of $\Delta\lambda$, if a procedure to exclude or filter out emissions creating gluons with $k_t < k_\perp$ has been used.

3.3 The Properties of the $\Delta\lambda$ Distributions

We will now exhibit a very noticeable regularity of the dipole cascades, cf. Fig. 3.2. In this figure, we show a plot of the average number of gluons as a function of $k_\perp$, $n(k_\perp)$, versus $\ell(k_\perp)$ for e^+e^--events with $\sqrt{s} = 200$ GeV and for a range of values of $k_\perp$ from 4 down to 1 GeV. We have switched off the gluon splitting process so that we end up with one colour connected set of partons. There are several interesting properties of this plot:

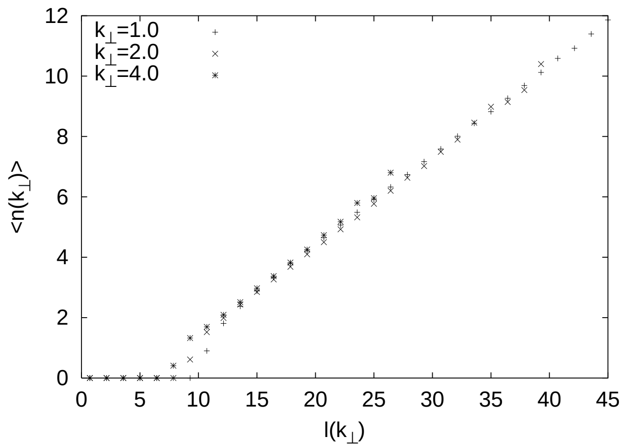

Figure 3.2: The figure shows a plot of $\langle n(k_\perp)\rangle$ versus $\ell(k_\perp)$ for an e^+e^--event with $\sqrt{s} = 200$ GeV from ARIADNE.

- There is a linear correlation between the average gluon multiplicity $\langle n(k_\perp)\rangle$ and the phase space variable $\ell(k_\perp)$ inside a very narrow band. The fact that the different lines obtained for different values of $k_\perp$ are so close to each other means that the slope of this linear correlation is rather insensitive to changes in the ordering variable in this range. It should be noted that the $\ell(k_\perp)$-distributions are widely varying for these $k_\perp$-values as we show in Fig. 3.3. We have used a running coupling (with $\Lambda_{QCD} = 0.22$ GeV, i.e. the default value in ARIADNE). The region with $\ell(k_\perp) > 20$ is mainly populated by the results from small $k_\perp$-values, $k_\perp < 2$ GeV.
- We find that the linear correlation in Fig. 3.2 is independent of the cms energy (we have used different cms energies ranging from 40 GeV and up to even 2000 GeV, though for small energies there are too few gluons emitted to allow detailed studies), cf. Fig. 3.4. Not only do we find a linear correlation at each value of cms energy (when the number of gluons is more than 2), the slope of the correlation varies rather weakly with respect to energy. This property is also not a function of the total thrust, or the presence of particularly hard emissions (e.g. gluon of $k_\perp > 7$ GeV for $\sqrt{s} = 200$ GeV). There is a minimum value of $\ell \simeq 10$, corresponding to no gluon emission (for $k_\perp = 1$ GeV and $\sqrt{s} = 200$ GeV), and there is a (small) transition region for a few more units, until the number of gluons exceeds two. But after that $dn/d\ell$ is a constant.
- As a consistency check we have used two procedures for sampling the events. It is possible to run the parton cascade in ARIADNE down to a

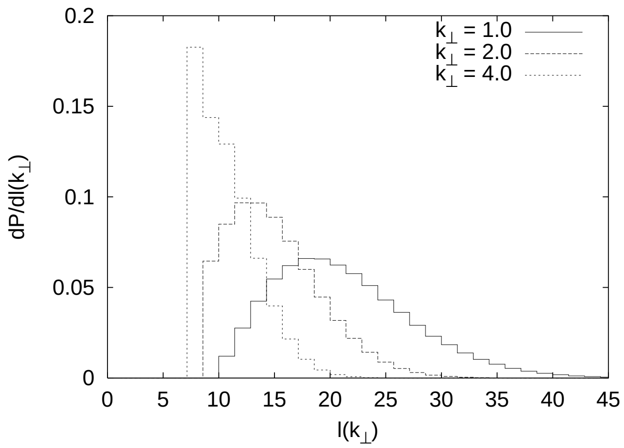

Figure 3.3: The $\ell(k_\perp)$-distribution for different $k_\perp$-values at $\sqrt{s} = 200$ GeV.

certain value of the ordering variable $k_\perp$, i.e. emit all gluons with larger $k_\perp$'s, sample the emerging directrix and investigate its properties, e.g. calculate the number of gluons emitted to that point, $n(k_\perp)$, the total length of the $\mathcal{X}$-curve, $\ell(k_\perp)$, the individual $\Delta\lambda(m_0)$'s and the local k_t's. After that we may continue the cascade for the same event down to smaller $k_\perp$-values and do the same exercise. Another possibility is to run the cascade down to a certain value $k_\perp \equiv k_{\perp cut}$ and collect a large sample of events to investigate. After this we can pick a new value of $k_{\perp cut}$ and repeat the process. The result in Fig. 3.2 does not depend upon which of the two methods for sampling the events we use.

We observe the same effect in the parton shower in PYTHIA as in ARIADNE. The ordering variable in PYTHIA is the parton virtuality Q^2, and the variable $\hat{k}_\perp^2 = z(1-z)Q^2$ (where z is the light-cone fraction taken by the emitted parton) is used as the argument for the running coupling. This is a good approximation for the transverse momentum in the case of massless parton kinematics. However, since transverse momentum itself is not the ordering variable in this case, there is no real lower limit to it. Therefore, in order to make the comparisons we filtered the events obtained from PYTHIA and combined partons such that all gluons had k_t above a certain value proportional to Q.

It is then possible to use PYTHIA to obtain an inclusive sample of $n_g(CQ)$ and $\ell(CQ)$. We just note that it is possible to tune the constant C such that, as shown in Fig. 3.5, there is the same $dn/d\ell$ as in ARIADNE. We find that $C \approx 0.5$. It is possible to switch off the coherence conditions in the parton

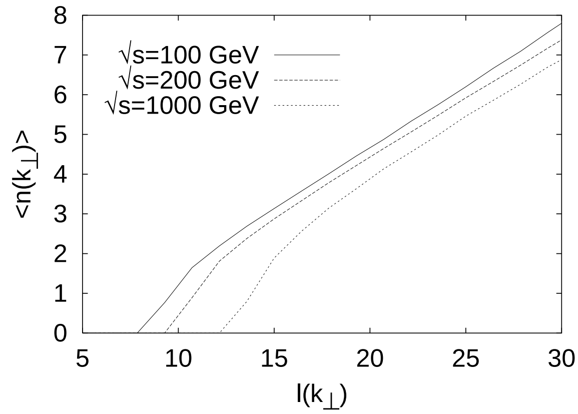

Figure 3.4: The figure shows a plot of $\langle n(k_\perp)\rangle$ versus $\ell(k_\perp)$ ($k_\perp = 1.0$ GeV) for different cms energies from ARIADNE.

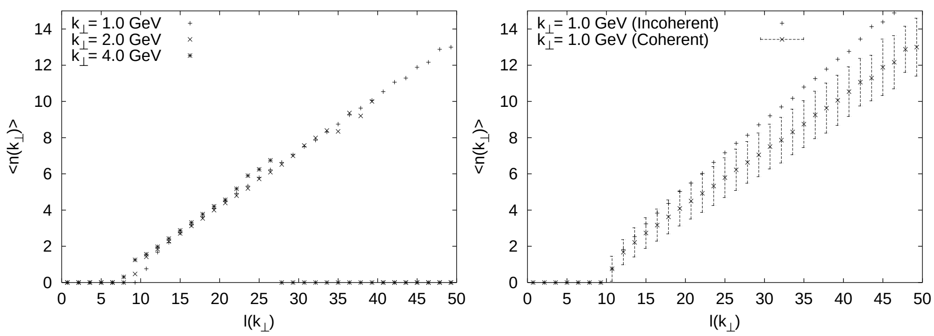

Figure 3.5: The figure to the left shows a plot of $\langle n(k_\perp)\rangle$ versus $\ell(k_\perp)$ for an e^+e^--event with $\sqrt{s} = 200$ GeV from PYTHIA. The figure to the right shows $\langle n(k_\perp)\rangle \pm \sigma$ versus $\ell(k_\perp)$ at $\sqrt{s} = 200$ GeV, $k_\perp = 1.0$ GeV for coherent and incoherent showers in PYTHIA.

shower in PYTHIA, since the strong angular ordering is implemented only after the generation using the ordering variable Q^2. We show the effect of this feature in Fig. 3.5. For the same C we obtain many more partons per unit phase space for an incoherent shower, although they still show a linear correlation to the ℓ-measure.

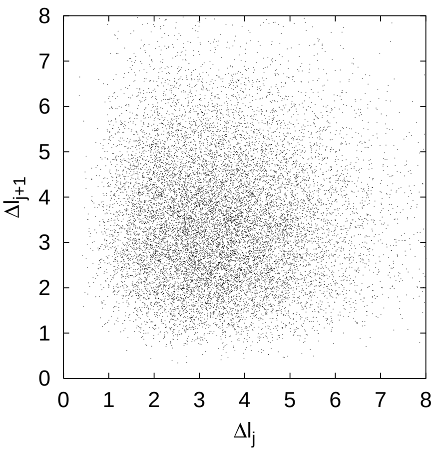

Figure 3.6: Scatter plot of two adjacent $\Delta\ell$ values

The linear relation between $\langle n\rangle$ and ℓ can be understood as follows. If one considers a variable such as ℓ defined as in Eq. (3.5) where the parts $\Delta\ell_j$ are distributed with the averages μ_j and the variances σ_j^2, then ℓ itself will mostly have a Gaussian distribution according to the central limit theorem. The average is $\bar{\mu} = \sum \mu_j$ and the variance $\bar{\sigma^2} = \sum \sigma_j^2$. The numbers $\bar{\mu}$ and $\bar{\sigma^2}$ are in general well-defined for large n unless the values of the $\Delta\ell_j$ are correlated. We find that the $\Delta\ell_j$'s indeed show very little correlation, even between adjacent dipoles, cf. Fig 3.6. We also find that the average μ_j shows only a weak dependence upon the total number of gluons in the event, n, for a wide range of n.

We will therefore go over to the investigation of the distribution of the $\Delta\ell_j$ defined in Eq. (3.5). We notice that the first and the last term in Eq. (3.5) are different from the other terms in one important aspect. They are contributions from dipoles involving a quark or an anti-quark (with different colour charges than gluons), whereas all the other terms come from purely gluonic dipoles. It turns out that the dipoles at the ends have slightly different distributions than all the rest. However, if the gluon splitting process is switched off, there are only two such dipoles in an event. This means that we can write for the average $\bar{\mu} = 2\langle\mu_{\rm q}\rangle + (n-1)\langle\mu_{\rm gg}\rangle$. In Fig. 3.4 we see this effect clearly, because it is only for $n > 2$ that we find a constant slope, i.e. when we have purely gluonic dipoles present. The properties we noted above are about variation of the number of gluons or dipoles with respect to $\ell(k_\perp)$ and the stability of the slope of the correlations, and should correspond to the properties of purely gluonic dipoles. Therefore, from now on we will not include the very first and the very

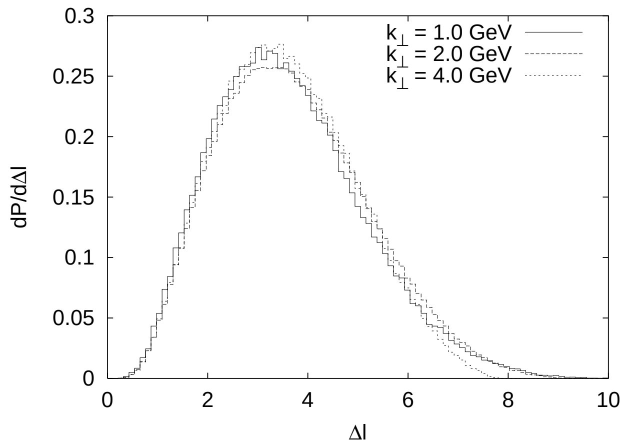

Figure 3.7: The $\frac{dP}{d(\Delta\ell)} \equiv P_\ell(\Delta\ell)$-distribution from ARIADNE.

last $\Delta\ell$-values in the investigations. We have seen that purely gluonic dipoles, irrespective of their position along the directrix, have the same distribution in size. In Fig. 3.7, we show the distribution $\frac{dP}{d(\Delta\ell)} \equiv P_\ell(\Delta\ell)$ from ARIADNE and observe that:

- The distribution P_ℓ has an average μ and a variance σ^2, consistent with the results in Fig. 3.2. We have found that it is independent of the cms energy, of the global event variables like thrust and the total ℓ-value for the event, and also of hard gluon emissions.
- The distribution P_ℓ is rather insensitive to the value of $k_\perp$. In Fig. 3.8, we show the average value of $\Delta\ell$ as a function of $\kappa \equiv \ln(k_\perp^2/\Lambda^2)$ and we find that it changes about 5 %, when the ordering variable goes from 0.8 to 3 GeV.
- There are no noticeable correlations between adjacent $\Delta\ell$'s as we have noted before. In Fig. 3.6, we show the scatter plot between two adjacent $\Delta\ell$, taken from stochastically chosen pairs in many different events. In Fig. 3.9, we show the values of the average $a(n)$ (defined as $a(n) \equiv \langle\sum_{j=1}^{n} \Delta\ell_j\rangle$), and the standard deviations around it, for chains of n connected $\Delta\ell$. For this figure the statistics was collected from events with a fixed number of gluons.
- In order to further investigate the independence of the $\Delta\ell$ values in an event we have examined events containing a fixed number (N) of gluons. We may then ask about the multiplicity distribution, $\hat{P}(N_\Delta)$, of events with N_Δ values of $\Delta\ell \leq \Delta$. We find a binomial distribution with the mean Np and

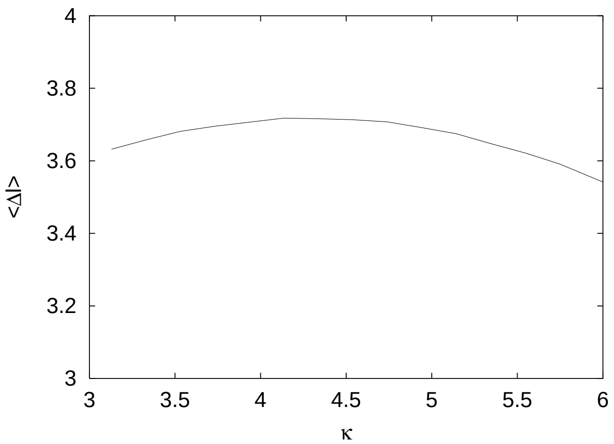

Figure 3.8: The average value of $\Delta\ell$ as a function of $\kappa \equiv \ln(k_\perp^2/\Lambda^2)$. Note that the variation in the average $\Delta\ell$ in the figure is much smaller than the width of the distribution of $\Delta\ell$ as seen in Fig. 3.7.

variance $Np(1-p)$ where $p = \int_0^\Delta dx P_\ell(x)$ as expected from uncorrelated dipoles. We have also investigated the average number of $\Delta\ell$-values, which are consecutive and satisfy $\Delta\ell \leq \Delta$. We find a geometric distribution, weighted with the average number of $\Delta\ell$ not fulfilling the condition (which is, once again, expected when we have uncorrelated dipoles). We also find that the distribution $P_{\ell n}$ obtained from the sum of the lengths of n consecutive $\Delta\ell$ is an n-fold convolution of the distribution P_ℓ.

The corresponding results in PYTHIA are very similar to the results in ARIADNE (with the appropriate choice of the constant C as discussed above). To the left in Fig. 3.10 , we show the distributions from PYTHIA and note that PYTHIA is somewhat more concentrated towards small $\Delta\ell$ values and also has a somewhat wider tail so that the average values are the same as in ARIADNE. The "incoherent" option gives a much more narrow distribution centred around smaller values, as expected.

It is also possible to investigate the distributions in terms of the λ-measure defined in Eq. (3.19). In Fig. 3.10 to the right, we show two distributions (one from ARIADNE and one from PYTHIA), to be called $P_\lambda(\Delta\lambda)$ using as before $2m_0 = k_\perp = CQ$ where m_0 is the argument of the λ-measure. Once again we find the same properties as for the distributions $P_\ell(\Delta\ell)$.

We conclude that, inside the whole region relevant to the hadronisation procedure in String Fragmentation, the partonic states are dominated by this

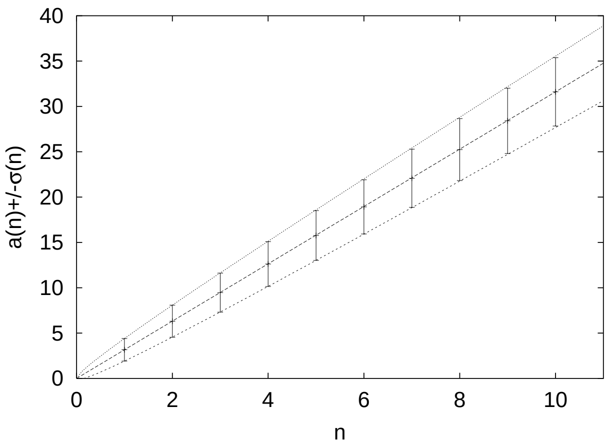

Figure 3.9: The figure shows the average $\Delta\ell$ (and the standard deviations around it) for chains of n connected $\Delta\ell$ called $a(n)$ $(a(n) \equiv \langle\sum_{j=1}^{n} \Delta\ell_j\rangle)$. The statistics is collected from events with a fixed number of gluons.

structure of independent entities. It is tempting to consider them as a kind of collective variables for the QCD force fields. The $\Delta\ell$ variables represent the local size of the dipoles between adjacent parton energy–momentum vectors, whereas the $\Delta\lambda$ values correspond to a similar although more non-local property depending upon a set of adjacent vectors.

These properties of the distributions of $\Delta\ell$'s are properties of gluonic dipoles, and result from perturbative QCD. In the next section we will make models in the LLA and the MLLA schemes based on simple gain loss considerations on the dipole cascade model, and show that it is possible to understand many qualitative features of these distributions.

The $\Delta\lambda$'s on the other hand are complicated objects, and there is no obvious way to calculate their distributions except by relying on the similarity between the λ-measure and ℓ. But the fact that there are as many $\Delta\lambda$'s as $\Delta\ell$'s, and the $\Delta\lambda$'s have parallels for each of the properties of the $\Delta\ell$'s discussed here, lead us to introduce the notion of Generalised Dipoles (GD) to be the "source" of the contributions to the $\Delta\lambda_j$'s. Whereas a dipole is spanned between two colour connected partons, a GD corresponds to one flat block or "plaquette" in the surface traced between the directrix and the $\mathcal{X}$-curve by the tangent to the $\mathcal{X}$-curve. Regularities in the properties of dipoles which are mirrored in the GD's would be passed on to the hadronised state in a hadronisation scheme based on the λ-measure, such as the one introduced in [8].

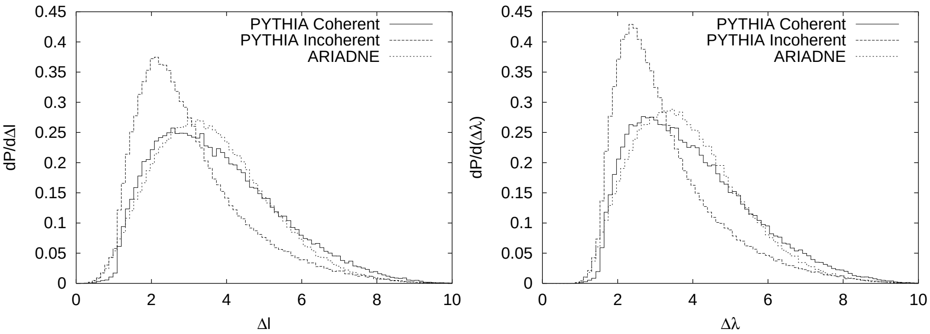

Figure 3.10: The figure to the left shows the $P_\ell(\Delta\ell)$-distribution from PYTHIA compared to the distribution obtained from ARIADNE. The figure to the right shows the corresponding plot for the $P_\lambda(\Delta\lambda)$ distribution.

3.4 Models to Describe the Dipole Distributions

3.4.1 A Simple Cascade Model

Multiplicity distributions were presented in the parton cascade formalism in [14] and in the dipole cascade formalism in [15] to leading logarithmic order. In this paper we will follow the approach presented in [16].

In order to provide a theoretical framework for our findings in the previous section, we will consider an analytical model for a dipole cascade. We will assume that there is a distribution, $f(\mu,\kappa)d\mu$, that describes the dipoles with size μ at the scale $\kappa \equiv \ln(k_\perp^2/\Lambda^2)$ (where $k_\perp$ is the ordering variable and $\mu \equiv \ln(M_d^2/k_\perp^2)$, in terms of the dipole masses M_d). We will consider the change in f when we make a small change in the scale κ. We note that $\mu+\kappa = ln\frac{M_d^2}{\Lambda^2}$ is independent of κ. If dipoles never decayed, the distribution $f(\mu,\kappa)$ would not change if $\mu+\kappa$ is kept constant as κ varies. Therefore any change in the distribution along the lines $\mu+\kappa = constant$ must purely come from decays.

There are two contributions to this. A dipole of size μ may decay into two smaller dipoles. A dipole of size bigger than μ may decay such that one of the daughter dipoles is of size μ. Gathering these terms together we get a partial integro-differential equation, cf. [16, 17], based upon Eq. 3.1 with $\alpha_{\text{eff}} = \frac{\alpha_0}{\kappa}$ for gluonic dipoles ($\alpha_0 = \frac{6}{11-2N_f/N_c}$):

$$Df \equiv \frac{\partial f}{\partial \kappa} - \frac{\partial f}{\partial \mu} = \frac{\alpha_0}{\kappa}\left[\mu f(\mu,\kappa) - 2\int_\mu d\mu' f(\mu',\kappa)\right] \tag{3.22}$$

The factor of 2 in the contribution from the larger dipoles stems from the fact that we are only considering "central" or purely gluonic dipoles here. When a gluonic dipole decays, there are 2 equivalent ways to obtain a gluonic dipole of size μ.

This integro-differential equation can be made into two coupled differential equations in terms of the first two moments of f, N_1 and N_2

$$\begin{aligned} N_j(\mu,\kappa) &= \int_\mu d\mu_1 (\mu_1)^{j-1} f(\mu_1,\kappa) \\ DN_1 &= -\frac{\alpha_0}{\kappa}(N_2 - 2\mu N_1) \\ DN_2 &= -N_1 + \frac{\alpha_0}{\kappa}\mu^2 N_1 \end{aligned} \tag{3.23}$$

For the normalisation we note that $N_1(0,\kappa)$ is the total number of dipoles available at the scale κ, to be called $\bar{n}$ in this section. $N_2(0,\kappa)$ is their combined length, to be called $\bar{\ell}$. The equations for these quantities can be obtained directly from Eqs. (3.23) in the LLA-scheme:

$$\begin{aligned} \frac{d\bar{n}}{d\kappa} &= -\frac{\alpha_0}{\kappa}\bar{\ell} \\ \frac{d\bar{\ell}}{d\kappa} &= -\bar{n} \end{aligned} \tag{3.24}$$

These equations are solvable in terms of combinations of the modified Bessel functions (cf. the next subsection) as soon as we have defined a "starting value", $\kappa_{max} \equiv L_0$, for the cascade.

In order to solve the coupled equations in Eq. (3.23), we introduce the combination $g(\mu,\kappa) = N_2 - \mu N_1$, which fulfils the equation:

$$Dg = \frac{\alpha_0}{\kappa}(\mu g) \tag{3.25}$$

with the boundary value

$$g(0,x) = \bar{\ell}(x) \tag{3.26}$$

It is related to N_1 through $N_1(\mu,\kappa) = -\frac{\partial}{\partial\mu} g(\mu,\kappa)$.

Including the boundary condition above, we obtain:

$$N_1(\mu,\kappa) = -\frac{\partial}{\partial\mu}\left\{\bar{\ell}(\mu+\kappa)\exp\left[-\int_\kappa^{\mu+\kappa} dy \frac{\alpha_0}{y}(\mu+\kappa-y)\right]\right\} \tag{3.27}$$

This is a derivative of two contributing factors. The first is $\bar{\ell}$ evaluated at $\mu+\kappa \equiv \ln(M_d^2/\Lambda^2)$, i.e. at the largest κ value where the dipole could have been produced. It is multiplied by the probability that the dipole has not decayed until κ. In field theoretical language this second contribution, the Sudakov form factor, corresponds to the sum of all the virtual corrections during the "lifetime" of the dipole. This Sudakov form factor can be easily calculated

$$S(\mu,\kappa) = \exp\left[-\int_{\kappa}^{\mu+\kappa} dy \frac{\alpha_0}{y}(\mu+\kappa-y)\right] = \frac{\exp(\alpha_0\mu)}{(1+\frac{\mu}{\kappa})^{\alpha_0(\mu+\kappa)}} \quad (3.28)$$

It fulfils

$$\begin{aligned} S(0,\kappa) &= 1 \\ \frac{\partial S}{\partial\mu}(\mu,\kappa) &= -\alpha_0 \ln(1+\frac{\mu}{\kappa})S \end{aligned} \quad (3.29)$$

The derivative vanishes at $\mu = 0$.

The distribution f is obtained by a partial differentiation of N_1, cf. Eq. (3.23)

$$f(\mu,\kappa) = -\frac{\partial N_1}{\partial\mu} \quad (3.30)$$

so that using Eqs. (3.24), (3.27) and (3.29) we obtain:

$$\begin{aligned} f(\mu,\kappa) = & [\bar{\ell}(L_0,\mu+\kappa)\alpha_0 \ln(1+\mu/\kappa)^2 + \\ & 2\bar{n}(L_0,\mu+\kappa)\alpha_0 \ln(1+\mu/\kappa)]S(\mu,\kappa) \end{aligned} \quad (3.31)$$

The result can be understood in a simple and useful way. The logarithmic factors in the parenthesis are equal to

$$\alpha_0 \ln(1+\mu/\kappa) = \int_{\kappa}^{\mu+\kappa} \frac{\alpha_0 dx}{x} \quad (3.32)$$

i.e. the probability that there will be a dipole breakup somewhere between $\mu+\kappa$, the largest virtuality where a dipole with size μ at κ can be produced, and κ, where it is found. There are two such factors multiplying all interior points in the dipoles at $\mu+\kappa$, counted by $\bar{\ell}(\mu+\kappa)$, and there is one factor multiplying twice the number of dipoles at $\mu+\kappa$ (because if there is already a dipole one can keep either its "left" side or its "right" side and produce the "other" side of the dipole with size μ by a breakup in between). Finally, the Sudakov form factor describes the probability that there is no decay affecting the existence of the dipole at κ.

In the limit when $L_0 \gg (\mu+\kappa)$, and $\mu+\kappa$ is significantly positive, the two functions $\bar{n}$ and $\bar{\ell}$ factorise and we may write in the LLA

$$\begin{aligned} \bar{n}(L_0,x) &\simeq V(L_0)(x)^{-\frac{1}{4}} \exp(-2\sqrt{\alpha_0 x}) \\ \bar{\ell}(L_0,x) &\simeq \sqrt{x/\alpha_0}\,\bar{n}(L_0,x) \end{aligned} \quad (3.33)$$

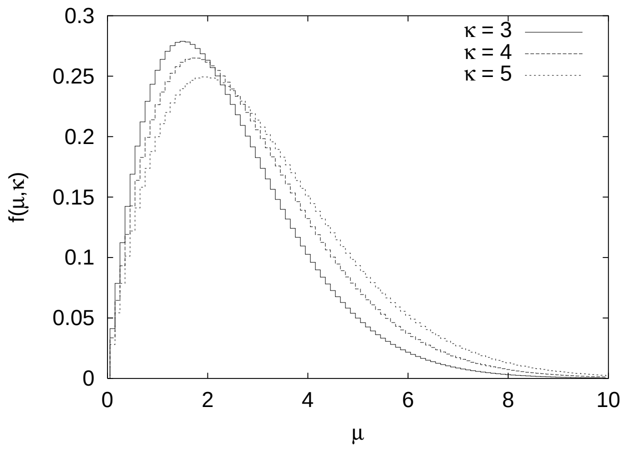

Figure 3.11: The $f_\kappa(\mu)$ function, obtained from Eq. 3.31, normalised to unity.

In Fig. 3.11, we show the function $f_\kappa(\mu)$, obtained from f in Eq. (3.31) by normalising it to unity, for a set of values of the parameter κ. There is a weak dependence upon the ordering variable κ and for large μ-values it has an essentially exponential falloff with a slope very similar to the ones we find in the distributions $P_\ell(\Delta\ell)$ and $P_\lambda(\Delta\lambda)$ in Section 3.3.

For small values of μ there are quantitative differences. The reason is that the LLA is not sufficient to describe the behaviour of small dipoles. In that case it is necessary to include both the contributions from the $(\sum_p)$ term in the dipole cross section in Eq. (3.1), and also to take into account the recoil contributions which are particularly noticeable for small dipoles. We will consider this question in the next subsection.

3.4.2 The $MLLA$ and Earlier Investigations

In the so-called Modified Leading Log Approximation, sub-leading effects from the polarisation sum are included [7, 18]. In general, the assumptions have been that the cms energy $\sqrt{s}$ (or rather its logarithm $L \equiv \ln(s/\Lambda^2)$) is very large and that the main contributions from the cascades will come from well-ordered emissions, i.e. that $k_{\perp j} \gg k_{\perp j+1}$ (at least for adjacent emissions).

Using this approximation, it is possible to write out analytical equations for the expected changes in the average ℓ (to be called $\bar{\ell}(\kappa)$) and the average n (similarly $\bar{n}(\kappa)$) for a given ordering variable $\kappa \equiv \ln(k_\perp^2/\Lambda^2)$ [7, 17, 18]:

$$\frac{d\bar{\ell}}{d\kappa} \quad = \quad -\bar{n}$$

$$\frac{d\bar{n}}{d\kappa} \quad = \quad -\alpha_{\rm eff}(\bar{\ell} - \bar{n}\delta) \tag{3.34}$$

Eqs. (3.34) are simplified versions of the Modified Leading Log Approximation (MLLA) formulae. A more elaborate treatment should include the difference between the quark and anti-quark endpoint dipoles with a different effective coupling α and a different correction δ, cf. [18], but these are small corrections if the starting value $L = \ln(s/\Lambda^2)$ is large.

The interpretation is that in a step $d\kappa$, $\bar{\ell}$ changes by $\bar{n}$ contributions from the scale change according to Eq. (3.5), just like the second line in Eq. (3.24). Further, the change in $\bar{n}$ in that step is given by the coupling times the available phase space. This phase space is given by $\bar{\ell}$ to first approximation; but there is a correction from each dipole from the term $\sum_p$ in Eq. (3.1). The polarisation sum $\sum_p \simeq 2$ near the centre of a dipole but decreases in the neighbourhood of the emitters. It has been shown [18] that the suppression of emissions because of this can be approximated by (and this is essentially the MLLA) a constant decrease in the dipole size $\delta = 11/6$ for gluonic dipoles (this number only depends upon the triple gauge boson vertex for 3 colours). In Eqs. (3.34) it is also assumed that the gluon splitting process $g \to q\bar{q}$ is neglected and therefore $\alpha_{\rm eff} \equiv \alpha_0/\kappa$ with $\alpha_0 = 6/11$ for all dipoles and not only the purely gluonic ones.

The decay of one dipole also affects the two adjacent ones due to recoils. A method to estimate this effect was suggested in [19]. Therefore an extra “loss-term” is added to the first line in Eq. (3.34):

$$\frac{d\bar{\ell}}{d\kappa} = -\bar{n} - C_r\frac{d\bar{n}}{d\kappa} \tag{3.35}$$

with a constant recoil correction estimated to be $C_r \simeq 2$.

These equations can be solved using the following combinations of the modified Bessel functions:

$$\begin{aligned} \mathcal{I}_1(x) &= \sqrt{2}x^{\gamma/2}I_\gamma(2\sqrt{\alpha_0 x}) \\ \mathcal{I}_2(x) &= \sqrt{2\alpha_0}x^{(\gamma-1)/2}I_{\gamma-1}(2\sqrt{\alpha_0 x}) \end{aligned} \tag{3.36}$$

and similarly for $\mathcal{K}_1$ and $\mathcal{K}_2$ in terms of the exponentially falling Bessel function K. Note that they are normalised so that

$$\mathcal{I}_1(x)\mathcal{K}_2(x) + \mathcal{I}_2(x)\mathcal{K}_1(x) = x^{\gamma-1} \tag{3.37}$$

and that there are simple differential relations between them:

$$\begin{aligned} \frac{d\mathcal{I}_1}{dx} &= \mathcal{I}_2(x) \\ \frac{d\mathcal{I}_2}{dx} &= \frac{\alpha_0}{x}\mathcal{I}_1(x) + \frac{(\gamma-1)}{x}\mathcal{I}_2(x) \end{aligned} \tag{3.38}$$

Similar relations hold for the exponentially falling modified Bessel function pair $(\mathcal{K}_1, -\mathcal{K}_2)$.

If we start the cascade at a large value of $L \equiv \ln(s/\Lambda^2) \gg \kappa$ we obtain, with the boundary values $\bar{\ell} = 0$ and $\bar{n} = 1$ at L, the results:

$$\begin{aligned} a &= L^{1-\gamma}\left[C_r \mathcal{K}_2(L) - \mathcal{K}_1(L)\right] \\ b &= L^{1-\gamma}\left[C_r \mathcal{I}_2(L) + \mathcal{I}_1(L)\right] \\ \bar{n} &= b\mathcal{K}_2(\kappa) - a\mathcal{I}_2(\kappa) \\ \bar{\ell} + C_r \bar{n} &= a\mathcal{I}_1(\kappa) + b\mathcal{K}_1(\kappa) \end{aligned} \tag{3.39}$$

using the notations $\gamma = 1 + \alpha_0(\delta + C_r)$.

It is difficult to obtain an analytically solvable partial integro-differential equation corresponding to Eq. (3.22). The method of moments runs into difficulties because the variation in the $\sum_p$ term in the cross section (Eq. (3.1)) affects the integral contribution, i.e. the gain from the decays of larger dipoles, in such a way that the equations for the first few moments are no longer independent of higher moments. Therefore, we will directly go over to the solution in Eq. (3.31) instead, and modify the ingoing terms according to the MLLA, keeping in mind the interpretation given there.

We assume that each dipole of size μ can decay only in the interior excluding a region $\delta/2$ on each extreme. Then the effective phase space at $(\mu + \kappa)$ in Eq. (3.31) is changed from $\ell(\mu + \kappa)$ into $[\ell(\mu + \kappa) - \delta \cdot n(\mu + \kappa)]$. A dipole of size μ is produced by a breakup first at a point $\kappa = \kappa_1$ and then at $\kappa_2 < \kappa_1$. The region where the "no emission probability" is to be calculated in the Sudakov form factor is changed in the MLLA, first by a loss of $\delta/2$ at κ_1 and then by a loss of a further $\delta/2$ at κ_2.

$$\begin{aligned} S_{\kappa_1,\kappa_2} &= \exp\left(-\int_{\kappa}^{\kappa_2} \frac{\alpha_0 dz(\mu + \kappa - \delta - z)}{z}\right) \times \\ &\quad \exp\left(-\int_{\kappa_2}^{\kappa_1} \frac{\alpha_0 dz(\mu + \kappa - \delta/2 - z)}{z}\right) \times \\ &\quad \exp\left(-\int_{\kappa_1}^{\mu+\kappa} \frac{\alpha_0 dz(\mu + \kappa - z)}{z}\right) = \\ &= \left(\frac{\kappa_1 \kappa_2}{\kappa^2}\right)^{\frac{\alpha_0 \delta}{2}} S(\mu, \kappa) \end{aligned} \tag{3.40}$$

where $S(\mu, \kappa)$ is the Sudakov form factor without the term δ as given in Eq. (3.28). Since this is a function of κ_1 and κ_2 now, we obtain, for the contribution to $f(\mu, \kappa)$ from situations where both gluons involved in a dipole are emitted below $\mu + \kappa$, the result:

$$f_1 \equiv 2(\bar{\ell} - \delta\bar{n})(\mu + \kappa) \int_{\kappa}^{\mu+\kappa} \frac{\alpha_0 d\kappa_1}{\kappa_1} \int_{\kappa}^{\kappa_1} \frac{\alpha_0 d\kappa_2}{\kappa_2} S_{\kappa_1,\kappa_2}$$

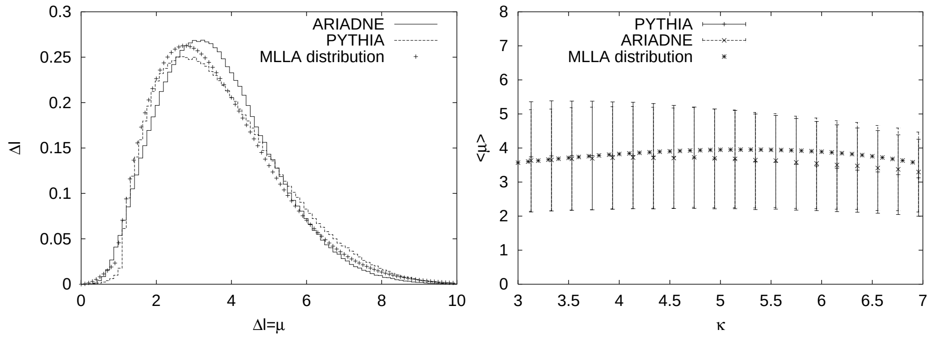

Figure 3.12: The figure to the left shows the distribution $f_\delta(\mu,\kappa)$, obtained from the MLLA approach at $k_\perp = 1GeV$, compared with the $P_\ell(\Delta\ell)$ distribution from ARIADNE and PYTHIA (cf. Fig. 3.10). The figure to the right shows the average value of μ as a function of κ, from the same distribution $f_\delta(\mu,\kappa)$. In the figure to the right, we also compare with the average value of ℓ (cf. Eq. (3.21)) as a function of κ obtained from ARIADNE and PYTHIA, and we also include the standard deviation in the result from PYTHIA and ARIADNE. This result is obtained using $\alpha_0 = 0.7$ and $C_r = 2$ in the MLLA distribution as explained in the text.

$$= \quad (\bar{\ell} - \delta\bar{n})(\mu+\kappa)\frac{4\left((1+\mu/\kappa)^{\frac{\alpha_0\delta}{2}} - 1\right)^2}{\delta^2} S(\mu,\kappa) \qquad (3.41)$$

The fact that the first break may be either on the "left" or on the "right" side contributes a factor of 2 in the above equation .

In the same way, for the second contribution related to the number of dipoles at $\mu+\kappa$, ie the situations where only one gluon involved in a dipole is produced below the scale $\mu+\kappa$, we obtain,

$$f_2 = \theta(\mu - \delta/2)\bar{n}(\mu+\kappa)\frac{4\left((1+(\mu-\delta/2)/\kappa)^{\frac{\alpha_0\delta}{2}} - 1\right)}{\delta} S(\mu-\delta/2,\kappa) \quad (3.42)$$

In this case there can never be a breakup until the dipole size has at least reached $\delta/2$, because one of the end points is already fixed at the virtuality $\mu+\kappa$.

We note for consistency that the result $f_\delta \equiv f_1 + f_2$ has the limit f in Eq. (3.31) when δ vanishes. In Fig. 3.12, we show the result of this $MLLA$ version of the dipole size distribution. We have used a fixed value $\delta = 11/6$ but we have allowed the parameters α_0 and C_r vary. The reason for allowing α_0 to vary is that it is feasible to shut off the gluon splitting process in Ariadne, but the running coupling will always receive contributions from the different number of "active" flavours at different virtualities. From the figure to the left, we conclude that it is in between the distributions from Ariadne and Pythia for the central dipoles when we use $\alpha_0 = 0.70$ (i.e. for three to four active flavours), and $C_r = 2$ (according to [19]). This result is rather insensitive to C_r and it can therefore not be used as a test for the claims in [19]. We have also checked the dependence upon the ordering variable. In Fig. 3.12 to the right, we show that f_δ also exhibits a slow change of its average value as a function of the (relevant) ordering variable like the Ariadne and Pythia P_ℓ distributions.

3.5 Concluding Remarks

The number of gluons emitted *above* a certain value of the ordering variable shows an interesting linear correlation (with Gaussian fluctuations) with the phase space available at that scale. We have called the phase space variable the ℓ-measure in this paper to distinguish it from the λ-measure, which is an infrared stable generalisation of the ℓ-measure, useful in the context of hadronisation.

Both these quantities are functions of not only the resolution scale ($k_{\perp cut}$ for a dipole cascade, Γ_0 in string fragmentation), but also of the precise geometry of the state under consideration. Therefore they change with every new gluon emitted in the system.

The resolution parameter relevant for hadronisation is a parameter fixed by the break-up properties of the string and the mass spectrum of the hadrons produced. The λ-measure is constructed in such a way that addition of gluons at transverse momenta much smaller than the scale Γ_0 does not change its value. In that way it is infrared stable.

However, since the resolution parameter for the ℓ-measure is the transverse momentum of the gluon to be emitted, the transverse momenta of all gluons already emitted must be higher in an ordered dipole cascade. Therefore, the only kind of infrared stability relevant for this measure would be the stability, when the ordering variable, which is also the resolution parameter, is small. Technically this is not the case. However, since in this approach we will never compute phase space available at a value of the ordering variable below the Λ_{QCD}, there is an effective infrared stability for the phase space, if all local transverse momenta k_{tj} are required to be above $k_\perp$. It is easily shown that the mass of any dipole with a gluon at one end is greater than the transverse momentum k_t of that gluon, which in turn, will be greater than Λ_{QCD}. Besides, we must remember that it is kinematically not possible for dipoles of mass smaller than $2\Lambda_{QCD}$ to emit gluons above Λ_{QCD}.

The two measures discussed here are quite strongly related. If one keeps only the last (often the dominant) term in the argument of the logarithm in the λ-measure, one gets an expression very similar to the ℓ-measure.

The linear correlation between the ℓ-measure and the number of gluons is a direct consequence of the following facts that we have demonstrated. The ℓ-measure is the sum of a series of terms $\Delta\ell_j$, one for each dipole. A given $\Delta\ell_j$ is the contribution from one particular dipole to the ℓ-measure, and is in some sense the "size" of that dipole. There are two kinds of dipoles. The first kind involves either the quark or the anti-quark energy–momentum. The second kind involves only the gluon energy–momenta. These two kinds of dipoles have different distributions in sizes.

It turns out that the size of the dipoles do not show any significant correlations. Therefore the ℓ-measure of a state consisting of a certain number of dipoles, which is just the sum of the corresponding $\Delta\ell_j$'s, is distributed like the sum of several independent random variables, i.e. like a Gaussian with a mean that is the sum of the means of the individual independent distributions. This shows up as a linear correlation between the number of partons and the ℓ-measure.

More interesting than the linear relation is the stability of the slope of these lines, which represents the number of gluons per unit phase space, with respect to changes in global event parameters like cms energy or thrust and even with changes in the ordering variable. It seems that parton cascades tend to form structures at one (relative) size when sizes are measured with the ℓ-measure with a resolution parameter proportional to the ordering variable. As we go down in the ordering variable, the running coupling should increase the number of emissions per unit phase space. However, the phase space variable itself scales appropriately to effectively absorb any increase of emissions per unit phase space.

We have also made another observation in this paper. Just like the ℓ-measure, the λ-measure can be thought of as a sum of terms $\Delta\lambda_j$, one for each vector along the directrix in colour order. Out of the two vectors involved in a particular $\Delta\lambda_j$, only one is a vector along the directrix. The other vector, in a sense a cumulative variable, is a weighted average of the vectors k_i's along the directrix with $i < j$.

It is interesting that all the properties of the ℓ-measure we have discussed here are also reflected in the λ-measure. There is a similar linear correlation to the number of gluons, similar lack of correlation among adjacent terms and similar stability with respect to change of global event variables and the ordering variable. Partitioning the λ-measure into a series of $\Delta\lambda_j$'s corresponds to partitioning the surface spanned between the directrix and the $\mathcal{X}$-curve into a series of "plaquettes" or flat regions along the directrix. Each plaquette is spanned between a parton energy momentum vector k_j, a vector q_{Tj-1} (weighted average of k_i's along the directrix with $i < j$), another vector q_{Tj} and a hyperbolic section of the $\mathcal{X}$-curve. The size of the plaquette $\Delta\lambda_j$ is the length of the section of the $\mathcal{X}$-curve, and is determined by k_j and q_{Tj-1}. Since these plaquettes share so many properties with dipoles, we will call them "Generalised Dipoles".

We note in passing that the possibility of partitioning the contributions to the λ-measure as contributions from connected flat regions has an interesting consequence for the fragmentation of a string according to the Lund model area law. When formulated as a process along the directrix [8, 21], string fragmentation is closely related to the λ-measure and the $\mathcal{X}$-curve. Particle production in this scheme can be thought of as partitioning the plaquettes mentioned here into smaller plaquettes, one for each hadron. Since the hadron energy–momenta will mostly come from these flat regions in the string, particles stemming from one GD will have energy–momenta aligned in a plane in Minkowski space, up to transverse momentum fluctuations. We have found such chains of particles and examined their properties. These chains, which we will call "coherence chains" are important for the study of Bose Einstein correlations in the Lund Model for multi-gluon systems, which we will elaborate on in a forthcoming publication.

We have also presented here an analytical model for the observations we have made about dipoles, in the LLA and MLLA schemes. There are limitations to this approach, since complications such as the polarisation sum make it very difficult to obtain differential equations which can be solved analytically. Nevertheless, our analysis based on simple gain-loss considerations broadly reproduces the qualitative features of the observations.

Acknowledgements

We would like to thank G. Gustafson, T. Sjöstrand and L. Lönnblad for helpful discussions. This work was completed by S. Mohanty and F. Söderberg, about two months after the untimely death of our collaborator Bo Andersson.

References

[1] G. Gustafson, U. Pettersson *Nucl. Phys.* **B306** (1988) 746.

[2] L. Lönnblad, *Computer Phys. Commun.* **71** (1992) 15.

[3] G. Corcella, I.G. Knowles, G. Marchesini, S. Moretti, K. Odagiri, P. Richardson, M.H. Seymour and B.R. Webber *J. High Energy Phys.* **0101** (2001) 010.

[4] T. Sjöstrand, P. Edén, C. Friberg, L. Lönnblad, G. Miu, S. Mrenna and E. Norrbin, *Computer Phys. Commun.* **135** (2001) 238.

[5] X. Artru, *Phys. Rept.* **97** (1983) 147.

[6] B. Andersson, G. Gustafson and B. Söderberg, *Z. Phys.* **C20** (1983) 317.

[7] Yu.L. Dokshitzer, V.A. Khoze, A.H. Mueller and S.I. Troyan, Basics of Perturbative QCD (Edition Frontières 1991).

[8] B. Andersson, S. Mohanty and F. Söderberg, *Eur. Phys. J.* **C21** (2001) 631.

[9] B. Andersson, G. Gustafson, P. Dahlqvist, *Nucl. Phys.* **B328** (1989) 76.

[10] G. Gustafson and A. Nilsson, *Z. Phys.* **C52** (1991) 553.

[11] Ya.I. Azimov et al. *Phys. Lett.* **B165** (1985) 147.

[12] L. Lönnblad, hep-ph/0112284.

[13] B. Andersson, P. Dahlqvist and G. Gustafson, *Z. Phys.* **C44** (1989) 455;*Z. Phys.* **C44** (1989) 461.

[14] Yu.L. Dokshitzer, V.S. Fadin, V.A. Khoze, *Z. Phys.* **C15** (1982) 325; A. Bassetto, M. Ciafaloni, G. Marchesini, A.H. Mueller, *Nucl. Phys.* **B207** (1982) 189.

[15] B. Andersson, P. Dahlqvist and G. Gustafson, *Phys. Lett.* **B214** (1988) 604.

[16] B. Andersson , *Nucl. Phys.* **B360** (1991) 109.

[17] B. Andersson, The Lund Model, (Cambridge University Press 1998).

[18] G. Gustafson, *Nucl. Phys.* **B392** (1993) 251; G. Gustafson, M. Olsson, *Nucl. Phys.* **B406** (1993) 293.

[19] P. Edén, G. Gustafson, *J. High Energy Phys.* **09** (1998) 015.

[20] B. Andersson, Closing talk for the XXXI International Symposium on Multiparticle Dynamics, Datong, China, Sep 2001.

[21] B. Andersson, *Acta Phys. Polonica B* **32** (2001) 3993.

Coherence Chains and Bose-Einstein Correlations in the Lund Model

Paper IV

LU TP 03-08
March 2003

Coherence Chains and Bose-Einstein Correlations in the Lund Model

Sandipan Mohanty[1]
Fredrik Söderberg[2]
Department of Theoretical Physics, Lund University.
Sölvegatan 14A, S-223 62 Lund, Sweden.

Abstract We extend an interference based approach for the analysis of Bose-Einstein Correlations in the Lund model to incorporate an approximate treatment of the correlations for general multi-gluon states.

[1]sandipan@thep.lu.se
[2]fredrik@thep.lu.se

4.1 Introduction

The fragmentation process in which the coloured partons are transformed into colourless hadrons is not understood from first principles, and therefore we have to rely on models for a description. The Lund string fragmentation model [1, 2, 3] is one such model, in which the dynamics of colour connected partons is modelled by proposing a string-like force field between a quark and an anti-quark with the emitted gluons as internal excitations along the string field. The probability for the formation of a set of hadrons from a given set of partons is given by what is known as the area law. The model can be formulated as a stochastic iterative process, and is therefore well suited for a Monte Carlo implementation. One such implementation is the well-known PYTHIA event generator [4].

For a state without gluons, the surface spanned by the string in space-time will be a (1+1)-dimensional plane. In general, for a multi-gluon string the surface will be a curved (1+1)-dimensional surface embedded in (1+3) dimensions. Calculating the energy-momenta of the hadrons according to the area law is rather difficult in this case. PYTHIA handles multi-gluon states according to the method presented in [5]. It has been found that this procedure fulfils the area law in an average sense but not on an event to event basis.

We have presented a paper [6] where we introduced a model for fragmenting a multi-gluon state, which fulfils the area law at every single step, at the price of small fluctuations introduced into the string state during hadronisation. The ideas presented in [6] have been developed and implemented in a Monte Carlo fragmentation program called ALFS [7]. In particular the effect of limited phase space for small cms energies have been introduced (effectively) through an energy dependent fragmentation function which differs for small invariant masses from the standard Lund model formula used in PYTHIA.

In the first part of this paper (section 4.4), we will make use of ALFS to study a set of properties of the hadronic state that are noticeable already in the analysis of the perturbative QCD parton cascades as we presented them in [8]. We learned that the multi-gluon states obtained from the parton cascades can be subdivided into a set of independent entities, that we called Generalised Dipoles (GDs) in [8]. The GDs are linked together along the colour field and they have certain properties which are independent of the total energy and global event variables such as thrust. Moreover, the sizes of the GDs relative to the cut-off scale (used to define the end of the partonic cascades) is remarkably stable against changes in the cut-off scale. In the first part of this paper, we will show that it is possible to define a set of corresponding quantities from the fragmentation process which we will call Coherence Chains (CC). In the second part of the paper we will use the idea of Coherence Chains to formulate a model for Bose-Einstein correlations for general multi-gluon states.

The CCs are defined by the property that, up to small transverse momentum fluctuations, the particle energy-momenta all belong to a plane, just as the particles stemming from the fragmentation of a simple string state without any interior gluonic excitations. In other words, we will show that the fragmentation of a multi-gluon state in our model resembles the linked fragmentation of many planar string regions.

In order to study the qualitative properties of CCs we will assume one common mass for all kinds of hadrons. In the applications in the second part of the paper, we will naturally include the full mass spectrum and the decay of resonances.

We will show that the hadron multiplicity distributions from the Coherence Chains, for a maximum allowed transverse momentum, are independent of the total energy and of global event variables such as thrust. We find that the only difference between the events is the occurrence of a different number of CCs. The number of Coherence Chains in an event depends upon the so-called λ-measure that was introduced in [9, 10] to describe the phase space available for hadron formation in multi-gluon states. The larger the energy and/or the gluonic activity, the larger is the available range of the λ-measure and the number of CCs.

In the second part of this paper, we will use the CCs to introduce a model for Bose-Einstein correlations in multi-gluon events. This model is a generalisation of the investigation in [11, 12], in which the Bose-Einstein effect for string states without gluons were studied. The Lund model is based on semi-classical approximations and classical probability concepts. This ignores possible interference effects due to the underlying quantum mechanical processes. In [11, 12] an amplitude was introduced that reproduces the area law and also gives rise to interference effects when there are identical bosons in the final state. The origin of the interference effect is the fact that identical hadronic states can be obtained with the hadrons ordered in different ways along the string. We will call these different "configurations" and they will give separate contributions to the production amplitude for this hadron state. The resulting interference effect was introduced in the Monte Carlo by an event weight.

It turns out that symmetrisation of the final state emerging out of the fragmentation of a string with gluonic excitations is much more complicated than for systems without gluons. We will make use of the proposed form for the matrix element in [11, 12] in our approach, and we will also use the concept of an event weight. In this case, there are severe constraints which limit the alternative configurations of identical particles in the final state, allowed by the string fragmentation model. Configurations which correspond to the exchange of two particles produced in two different planar regions of the string, are either impossible or highly suppressed. In the approximation presented here, we will only take into account exchange of particles in the same planar region.

As we will show in the first part of the paper, an event can be subdivided into a set of Coherence Chains, where all momenta of the particles are nearly aligned in a plane, and this partitioning of the event is insensitive to very soft gluons. The Coherence Chains therefore describe the string regions over which interference effects between identical particles would be considered.

We will develop this scheme in the second part of this paper and show that the CCs stemming from the Generalised Dipoles in coherent perturbative cascades are sufficiently large so that the ensuing distributions show an enhancement for the probability for small momentum differences between identical bosons. We will be satisfied with a study of the hadronisation properties of events stemming from e^+e^--annihilation and the ensuing bremsstrahlung, defined by the perturbative QCD cascades.

In subsection 4.2, we will briefly describe the features of the fragmentation of the multi-gluon states according to [6, 7] and in subsection 4.3 the properties of the Generalised Dipoles according to [8]. In section 4.4, we will define the Coherence Chains and exhibit their properties. In section 4.6, we introduce our BEC model based upon the Coherence Chains and study the correlations arising among the identical pions. We end with a set of concluding remarks in section 4.7.

PART I: Introduction to Coherence Chains

4.2 The Lund Area Law Applied to Multi-gluon States

In the Lund string model a colour flux tube is assumed to stretch between the partons at the end of the parton cascades. This colour field is approximated by a massless relativistic string with a constant energy-density [1, 2, 3].

When a quark and an anti-quark move apart, they are assumed to stretch a string-like field between them. Consequently, they will lose energy to the string. After a given time, they lose all their energy and are pulled back towards each other. The ensuing motion is periodic.

If the energy stored in the string is large enough, formation of $q\bar{q}$-pairs along the string becomes possible and the string will break into smaller string pieces. A q from one such break-up point ("vertex") together with a $\bar{q}$ from an adjacent vertex along the string field form a hadron (on mass shell) composed of the pair and the field in between. Transverse momentum is generated at these string break-up vertices as described in [13]. The energy-momentum contained in the string piece between the two adjacent vertices and the transverse momenta carried by the quark and the anti-quark add to make the energy-momentum of the particle formed.

Therefore, the hadronisation process can be modelled by a break-up of the original string into smaller string pieces, each describing a hadron with a given energy-momentum. The probability for the production of a set of n hadrons with energy-momenta $\{p_\alpha\}$ with total energy-momentum P_{tot} is given by the area law [1, 2, 3]:

$$dP_n(\{p_\alpha\}; P_{tot}) \propto \tag{4.1}$$
$$\propto \left(\prod_{\alpha=0}^{n-1} N_\alpha d^4 p_\alpha \delta(p_\alpha^2 - m_\alpha^2) \right) \delta(\sum_{\alpha'=0}^{n-1} p_{\alpha'} - P_{\text{tot}}) \exp(-bA) \exp(-\frac{1}{2\sigma^2} \sum_{\beta=0}^{n} k_{\perp\beta}^2)$$

Here A is the area spanned by the string before it decays, and $k_{\perp\alpha}$ are the transverse momenta generated at the vertices where the string breaks. (We assume that transverse momentum is conserved at every breakup vertex. A model where transverse momentum is only conserved within a finite range in rapidity was discussed in [18].) In order to describe the break-up of a string with internal gluonic excitations, it will be useful to consider string motion in a little more detail.

The surface spanned by a string (which does not break) during one period is a minimal surface which means that the surface is completely determined by its boundary curve. This boundary curve, a four-vector valued curve $\mathcal{A}$, is usually called the directrix. The position of an arbitrary point $X(t, \sigma)$ on the surface of the string (open string; parametrised by time t and the energy σ between the quark end point and the point X) is related to the directrix $\mathcal{A}(t)$ in the following way.

$$X(t, \sigma) = \frac{1}{2} [\mathcal{A}(t + \sigma) + \mathcal{A}(t - \sigma)] \tag{4.2}$$

The function $\mathcal{A}(t)$ has the following periodicity and symmetry properties for a string which starts at a single point at time $t = 0$:

$$\begin{aligned} \mathcal{A}(t + 2E) &= \mathcal{A}(t) + 2P_{\text{tot}} \\ \mathcal{A}(-t) &= -\mathcal{A}(t) \end{aligned} \tag{4.3}$$

We see from Eq.(4.2) and Eq.(4.3) that the string surface is described by a left moving and a right moving wave, which bounce at the endpoints. The directrix of a string stretched between a certain set of partons is obtained by laying out the energy-momenta of the quark, the gluons and the anti-quark in colour order.

The minimal area nature of the string world surface also means that properties of hadrons created during string fragmentation are stable against small perturbations on the boundary, i.e. that the model is infrared stable.

We have recently derived a process for fragmenting a multi-gluon string state into final state hadrons in accordance with the Lund model area law [6]. As the directrix completely determines the string state we have chosen to present the fragmentation of a multi-gluon string state as a process along the directrix.

In the case of a flat string, the Lund fragmentation process typically results in a state like the one drawn in Fig.4.1 to the left. This figure shows the vertices where new $q\bar{q}$-pairs are produced and the corresponding vertex vectors $\{x_\alpha\}$. The momenta of the produced hadrons, $\{p_\alpha\}$, are also shown in this figure. This process can be formulated in terms of the directrix in a way which can be generalised to strings with gluonic excitations.

In [6], we formulated an iterative process along the directrix to describe string fragmentation. We defined (abstract) dynamical variables called "vertex vectors" x_α. These variables would correspond to true space-time locations for production of quark anti-quark pairs if the string had no gluonic excitations. Each particle energy-momentum vector p_α is constructed as a linear combination of a vertex vector x_α and a certain section of the directrix k_α. The same pair of vectors x_α and k_α also determines the next vertex vector $x_{\alpha+1}$.

$$\begin{aligned} p_\alpha &= z_\alpha x_\alpha + \frac{1}{2}\left(1 - \frac{z_\alpha^2 x_\alpha^2}{m_\alpha^2}\right) k_\alpha \\ x_{\alpha+1} &= (1 - z_\alpha) x_\alpha + \frac{1}{2}\left(1 + \frac{z_\alpha^2 x_\alpha^2}{m_\alpha^2}\right) k_\alpha \end{aligned} \tag{4.4}$$

Since with this construction, $x_\alpha + k_\alpha = p_\alpha + x_{\alpha+1}$, we associate a "plaquette" bounded by these four vectors with the particle indexed α, cf. Fig.4.1 to the right. Each of the vectors x_α is shared between two plaquettes, and hence production of a set of hadrons from a given string or directrix means construction of a set of connected plaquettes along the directrix in this model. The initial value x_0, for the series of vertex vectors, is taken to be the first segment of the directrix. The numbers z_α are related to the area of the plaquettes, and are required to be distributed according to the following distribution, in order that the construction of plaquettes would be weighted according to the area law:

$$f(z)dz = N\frac{dz}{z}(1-z)^a \exp\left(-\frac{bm^2}{z}\right) \tag{4.5}$$

After the selection of z_α and hence a properly distributed area for the plaquette, the size of k_α is chosen so that the plaquette does indeed have that area.

The distribution in Eq.(4.5) is called the Lund symmetric fragmentation function. It can be derived from the area law in Eq.(4.1) in the limit of large centre of mass energies. The effective fragmentation function, which is used in ALFS, is however energy dependent, and reduces to the above in the limit of large energies [7].

There is a one-to-one correspondence between the areas of the plaquettes constructed in this way and certain areas which can be associated with the

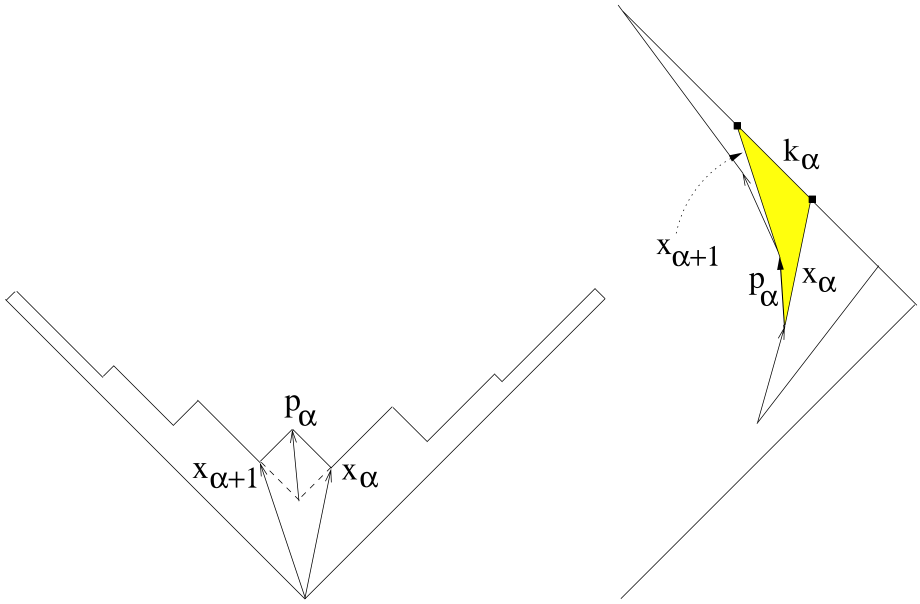

Figure 4.1: The figure to the left shows a typical Lund string break-up for a string state without gluons. The figure to the right shows the corresponding plaquette bordered by x_α, $x_{\alpha+1}$, p_α and a segment from the directrix k_α, as described in the text.

production of individual hadrons in the string fragmentation model without gluonic excitations. Therefore, the sum of the areas of the plaquettes which is also the area between the directrix and the "hadronic curve"[3], i.e. the curve obtained by placing the hadron energy-momenta one after the other in rank order, could be used as the area in the Lund model area law. Therefore, the area law on the whole event can be implemented by weighting the construction of each plaquette according to its area, which amounts to choosing the variables "z_α" in Eq.(4.4) according to the Lund symmetric fragmentation function and selecting k_α's of the appropriate sizes.

In connection with the plaquette building process in Eq.(4.4) one observes that the vertex vectors contain a memory of the earlier partonic energy-momenta in the iteration process, and hence along the directrix.

The gluon corners pose a problem because the generated z_α value implies a value of the area of the plaquette which does not fit in the space between the hadronic curve and the directrix around the gluon corner. In [6], we solved

[3]The hadronic curve was called the X-curve in [6]

this problem by modifying the directrix locally around the gluon corners. We found that the required distortions of the directrix only have small and local implications on the string state because the string surface is a minimal surface.

The model described above is implemented in the Monte Carlo simulation program ALFS [7] and we will make use of this program in the investigations of the Coherence Chains in section (4.4). We will come back to the hadronisation process in subsection 4.4, but before that we will discuss some properties of the parton cascades relevant to the present investigation, in section 4.3.

4.3 The Generalised Dipoles

The Generalised Dipoles were introduced in [8]. In this section, we will recapitulate some of their properties, since there is a close resemblance between the Generalised Dipoles and the Coherence Chains defined later in this paper.

Two different phase space measures were discussed in [8], the λ-measure and the ℓ-measure. They are both strongly related to the Generalised Dipoles, but they were originally introduced for different purposes.

1. The quantity we called the ℓ-measure in [8] was introduced in [15]. In the dipole model, the available phase space for gluon emission, ℓ, in the Leading Log Approximation (LLA) [14] and in the Modified Leading Log Approximation (MLLA) [14] schemes is a sum of a series of terms, $(\Delta\ell)_\alpha$, one for each pair of colour-connected partons, i.e. each pair of consecutive vectors along the directrix [15]. These terms are contributions to the phase space from individual dipoles in the Dipole cascade model [15]. The phase space for the emission of a gluon with transverse momentum $k_\perp^2$, from a system of n_g gluons can be expressed as:

$$\ell \quad = \quad \sum_{\alpha=0}^{n_g} (\Delta\ell)_{\alpha,\alpha+1} = \sum_{\alpha=0}^{n_g} \ln\left(\frac{s_{\alpha,\alpha+1}}{k_\perp^2}\right) = \ln \prod_{\alpha=0}^{n_g} \left(\frac{s_{\alpha,\alpha+1}}{k_\perp^2}\right), \quad (4.6)$$

   i.e. as a sum over the contributions from the partonic dipoles. $s_{\alpha,\alpha+1}$ is defined as $(\mathcal{A}_\alpha + \mathcal{A}_{\alpha+1})^2$.

2. The λ-measure was introduced in [9] as a generalised rapidity range for measuring the hadronic phase space. In [8] we noted that it can be subdivided into a set of parts called $\Delta\lambda$, with interesting properties. Every $\Delta\lambda$ contribution is built up from one parton energy-momentum vector, $\mathcal{A}_{\alpha+1}$, and from one more abstract vector, ${q_T}_\alpha$[4], according to the recursive formula below:

$$\lambda \equiv \sum_{\alpha=0}^{n_g} \Delta\lambda_\alpha = \sum_{\alpha=0}^{n_g} \ln\left(1 + \frac{q_{T\alpha}\mathcal{A}_{\alpha+1}}{m_0^2}\right) \quad (4.7)$$

[4] The vector q_T was called q in the original paper [9]

$$
\begin{aligned}
q_{T\alpha+1} &= \gamma_{\alpha+1} q_{T\alpha} + \frac{1+\gamma_{\alpha+1}}{2}\mathcal{A}_{\alpha+1} \\
\gamma_{\alpha+1} &\equiv \frac{1}{1+q_{T\alpha}\mathcal{A}_{\alpha+1}/m_0^2} \\
q_{T0} &= \mathcal{A}_q
\end{aligned}
\tag{4.8}
$$

The λ-measure is infrared stable and it is insensitive to gluons with $k_\perp$ small compared to m_0. However, if the scale m_0 is smaller than the smallest $k_\perp$, then there is a similarity between λ and ℓ. Thus we found in [8] that $\lambda(m_0 = \frac{1}{2}k_\perp) \approx \ell(k_\perp)$. The $\Delta\ell$'s are contributions from the parton-parton dipoles to the total ℓ-measure, whereas the $\Delta\lambda$'s are more abstract quantities.

In [8], we found that the $\Delta\ell$ and the $\Delta\lambda$ distributions have the following properties.

- The distribution $\frac{dP}{d(\Delta\ell)} \equiv P_\ell(\Delta\ell)$ is independent of the cms energy and of global event variables such as thrust and the total ℓ value. It is also independent of presence of particularly hard gluon emissions in the event.

- The distribution $P_\ell(\Delta\ell)$ is rather insensitive to the value of $k_\perp$.

- There are no correlations between adjacent $\Delta\ell$'s

- All the above properties of the ℓ-measure are also reflected in the λ-measure. There are as many $\Delta\lambda$'s as $\Delta\ell$'s in an event. Therefore, just as $\Delta\ell$ measures the size of colour dipoles, we introduced the concept of Generalised Dipoles as the abstract entities whose size would be represented by $\Delta\lambda$.

It is possible to give a geometrical picture of the Generalised Dipoles. In the Lund string fragmentation model, for a string with no gluonic excitations, the hadrons are produced along a hyperbola [1, 2, 3] on the average. For a string with gluonic excitations, the hadrons are produced along a set of connected hyperbolae along the directrix [9, 10], called the χ-curve[5] in [8]. The λ-measure is related to the length of the χ-curve and it is also proportional to the area spanned between the χ-curve and the directrix [9]. Subdividing the λ-measure according to Eq.(4.7) means that we subdivide this area into smaller "plaquettes" very similar to the ones that we defined in subsection 4.2. These plaquettes are bordered by q_{T_α} and $q_{T\alpha+1}$, a hyperbolic segment of the χ-curve and a parton energy-momentum vector from the directrix.

These properties of the GDs will have important implications for the fragmentation products of the string as we will see in the next section.

[5]The χ-curve was called the x-curve in the original paper [9]

4.4 The Coherence Chains

In this section, we will define and examine the Coherence Chains (CC). For simplicity, we will use a single hadron mass in this study. The idea is to look for "planar" regions in the space of the final state particle energy-momenta.

4.4.1 The Definition of a Coherence Chain

Let us consider a final state, obtained from our fragmentation model, described by means of an X-curve containing the hadron energy-momenta $\{p_\alpha\}$ laid out in rank-order. By a "planar region" we will mean a rank-connected subset of hadron energy-momenta (excluding hadronisation transverse momenta) denoted $p_{l\alpha}, p_{l\alpha+1}, \ldots, p_{l\alpha+n-1}$ which can be written as a linear combination of an "initial" vertex vector x_α and the sum of the corresponding directrix pieces $\{k_j\}$ together with a small transverse component $\delta(\alpha, n)$, which satisfies $\delta \cdot x_\alpha = \delta \cdot K = 0$:

$$\begin{aligned} K(\alpha,n) &= \textstyle\sum_{j=\alpha}^{\alpha+n-1} k_j \\ P(\alpha,n) \equiv \textstyle\sum_{j=\alpha}^{\alpha+n-1} p_{lj} &= u(\alpha,n)x_\alpha + v(\alpha,n)K(\alpha,n) + \delta(\alpha,n) \end{aligned} \tag{4.9}$$

Due to the facts that $P(\alpha,n), K(\alpha,n)$ and x_α are time-like or light-like vectors the remainder $\delta(\alpha,n)$ must be space-like (or vanishing). We define the set of rank-connected hadrons as a Coherence Chain $CC(n,\delta^2)$ of length n and size δ^2 ($\delta^2 > 0$) if:

$$\begin{aligned} -\left[\delta(\alpha,n)\right]^2 &\leq \delta^2 \\ -\left[\delta(\alpha,n+1)\right]^2 &> \delta^2 \end{aligned} \tag{4.10}$$

It is easy to find an iterative procedure to find the $CC(n,\delta^2)$ from the fragmentation products. We start on a hadron energy-momentum vector and the corresponding vertex vector (for this situation the first condition in Eq.(4.10) is trivially satisfied according to Eq.(4.4)). We then add the energy-momentum vector of the next hadron in rank order and check the resulting $\delta(\alpha,n)^2$-value and continue until the first relation in Eq.(4.10) fails. After that we start on the next hadron and repeat the procedure to obtain the next chain.

Especially for small values of δ^2, the event will contain a set of hadrons which cannot be connected to any of their neighbours in rank. We will call them "solitaires". They can be thought of as $CC(1,\delta^2)$, but we will exclude them in the following investigation of the Coherence Chains, because they contain just one hadron each, and the concept of a "chain" is better formulated with more than one element. For a given value of δ^2, the procedure above will subdivide each fragmentation event into a set of $CC(n,\delta^2)$ with different values of n and we will now consider the properties of these objects.

4.4.2 The Properties of the Coherence Chains

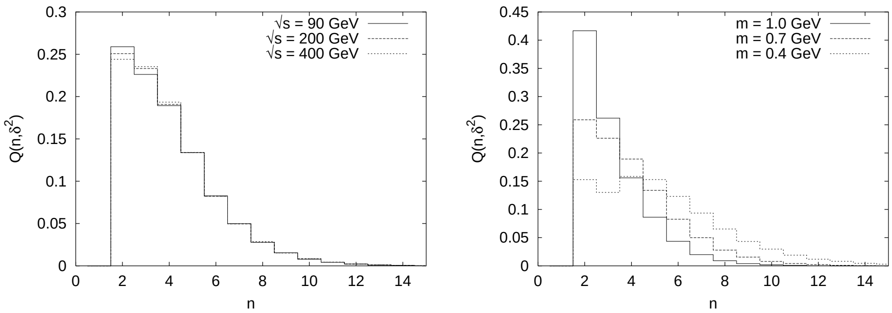

Figure 4.2: The figure to the left shows the $Q(n, \delta^2)$ distribution for different $\sqrt{s}$ values. A single hadron mass of $m = 0.7$ GeV has been used for this result. The figure to the right shows the $Q(n, \delta^2)$ distribution for different values of the common mass at $\sqrt{s} = 90$ GeV. Both the plots are obtained using $\delta^2 = 0.10$ GeV^2.

A Coherence Chain has a length (multiplicity) given by n and a (transverse) size given by δ^2. We will first keep δ^2 fixed and examine the dependence of the multiplicity on different event variables, and after that we will study the dependence upon δ^2.

We consider multi-gluon events, obtained e.g. from the Ariadne Monte Carlo implementation of the Dipole Cascade Model [16], and hadronise the strings using Alfs. After hadronisation we trace all the Coherence Chains in the final states. From an inclusive sample of such events, we determine the distribution $Q(n, \delta^2)$, of the hadron multiplicity n inside Coherence Chains. The resulting distributions are shown in Fig.4.2 and we note the following properties.

- The distribution $Q(n, \delta^2)$ is almost independent of the energy of the event. The distribution Q does, however, depend upon the hadron mass value used. Besides these two properties, we have also found that the distribution is insensitive to the presence of gluons with particularly high transverse momenta in the events. Moreover, it is independent of global event variables such as thrust, sphericity etc.

- The multiplicity of hadrons (n_1, n_2) in two adjacent Coherence Chains are independent of each other. Fig.4.3 shows $\langle n_2 \rangle$ for different values of n_1. As a further check of the independence, we have examined the distribution of

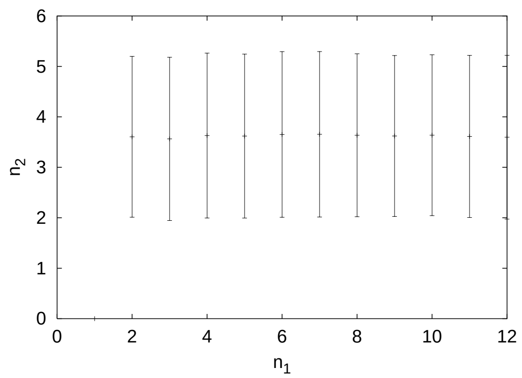

Figure 4.3: The figure shows $\langle n2 \rangle$ versus $n1$ for $\sqrt{s} = 90$ GeV, $m = 0.7$ GeV and $\delta^2 = 0.10$ GeV^2. The error-bars indicate the standard deviation.

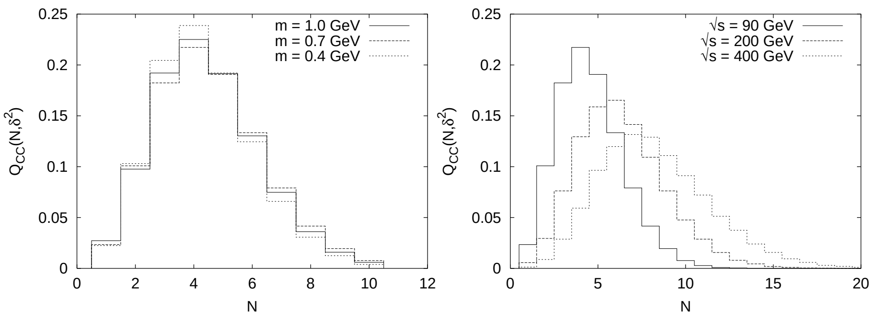

Figure 4.4: The figure to the left shows the $Q_{CC}(N, \delta^2)$ distribution at $\delta^2 = 0.10$ GeV^2 and $\sqrt{s} = 90$ GeV for different (common) mass values. The figure to the right shows the $Q_{CC}(N, \delta^2)$ distribution for different values of $\sqrt{s}$ obtained using a single hadron mass of 0.7 GeV.

$CC(n, \delta^2)$ with $n \leq r$ in the individual events. If we chose events with a chain multiplicity N we find a binomial distribution with the mean value Np using $p = \sum_1^r Q(j, \delta^2)$ and a variance $Np(1-p)$ (which is expected if there is no correlation).

The distribution of the number N, of Coherence Chains in a single event, to be called $Q_{CC}(N, \delta^2)$ has the following properties.

- The energy dependence of the distribution is shown in Fig.4.4. At high energies more CCs tend to form.

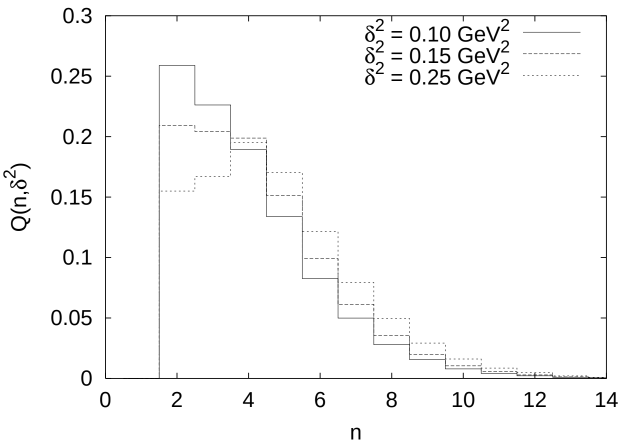

Figure 4.5: The figure shows the distribution $Q(n, \delta^2)$ for different values of δ^2. $\sqrt{s} = 90$ GeV and $m = 0.7$ GeV.

- In Fig.4.4, we show the distribution $Q_{CC}(N, \delta^2)$ for different values of the hadron mass. We find that the distribution is almost independent of the hadron mass.
- The distribution depends upon the total λ measure for the event but for a given value of λ_{tot} it is independent of the energy, the global event variables and of the number of "hard" gluon emissions.

These properties are similar to those found in connection with the Generalised Dipoles in [8], as described in subsection 4.3. In the next subsection, we will investigate the connection between these two concepts.

4.4.3 The Correlation Between the Coherence Chains and the Generalised Dipoles

We will see in the next section that the CCs play an important role in connection with Bose-Einstein correlations in multi-gluon events. In our model for the Bose-Einstein correlations, they roughly describe how far coherent interference effects extend among the final state hadrons. String fragmentation, as noted earlier, is infrared stable, i.e. many properties of the final state of hadrons are stable against introduction of very soft gluons. The process of hadronisation resolves the partonic state on the scale of hadron masses. Similarly, the parameter δ^2, since it affects which particles are included in a chain, could be interpreted as a resolution parameter relevant for Bose-Einstein correlations,

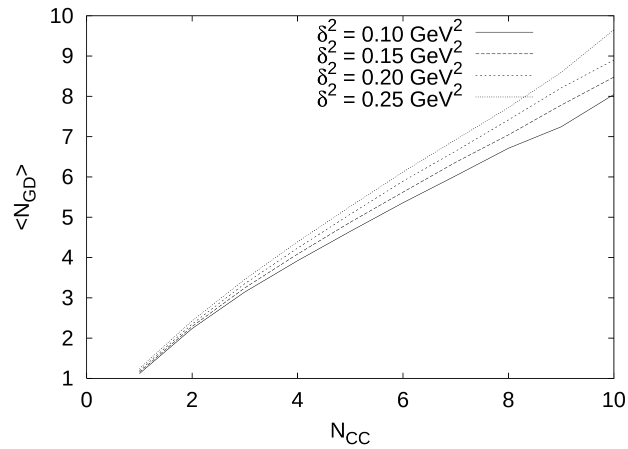

Figure 4.6: The figure shows the average number of Generalised Dipoles ($\langle N_{GD}\rangle$) vs the number of Coherence Chains (N_{CC}) in an event for different values of δ^2. The result is obtained using $m = 0.7$ GeV and $\sqrt{s} = 90$ GeV.

and an optimal value for it could be fixed from experimental data. In Fig.4.5, we show how the $Q(n, \delta^2)$ distribution varies with δ^2. When δ^2 is larger, we see that longer Coherence Chains tend to form. In Fig.4.6 we show the average number of Generalised Dipoles present in an event as a function of the number of Coherence Chains detected for different values of δ^2. This shows that for larger values of δ^2, there are more dipoles for every Coherence Chain, but the number of dipoles per chain is always close to 1.

Every partonic state is composed out of a set of Generalised Dipoles that define planar regions by means of the (initial) q_T-vector $q_{T\alpha}$ and the corresponding directrix vector $\mathcal{A}_{\alpha+1}$. In principle such a region would decay just as a flat string, i.e. there will be a set of hadrons produced inside that plane, which would be subsequently grouped into a Coherence Chain.

However, the introduction of fragmentation transverse momenta in the process diffuses the relationship between the Coherence Chains and the Generalised Dipoles. Also, in the string fragmentation model in ALFS, there is a special procedure to create plaquettes around gluon corners. Since it is normally not possible to fit a planar plaquette weighted with its area in the region between the X-curve and the directrix around gluon corners, the directrix is slightly modified around these corners. Two plaquettes are created with their k vectors not exactly parallel to the local segments of the directrix. Therefore, the two resulting plaquette planes are not aligned with the rest of the plaquettes formed away from the gluon corners. Since the k vectors in the plaquettes are normally sections of the directrix, the procedure around gluon corners is equivalent to slight local deformations of the original directrix on the scale of hadron masses. Normally, this means that our process for finding Coherence Chains using Eq.(4.10) marks the end of a chain around these corners. If this happens, the two particles around each gluon corner may be labelled as solitaires, or with smaller chances, form a chain of two particles themselves.

For a soft gluon very often the deformations are so small that one or both of the particles formed with the corner crossing procedure are incorporated into the Coherence Chain. This in itself introduces fluctuations in the total number of CCs detected. If there are only one or two particles with plaquettes which have their k vectors aligned with a gluon energy-momentum vector, they can be "gobbled up" by a bigger Coherence Chain comprising of neighbouring hadrons.

Thus, it is reasonable that the number of CCs is correlated with the number of GDs, and that the correlation is not strictly one-to-one. Since δ^2 is the maximum allowed transverse momentum for a new particle to be included in a CC, the larger its value, the more likely it is that a Coherence Chain will extend beyond a corner crossing and include hadrons from more than one GDs. The effect would be a reduction of the total number of CCs in the event and an increase of the average number of particles in a CC, and that is precisely what is seen in Fig.4.5 and Fig.4.6.

PART II: The Coherence Chains and Bose-Einstein Correlations

It has been shown that Bose-Einstein correlations (BEC) could be introduced into the Lund model as a coherent interference effect [12]. In this approach, it is construed that the Lund model area law, derived using classical probability concepts, stems from an underlying quantum mechanical amplitude. For the production of a system of hadrons containing several identical bosons, one obtains a set of contributions to the amplitude, corresponding to different ways of permuting the final state momenta among the identical particles. The treatment in [12] was restricted to Bose-Einstein correlations for hadrons formed from a string without gluons. The hadronisation procedure in ALFS and the existence of Coherence Chains allows an extension of the model to multi-gluon strings. We present here this approach to model the BEC.

4.5 The Bose-Einstein Effect: Flat Strings

4.5.1 Notation and Preliminaries

Consider the decay of a string into a set of n hadrons in the Lund model. This requires $n-1$ vertices along the string where $q\bar{q}$ pairs are produced. Each hadron is composed out of a quark from one vertex and an anti-quark from a neighbouring vertex. The hadrons, which contain the initial quark or anti-quark stretching the string, need only one more break-up along the string for their formation, but we associate two imaginary vertices with the original q and $\bar{q}$, and place them at the turning points of those particles. Thus every hadron can be viewed as if it was produced between two vertices, which gives us $n+1$ vertices in total.

We will use the following convention for numbering particles and vertices. Particle properties such as energy-momenta, can be numbered from 1 to n according to the rank order of the particle; or from 0 to $n-1$ so that p_0 would refer to the energy-momentum of the first rank particle etc. We will use this latter convention of numbering elements in a sequence in this paper. Thus, we have a set of (n) hadrons:

$$\begin{aligned} \{h_\alpha | \alpha \in [0, n-1]\} \\ \text{with energy-momenta} \\ \{p_\alpha | \alpha \in [0, n-1]\} \\ \text{whose creation is associated with plaquettes} \\ \{P_\alpha | \alpha \in [0, n-1]\} \\ \text{formed between vertices} \\ \{v_\alpha | \alpha \in [0, n]\} \end{aligned} \tag{4.11}$$

Given a rank-ordered set of n hadron energy-momenta, we will show that it is possible to determine the $(n-1)$ intermediate vertices and the n plaquettes involved in the production process. The two imaginary vertices associated with the initial $q\bar{q}$ pair are assumed to be known, and they define the string plane.

We let $(p_{l\alpha}, p_{\perp\alpha})$ denote the longitudinal[6] and transverse components of the hadron energy-momentum vector relative to the plane of the string (or local planar region in a gluonic string). Further, let $k_{\perp\alpha}$[7] denote the transverse momentum generated at the vertex v_α in the string break-up process.

Every plane in Minkowski space, which contains a time like vector, has two light-cone directions. If we identify one of them as the positive and the other

[6]We define the "longitudinal component" of a general four-vector with respect to a plane in Minkowski space as its component in that plane.

[7]The vector $k_{\perp\alpha}$, defined in connection with transverse momentum generation, is not the transverse component of k_α which is defined in connection with Eq.(4.4).

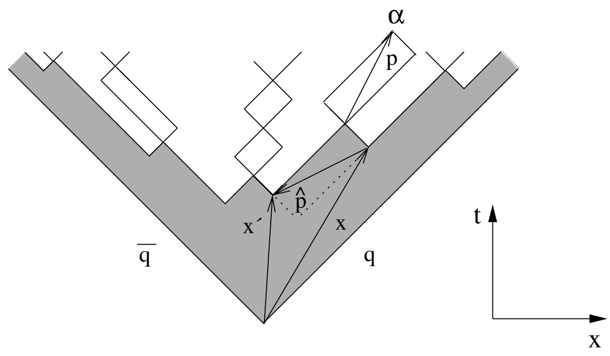

Figure 4.7: The figure shows the fragmentation of a flat string. The longitudinal momentum vector of a hadron $p_\alpha \equiv p$ and its dual vector $\hat{p_\alpha} \equiv \hat{p}$ is shown. The dual vector correspond to the difference between the two vertices involved in the creation of the hadron.

as the negative light-cone direction, the vectors $p_{l\alpha}$ could be specified in terms of the components $(p^+_{l\alpha}, p^-_{l\alpha})$ along the light-cones. We define a dual vector to $p_{l\alpha}$ through its components as $\hat{p}_\alpha = (-p^+_{l\alpha}, p^-_{l\alpha})$. It follows that:

$$\begin{aligned} \hat{p}_\alpha \cdot p_{l\alpha} &= 0 \\ \hat{p}^2_\alpha &= -p^2_{l\alpha} = -(m^2_\alpha + p^2_{\perp\alpha}) = -m^2_{\perp\alpha} \end{aligned} \tag{4.12}$$

One could alternatively define $\hat{p}_\alpha$ in terms of the properties in Eq.(4.12). These would determine the vector up to a sign, since we demand that it is a vector in the string plane like the longitudinal momentum. The sign ambiguity is equivalent to the ambiguity in naming one light-cone direction as positive and the other as negative. An iterative string fragmentation algorithm allows a straight forward identification of one light-cone direction as positive and another as negative. In Fig.4.7, which shows the fragmentation of a flat string, it is easy to see that the dual to the longitudinal momentum vector introduced above would correspond to the difference between the two vertices involved in the formation of the particle.

$$\hat{p}_\alpha = x_{\alpha+1} - x_\alpha \tag{4.13}$$

This relation can then be applied to the "plaquette" associated with the formation of the particle labelled α. Eq.(4.4) and Eq.(4.13) give:

$$\hat{p}_\alpha = k_\alpha - p_{l\alpha} \tag{4.14}$$

This vector satisfies all the defining properties of $\hat{p}_\alpha$ outlined above. Eq.(4.14) then helps identify the negative light-cone direction in the plane of the plaquette with the direction of k. With this background, it is easy to see the following:

Property 1 *Once (i) the string plane (ii) the energy-momentum of a particle, and (iii) the starting vertex (both vertex vector and vertex transverse momentum) for a plaquette are specified, the plaquette is completely determined.*

The vector $\hat{p_\alpha}$ can be constructed from the light-cone components of p_α. We can then find the remaining information for the plaquette, i.e. $x_{\alpha+1}$ from Eq.(4.13), k_α from Eq.(4.14) and $k_{\perp\alpha+1}$ from the following relation:

$$k_{\perp\alpha+1} = k_{\perp\alpha} + p_{\perp\alpha} \tag{4.15}$$

If $\hat{k}$ is a known light like vector, the above can be schematically represented as follows:

$$v_\alpha \oplus p_\alpha \to (v_{\alpha+1}, k_\alpha) \text{ when } (k_\alpha \cdot \hat{k} = 0) \tag{4.16}$$

Therefore, given a starting vertex vector x_0, a vertex transverse momentum $k_{\perp 0}$ and a set of hadrons with momenta as in Eq.(4.11), it is possible to reconstruct the entire set of plaquettes completely.

$$\begin{aligned} k_{\perp 1} &= k_{\perp 0} + p_{\perp 0} \\ k_{\perp 2} &= k_{\perp 1} + p_{\perp 1} = k_{\perp 0} + p_{\perp 0} + p_{\perp 1} \\ \ldots &= \ldots \\ k_{\perp\alpha} &= k_{\perp 0} + \sum_{\beta=0}^{\alpha-1} p_{\perp\beta} \end{aligned} \tag{4.17}$$

$$\begin{aligned} x_1 &= x_0 + \hat{p}_0 \\ x_2 &= x_1 + \hat{p}_1 = x_0 + \hat{p}_0 + \hat{p}_1 \\ \ldots &= \ldots \\ x_\alpha &= x_0 + \sum_{\beta=0}^{\alpha-1} \hat{p}_\beta \end{aligned} \tag{4.18}$$

For later reference we note the following:

Property 2 *If the plaquettes* $[0,\ldots,n-1]$ *are known to have the property* $k_\alpha \cdot k_\beta = 0$ *for* $\alpha, \beta \in [0, n-1]$*, the vectors* x_n *and* $k_{\perp n}$ *reconstructed like in Eq.(4.17) and Eq.(4.18) are independent of the order of the particles* $[0,..,n-1]$.

The intermediate vertices $[1,\ldots,n-1]$ on the other hand, have different vectors $(x_\alpha, k_{\perp\alpha})$ associated with them. Therefore, the area under these vertices and the Gaussian suppression factor for the transverse momenta in the reconstructed vertices will depend on the order of the particle energy-momenta in the reconstruction process.

4.5.2 The Amplitude

The area law in Eq.(4.1) has a formal resemblance to a quantum mechanical transition probability. It is the product of the final state phase space and a factor which can be interpreted as the square of a matrix element in a quantum mechanical calculation [11, 12]:

$$dP \propto \prod_{\alpha=0}^{n-1} d^4 p_\alpha \delta(p_\alpha^2 - m_\alpha^2) \delta(\sum_{\alpha'=0}^{n-1} p_{\alpha'} - P_{tot}) \times |\mathcal{M}|^2 \tag{4.19}$$

An amplitude which would yield the area law was discussed in [12]:

$$\mathcal{M} = \exp\left[(i\frac{1}{2\kappa} - \frac{b}{2})A - \frac{1}{4\sigma^2} \sum k_{\perp\alpha}^2 \right] \tag{4.20}$$

Here κ is the string constant (phenomenologically $\kappa \simeq 0.2$ GeV^2), $b \simeq 0.7$ GeV^{-2} and $\sigma \simeq 0.3$ GeV is the size of hadronisation transverse momentum fluctuations. The area is evaluated in energy-momentum space using light cone coordinates. The expression in Eq.(4.20) is motivated by the fact that the action for the (non-breaking) relativistic string is given by κ times the invariant area spanned by the string. Thus $\frac{ib}{2}A$ can be interpreted as an imaginary part of the action, responsible for the break-up of the string.

Suppose two hadrons labelled a and b occurring at rank orders (indices) α and β are identical particles. We could reconstruct another set of vertex vectors and transverse momenta by using these particles in interchanged rank orders, in the procedure outlined in subsection 4.5.1. The vertices $[0, \ldots, \alpha]$ and $[\beta+1, \ldots, n]$ will be unaffected by this change, and in fact all the properties of the plaquettes $[0, \ldots, \alpha-1]$ and $[\beta+1, \ldots, n-1]$ will be unaffected by this permutation. However, the vertices $[\alpha+1, \ldots, \beta]$ and the plaquettes $[\alpha, \ldots, \beta]$ may be changed, and therefore the total area of these plaquettes and the transverse momentum suppression factor calculated for these vertices would add up to different values after the exchange.

The exchanged configuration of vertices is a valid alternative way the string could have fragmented to give rise to exactly the same set of hadrons. The amplitude for that alternative process would depend on the area under the reconstructed vertices and the new transverse momentum suppression factor. We illustrate this in Fig.(4.8), where we show that the amplitude of the initial configuration and the exchanged configuration will involve different areas. Since the probability for the formation of the final state is the square of the total amplitude, and there are two possible contributions for the generation of the final hadron state from the same initial parton state, one should add these two contributions and square the sum. This would give rise to an interference term. Since the Monte Carlo implementations of the Lund model are built

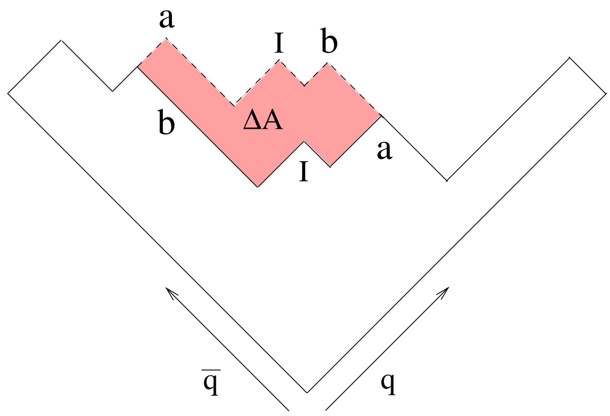

Figure 4.8: The figure shows the decay of a string state with the identical bosons a and b produced with the intermediate state I in between them. The string state drawn with dashed lines is another production possibility (configuration), since the bosons a and b are identical. Each configuration will contribute to the amplitude, and the interference term can be parametrised by the area difference between the two configurations, ΔA, as described in the text.

upon classical probability concepts they will only take into account the squared amplitudes of individual configurations. The effect of the interference term could be introduced as an event weight which would associate a total probability of $|(\mathcal{M}_1 + \mathcal{M}_2)|^2$ with the direct and exchanged configurations together, rather than just $(|\mathcal{M}_1|^2 + |\mathcal{M}_2|^2)$.

The alternative or exchanged configuration of vertices giving rise to the same set of final state hadrons is an allowed set of vertices, and it will occur during a Monte Carlo simulation naturally according to its own probability. The total probability for the hadronic state has to be split between these two configurations. If there are several alternative configurations, the total amplitude is to be calculated by summing over all possible permutations of identical particles, and the squared amplitude is to be split between all those permuted configurations. There is no unique prescription for the weight that should be associated with any one of these configurations as long as the correct total probability is assigned to the ensemble of configurations which can be obtained by a permutation of identical particles in a generated event. One form of event weight was suggested and used in [12]:

$$w_P = 1 + \sum_{P' \neq P} \frac{2Re(\mathcal{M}_P \mathcal{M}^*_{P'})}{|\mathcal{M}_P|^2 + |\mathcal{M}_{P'}|^2} \tag{4.21}$$

For reasons which will be elaborated upon in section 4.6.3, we deemed this choice of event weight unsuitable for our purposes, and instead chose the following event weight:

$$w_P = \frac{|\sum_{P'} \mathcal{M}_{P'}|^2}{\sum_{P'} |\mathcal{M}_{P'}|^2} \tag{4.22}$$

We note that unlike the weight in Eq.(4.21), the above weight partitions the total probability for the production of a certain set of hadrons into individual configurations of identical bosons in such a way that each configuration is re-weighted by the same factor. We also note that the weight in Eq.(4.22) is manifestly positive definite. We discuss this choice and its implications further in section 4.6.3. In the next section, we present our method to calculate this weight for a given event.

4.5.3 Calculation of the Event Weight

The calculation of the event weight in Eq.(4.22) involves an estimation of the amplitude contributions corresponding to all possible rearrangements of the identical particles in the event. If $\mathcal{M}_0$ is the amplitude term corresponding to a generated event, and $\mathcal{M}_1$ is the amplitude term of another configuration of identical bosons in the generated event, we have

$$\mathcal{M}_1 = \mathcal{M}_0 \exp\left[(i\frac{1}{2\kappa} - \frac{b}{2})\Delta A - \frac{1}{4\sigma^2}\Delta \sum k_{\perp\alpha}^2\right] \tag{4.23}$$

where $\Delta f \equiv f(configuration\ 1) - f(configuration\ 0)$. We note that the dependence on the transverse momenta relies on the assumption that $k_\perp$ must be exactly conserved in every break-up. This could however be modified if $k_\perp$ is only conserved within a finite rapidity range [18].

The amplitudes $\mathcal{M}_{P'}$ can all be expressed in terms of the amplitude of the generated event, the area differences and the difference of summed up squared transverse momenta. We observe that the amplitude of the original event will cancel between the numerator and the denominator in Eq.(4.22). Thus

$$w_p = \frac{|1 + \sum_{P' \neq P} S \cdot \exp\left((i\frac{1}{2\kappa} - \frac{b}{2})\Delta A - \frac{1}{4\sigma^2}\Delta \sum k_{\perp\alpha}^2\right)|^2}{1 + \sum_{P' \neq P} |S \cdot \exp\left((-\frac{b}{2})\Delta A - \frac{1}{4\sigma^2}\Delta \sum k_{\perp\alpha}^2\right)|^2} \tag{4.24}$$

In Eq.(4.24) we have also included a factor S in front of all the amplitudes. This factor depends on the spin of the particles being exchanged. If the particles being symmetrised are spin 1 particles, they should be treated as indistinguishable states only if they are in the same spin state. Since we do not keep track of the spin of the particles in this analysis, we consider them as identical with a probability of $\frac{1}{3}$. When two fermions are exchanged in an alternative configuration, the amplitudes should be added with an additional negative sign, and this can be included through this spin factor. When multiple particles appear at exchanged ranks in an alternative configuration, the spin factor is calculated appropriately, i.e. it receives a contribution of -1 for an odd permutation of identical fermions, 1 for an even permutation of the same, 1 for any permutation of scalar bosons and vector bosons which are regarded as being in the same spin state.

For the lowest non-trivial order of permutations, in which only one pair of identical particles are exchanged in ranks the terms ΔA and $\Delta \sum k_{\perp\alpha}^2$ can be shown to be:

$$\begin{aligned} \Delta A &= -2(p_{l\beta} - p_{l\alpha}) \cdot \left[x_\beta - x_{\alpha+1} + \frac{1}{2}(\hat{p}_\alpha + \hat{p}_\beta) \right] \qquad (4.25) \\ \Delta \sum_{\alpha'=\alpha}^{\beta+1} k_{\perp\alpha'}^2 &= \Delta \sum_{\alpha'=\alpha+1}^{\beta} k_{\perp\alpha'}^2 \\ &= (\beta-\alpha)(p_\beta - p_\alpha)^2 + 2(p_\beta - p_\alpha) \cdot \left(\sum_{\alpha'=\alpha+1}^{\beta} k_{\perp\alpha'} \right) \end{aligned}$$

where identical particles with indices α and β ($\alpha < \beta$) are exchanged to form the exchanged configuration of vertices.

For a general permutation, ΔA and $\Delta \sum k_{\perp\alpha}^2$ can be expressed according to the following formulae. Given that $\{e_0, e_1, e_2, \ldots, e_{n-1}\}$ is a permutation of $\{0, 1, 2, \ldots, n-1\}$:

$$\begin{aligned} \Delta A &= \frac{1}{2} \sum_{\alpha,\beta=0}^{n-1} (\epsilon_{e_\alpha e_\beta} - \epsilon_{\alpha\beta}) k_\alpha \hat{p}_\beta \qquad (4.26) \\ \Delta \sum_{\alpha=0}^{n} k_{\perp\alpha}^2 &= \sum_{\alpha,\beta=0}^{n-1} [\max(\alpha,\beta) - \max(e_\alpha, e_\beta)] p_{\perp\alpha} p_{\perp\beta} \end{aligned}$$

where $\epsilon_{\alpha\beta}$ is defined as:

$$\epsilon_{\alpha\beta} = \begin{cases} +1, & \alpha > \beta; \\ 0, & \alpha = \beta; \\ -1, & \alpha < \beta \end{cases} \qquad (4.27)$$

4.6 The Bose-Einstein Effect: Gluonic Strings

We will proceed to extend the BE model described above to multi-gluon states, but we will first state some of the problems one must encounter in doing so.

The reason why the process in the previous section could be consistently formulated for a flat string, is that it is possible to find another set of vertex locations which would produce the same set of hadrons. In the presence of gluons, the situation is far more complicated. If the identical particles being exchanged happen to be separated by one or more gluon corners, one can not find an alternative set of vertices which would lead to the same set of final state particles from the same partonic configuration.

The vectors constituting the plaquettes generated during string fragmentation in ALFS have many geometrical relations between them. If we try to interchange only the momentum of two particles while keeping the plaquette planes in their original locations, we would need to project the particle momentum to longitudinal and transverse components relative to its new plaquette. It is then impossible to arrange that the recalculated vertex transverse momenta are orthogonal to the two plaquettes they are connected to, for all vertices. Also, if the particles are exchanged across a hard gluon corner, the new location for a momentum might be unnatural, i.e. large transverse momenta might be required relative to the new location of the particle, and large transverse momenta are suppressed because of their Gaussian distribution. If the vectors k are exchanged along with the momenta, the relocated plaquettes cease to be planar. In all such methods we considered, we found that once we exchange two particles created out of plaquettes with k vectors which are not parallel, the reconstructed configurations violate some basic geometrical relations obeyed by plaquettes in ALFS, which rules them out as possible outcomes of fragmentation events. Even if we choose to be lenient about some geometrical relations as long as total energy-momentum conservation is satisfied, the rearrangements result in extremely unlikely values for the vertex transverse momenta.

It may be possible to find another set of k vectors for the two plaquettes involved in the exchange and all the plaquettes between them which would preserve all geometrical relations after the exchange; but such a procedure is not consistent with the idea that one could treat the parton showers and hadronisation separately, which is at the heart of most simulation methods. At this moment we would be satisfied with finding approximations which would still stick to the established parton shower techniques, while at the same time trying to incorporate interference effects at the hadronisation stage on these multi-gluon states.

4.6.1 The Factorisation of the Event Weight

As an approximation, we will completely ignore all possible interference effects between different partonic states leading to the same set of hadrons. In such a case, the amplitude for a process in which two identical bosons are exchanged across a gluon corner must be zero, since, as noted above, it is impossible to reconstruct an alternative set of vertices leading to the same particle momenta without altering the partonic state. One would then consider exchanges of identical particles only inside flat regions or GDs in the string.

The amplitude in Eq.(4.20) can be looked upon as the product of factors corresponding to the creation of individual particles:

$$\begin{aligned} \mathcal{M} &= \prod_{\alpha'=0}^{n-1} \mathcal{M}(v_{\alpha'}, \delta A_{\alpha'}, v_{\alpha'+1}) \\ &= \prod_{\alpha'=0}^{n-1} \exp\left[(i\frac{1}{2\kappa} - \frac{b}{2})\delta A_{\alpha'} - \frac{1}{8\sigma^2}(k_{\perp\alpha'}^2 + k_{\perp\alpha'+1}^2)\right] \end{aligned} \tag{4.28}$$

One could link each of the $\mathcal{M}(v_{\alpha'}, \delta A_{\alpha'}, v_{\alpha'+1})$ to the production of one particle or with what is schematically represented in Eq.(4.16). In ALFS, this factorisation of the amplitude to a set of factors, one for each particle, is valid even for gluonic strings. This is because there is a unique planar area associated with the creation of each particle: the area of a plaquette. The sum of the areas of the plaquettes is the area in the area law. In other words, the fragmentation procedure in ALFS divides the area in the area law into a set of planar areas, one for each particle.

In order to analyse the change in the amplitude when identical particles with indices between α and β are permuted arbitrarily, we will rewrite Eq.(4.28) in the following way:

$$\begin{aligned} \mathcal{M} &= \left(\prod_{\alpha'=0}^{\alpha-1} \mathcal{M}(v_{\alpha'}, \delta A_{\alpha'}, v_{\alpha'+1})\right) \cdot \\ &\cdot \left(\prod_{\alpha'=\alpha}^{\beta} \mathcal{M}(v_{\alpha'}, \delta A_{\alpha'}, v_{\alpha'+1})\right) \cdot \left(\prod_{\alpha'=\beta+1}^{n-1} \mathcal{M}(v_{\alpha'}, \delta A_{\alpha'}, v_{\alpha'+1})\right) \end{aligned} \tag{4.29}$$

If v_α and $v_{\beta+1}$ remain unchanged under the permutations, it is clear that contributions from the first and the third parentheses would be unchanged. But Property 2 guarantees that v_α and $v_{\beta+1}$ remain unchanged under the permutations, if the plaquettes α through to β have their k vectors parallel, or if these plaquettes are parts of the same plane in Minkowski space.

Using the shorthand $\mathcal{M}_\alpha \equiv \mathcal{M}(v_\alpha, \delta A_\alpha, v_{\alpha+1})$, we can now write, for an arbitrary gluonic string, which has fragmented into a group of hadrons like in Eq.(4.11)

$$\begin{aligned} \mathcal{M} &= \left(\prod_{\alpha=0}^{\beta_1} \mathcal{M}_\alpha\right) \cdot \left(\prod_{\alpha=\beta_1+1}^{\beta_2} \mathcal{M}_\alpha\right) \cdot \left(\cdots\right) \cdots \left(\prod_{\alpha=\beta_r+1}^{n-1} \mathcal{M}_\alpha\right) \\ &= \left(\mathcal{M}^A\right) \cdot \left(\mathcal{M}^B\right) \cdots \end{aligned} \tag{4.30}$$

where the connected plaquettes collected into each of the parentheses above are assumed to have their k vectors parallel. In the second line of the equation, the superscripts “A”, “B”, etc represent these collections of plaquettes which are created with their k vectors parallel. We will call them “coherence regions” for the moment. To calculate the amplitude of an alternative configuration of vertices leading to the same set of particles, in which two particles in group A (for example) occur at interchanged orders, we need to calculate the altered amplitude contribution from group A, and multiply that to the amplitudes from group B,C,... which are not affected by the exchange. One can therefore evaluate permutations inside each coherence region independently.

The total amplitude is obtained by summing over the amplitudes of all allowed permutations of identical particles. If $\pi_i(A)$ represents a particular permutation of identical particles in coherence region A,

$$\begin{aligned} \mathcal{M} &= \sum_{i,j,k\ldots} \left(\mathcal{M}^{\pi_i(A)}\right) \cdot \left(\mathcal{M}^{\pi_j(B)}\right) \cdot \left(\mathcal{M}^{\pi_k(C)}\right) \cdots \\ &= \left(\sum_i \mathcal{M}^{\pi_i(A)}\right) \cdot \left(\sum_j \mathcal{M}^{\pi_j(B)}\right) \cdot \left(\sum_k \mathcal{M}^{\pi_k(C)}\right) \cdots \\ &= \mathcal{M}^A_{tot} \cdot \mathcal{M}^B_{tot} \cdot \mathcal{M}^C_{tot} \cdots \end{aligned} \tag{4.31}$$

Along with the result,

$$\sum_{i,j,k\ldots} |\left(\mathcal{M}^{\pi_i(A)}\right) \cdot \left(\mathcal{M}^{\pi_j(B)}\right) \cdot \left(\mathcal{M}^{\pi_k(C)}\right) \cdots|^2 = \tag{4.32}$$

$$\left(\sum_i |\mathcal{M}^{\pi_i(A)}|^2\right) \cdot \left(\sum_j |\mathcal{M}^{\pi_j(B)}|^2\right) \cdot \left(\sum_k |\mathcal{M}^{\pi_k(C)}|^2\right) \cdots$$

we obtain a generalisation of the weight in Eq.(4.22) for multi-gluon strings:

$$w = w^A \cdot w^B \cdot w^C \cdots \tag{4.33}$$

Thus we have shown that if we associate an amplitude of zero for the exchange of bosons across gluon corners, the Bose-Einstein event weight factorises into a product of individual weights for coherence regions. The weights for coherence regions can be evaluated independently by permuting particles inside the region and finding a weight as in the case of a flat string, using Eqs.(4.22,...,4.25). In the approximation we have considered up to this point, the hadrons emerging out of the hadronisation process with plaquette planes aligned with one GD in the partonic state will be grouped into one coherence region.

4.6.2 A BEC Model Based on Coherence Chains

The GDs used in the above are, strictly speaking, functions of the cut-off scale used in the parton shower. In [8] we noted that these GDs have interesting scaling properties, in that they seem to have nearly the same distribution in sizes relative to the cut-off scale, for a wide range of the value of the cut-off scale. But compared to a fixed scale, the smaller the cut-off, the larger the number of gluons, and hence the smaller the GDs, even though there might be more of them. This makes it unsatisfactory to not consider exchanged amplitudes across gluon corners. Smaller the cut-off, less the chance that two identical bosons would be found in one GD. In fact, one can imagine making the cutoff scale, and hence the GDs, so small that in the whole event there wont be any instances left of two identical particles in the same GD. Since the cut-off scale is tuned from other considerations, it seems like an artificial limitation of this particular approximation.

However, as the cut-off scale is lowered, the system also exhibits softer and softer gluons. If one such state is interchanged for another, the system does not look radically different either at the partonic or the hadronic level. One could argue that the amplitudes to produce those “slightly different” partonic states should be very similar, and at least some properties of the emerging system of hadrons would be insensitive to any small differences they might have.

This is where the concept of Coherence Chains helps. Defined on the hadronic state, they are answers to the question: “Could this set of hadrons be treated as if they came from one flat region on a string ?”. The hadrons might actually come from a region of the string which contains many gluons. But if it can still be regarded as flat, up to a certain scale in transverse momentum, we will assume that they could be identified with our coherence regions in the previous subsection.

The procedure to calculate the event weight in this approach would therefore be as follows. We first identify all Coherence Chains in an event. The energy-momentum vectors of the particles in every Coherence Chain are projected into longitudinal and transverse components relative to the plane of the Coherence Chain. A set of plaquettes is reconstructed on this plane using the particle energy-momenta and the starting vertex for the Coherence Chain. A weight is calculated for each Coherence Chain, considering permutations of identical particles inside the Coherence Chain. The weights obtained in all the Coherence Chains are then multiplied to give the total event weight.

Defining a Coherence Chain is tantamount to identifying the amplitudes of all partonic states which could give rise to hadronic states similar to the one used in the construction of the Coherence Chains. Thus, the Coherence Chain approximation of the analysis of BEC is built upon the expectation that the BEC would be insensitive to the small differences in the amplitudes for the formation of different partonic configurations involving very soft gluons. The use of Coherence Chains allows us lower the parton shower cut-off without making BE calculations like in Eq.(4.33) impossible.

4.6.3 A Few Comments About the Event Weight and Our Weighting Procedure

We expect that the weighting only affects the hadronisation process and does not modify the probability for different intermediate partonic states. An event weight gives the relative size of the true probability that should be associated with one particular event compared to the probability with which a Monte Carlo generates it. One could then count "1.3" events for an event which has a weight 1.3 in any statistics one might be interested in. This approach was found unsuitable for our BEC analysis.

The reason was that we found a multiplicity dependence in the weights. This means that events with higher number of particles would be counted more often, and that would change the multiplicity distributions generated in the Monte Carlo. In [12], a simple re-tuning of the Lund model parameters was used to shift the multiplicity distributions back to unweighted positions. This can not be done for multi-gluon strings, because the multiplicity of the event increases with gluonic activity and multi-gluon events would therefore end up being weighted higher than events with few or no gluons. The multiplicity distribution would shift more for multi-jet events compared to events with few jets, and an effective re-tuning would have to involve the particular partonic state.

Another way to use a Bose-Einstein event weight is to use it as an internal acceptance probability for the particular hadronisation event, while keeping the partonic configuration unchanged until an event gets accepted. In this method, we always associate one hadronic state with one partonic configuration, thereby keeping the relative normalisations of different kinds of partonic configurations unaffected.

It is desirable that a weight which is to be used as a rejection weight be positive definite. The weight used in [12], i.e. the weight in Eq.(4.21), was not positive definite. Since we needed the weight as a rejection weight, we decided in favour of the manifestly positive definite weight in Eq.(4.22).

Multiplicity distributions will still shift as the events with higher multiplicity have higher weights and have a higher chance of being accepted. But if the shift is larger for events with more jets, compared to events with simpler geometry, jet multiplicities from weighted events, when tuned to match those of the unweighted events for 2-jet systems, would not match up for higher number of jets. Since the unweighted Monte Carlos are known to describe experimental multiplicity distributions quite well, this would be an unhealthy feature of the model.

In this connection, we see the significance of certain stability properties of the Coherence Chains, discussed in section 4.4. We recall that the distribution in the number of particles included inside a CC was relatively insensitive to the global event variables. In an event with many jets, there are probably a large number of Coherence Chains. However, the number of particles inside one Coherence Chain still has the same distribution. This multiplicity will be shifted to higher values by BE weighting. But once we re-tune the program so that the correct multiplicity distribution is obtained for events with simple geometry, i.e. few CCs, the events with a larger number of CCs would automatically stand re-tuned, as they are merely larger collections of CCs of the same kind. Also, since the distribution in size of the Coherence Chains was rather insensitive to the centre of mass energy of the event, we expect that it would be possible to re-tune the Lund model parameters in a similarly energy insensitive way.

4.6.4 Resonance Decays

Since a large fraction of all the pions in the final state are produced as decay products of short lived resonances, it is important to consider their influence on the Bose-Einstein weight for an event. The decay of a resonance is normally thought of as a process which is very different from the string breakup. In this investigation, we will adopt the same approach to resonances as in [12]. We will assume that resonances with width larger than a certain cut-off, decay on a time scale short enough for the decay products to directly contribute to interference effects involved in the hadronisation process. We will also choose this cut-off in width at about 0.02 GeV, so that only the decay products of a few resonances like the ρ and the K^*-resonances are considered during the Bose-Einstein calculations.

Even though resonance decay of the ρ is considered to be isotropic, when the energy momenta of its decay products are projected as longitudinal and transverse components relative to the string plane, they always give reasonable values since the mass of the resonance happens to be about twice the scale for hadronisation transverse momenta for hadrons. Had the hadronisation transverse momentum scale been about one tenth of its phenomenological value (about 0.4 GeV for a hadron), it would have been quite unnatural to regard the decay products from a ρ decay as if they came directly from the decay of the string.

Once an order has been assigned to the decay products, the plaquette reconstruction process of section 4.5.1 can assign new plaquettes corresponding to the decay products in place of the plaquette corresponding to the resonance. Without going into much detail, we state that sometimes (eg. $\rho^0 \to \pi^+\pi^-$) the rank order of decay products can be deduced from the requirement of consistency with the decay of the original string. However, in many cases it is not possible to assign a unique order from such considerations. For such situations, we have chosen to reconstruct in all possible orders, to find the area law probabilities that would be associated with different orderings and then to select one of them based on the Bayesian probability for that particular ordering.

4.6.5 Higher Order permutations and Computing Time

As pointed out in [12], certain higher order permutations of identical particles might lead to configurations with significant contributions to the amplitude, while many lower order contributions might be negligible. Calculating the contribution of all permutations of identical particles takes an unacceptable amount of time. In [12], Andersson and Ringnér suggested a method to estimate which configurations might make significant contributions and generate only those configurations.

The concept of a "link" between two ranks was introduced from purely practical considerations. Two ranks, α and β, are said to have a link between them if and only if:

- The particles at ranks α and β are identical
- $Q^2 = -(p_\alpha - p_\beta)^2 < Q^2_{\max} \simeq 1\mathrm{GeV}^2$
- $|\hat{P}^2| = |(x_{\alpha+1} - x_\beta)^2| < |\hat{P}^2_{\max}| \simeq 20\mathrm{GeV}^2$ (slightly different from the condition used by Andersson and Ringnér)

Consider a permutation of the indices $\{e_0, e_1, \ldots, e_{n-1}\}$. It turns out, as expected from the expression for the amplitude terms in Eq.(4.23), that normally the contribution of the permutation is either strictly 0 or negligible, if there is no link between the ranks α and e_α. Therefore, only a small error is made in some rare events by considering permutations with the constraint that for all α, there is a link between α and e_α. The advantage in terms of computing time because of the use of this procedure is tremendous, and justifies its use.

We also point out that multi-jet events will typically have a much larger multiplicity than events with simpler structure. Even though the coherence chains breakup the events into smaller groups over which symmetrisation of

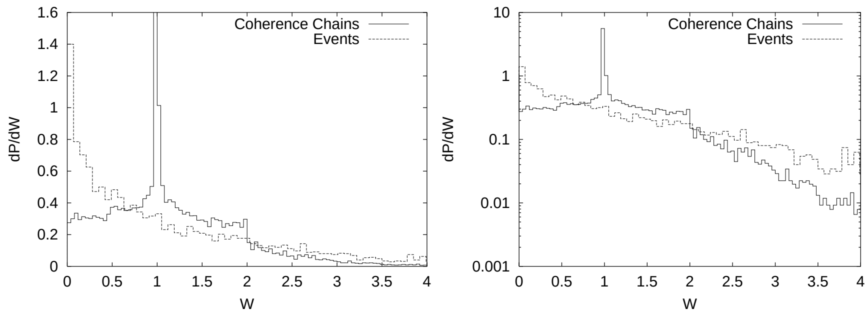

Figure 4.9: The figure to the left shows the weight distribution for an inclusive sample of events and the corresponding weight distribution for the Coherence Chains. We have used $\delta^2 = 0.10$ GeV^2 and $\sqrt{s} = 90$ GeV. The figure to the right shows the same result using a log scale instead. Note that the weight distribution for CCs extends beyond the range of the y-axis in the left-hand plot.

the amplitude is carried out, going through all permutations may still be prohibitively computation intensive. A coherence chain with 6 π^+s and 6 π^-s, for instance, will involve about 500 000 possible configurations. Though such chains are not the most common, they are not forbidden. Events with many identical particles in one chain will therefore slow down the simulation considerably, without affecting the end results, unless the above constraint is used to select the appropriate permutations.

4.6.6 Results

In this subsection, we will present a study of the distributions obtained from a Monte Carlo implementing the BE model described earlier.

The weight distribution for an inclusive sample of events at a centre of mass energy of 90 GeV is shown in Fig.4.9. As pointed out earlier, this weight is the product of as many terms as there are Coherence Chains in the event. In Fig.4.9, we also show the weight distribution for Coherence Chains. As with most properties of Coherence Chains, this weight distribution is rather insensitive to changes in the centre of mass energy and thrust of the event.

The "cliff" in the weight distribution for Coherence Chains at a weight value of 2 can be understood as follows. The events in which exactly one alternative permutation of the identical particles exists, have only two terms in the expression for the total amplitude. For this situation, the weight in Eq.(4.22) can not be larger than 2. But if there are more allowed permutations,

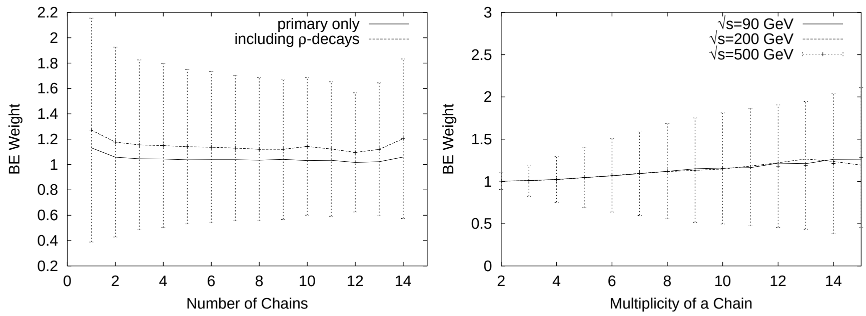

Figure 4.10: The plot to the left shows the mean weight of Coherence Chains vs the total number of chains in the event. The plot to the right shows the mean weight of Coherence Chains vs the number of particles included in the chains. The result was obtained using $\sqrt{s} = 90$ GeV and $\delta^2 = 0.10$ GeV^2.

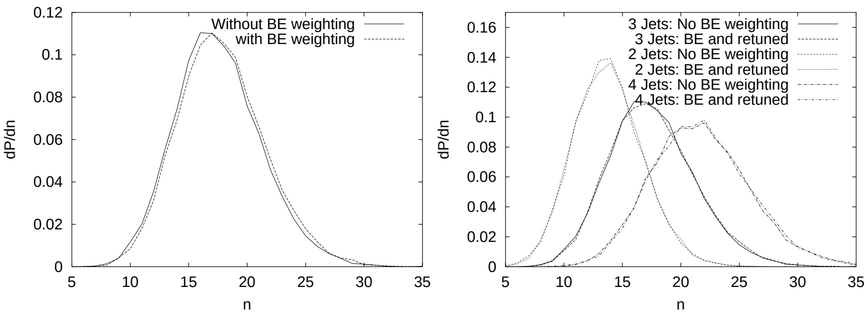

Figure 4.11: The weight shifts the multiplicity distribution, but it can be restored by a simple re-tuning of Lund model parameters as described in the text.

the weights could be either greater or smaller than 2. So, the weight distribution receives contribution from different (but not disjoint) sets of events on either side of 2. We plot the mean weight of Coherence Chains vs the total number of chains in the event in Fig.4.10. It shows that events with more Coherence Chains have the same kind of chains but in greater numbers, and that the weights of individual chains are similar to the weight of chains in other kinds of events. The weight of CCs plotted against the number of particles included in the chains is shown in Fig.4.10. We see that the average weight for events with higher multiplicities is slightly higher than for events with smaller multiplicities.

As discussed earlier, a higher average weight for chains with higher multi-

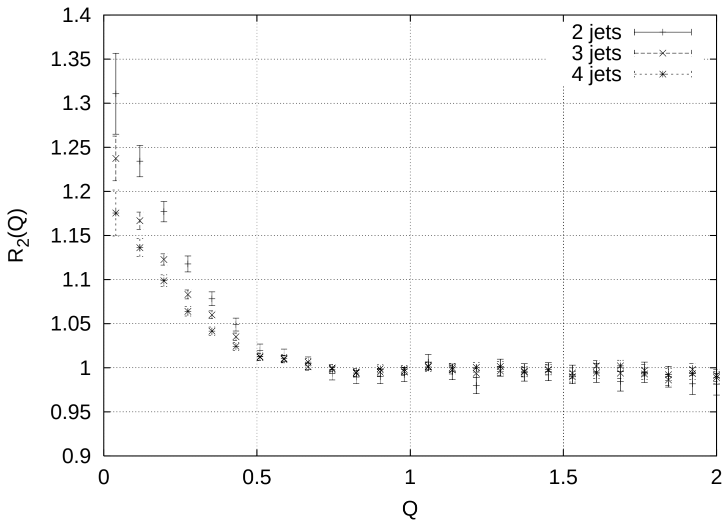

Figure 4.12: The figure shows the two particle correlation function for 2,3 and 4 jet events. $\sqrt{s}$ = 90 GeV and δ^2 = 0.25 GeV^2. The sample consists of the particles used in the symmetrisation.

plicity would shift the multiplicity distributions towards higher multiplicities, as is seen in the left-hand plot in Fig.4.11. However, as mentioned earlier, once the multiplicity distribution for one type of events, 3-jet events for instance, is tuned through an adjustment of the Lund model parameters, the multiplicity distribution on Coherence Chains would have been tuned back to their proper values. Since other kinds of events merely have a collection different average number of Coherence Chains, their multiplicity distributions would be automatically re-tuned. We demonstrate this in the right-hand plot in Fig.4.11, which shows multiplicity distributions in 2-jet, 3-jet and 4-jet events. After the application of BE weights, the multiplicity distributions shift to higher values like in the left-hand plot in Fig.4.11. We then re-tuned the Lund model b parameter (cf. Eq.(4.5)), so that the 3-jet multiplicity distribution was restored. With the re-tuned parameter values, we generated multiplicity distributions for 2-jet and 4-jet events with BE weights applied, and found them to be restored as well.

It should be mentioned here that Fig.4.10 shows a slight increase of the average weight for events in which there is only one chain. Either such events have no gluons in them, or only have very soft gluons which were overlooked by the Coherence Chain. Thus, the entire set of hadrons is included in one CC, which ends up with a slightly higher multiplicity than chains in events which

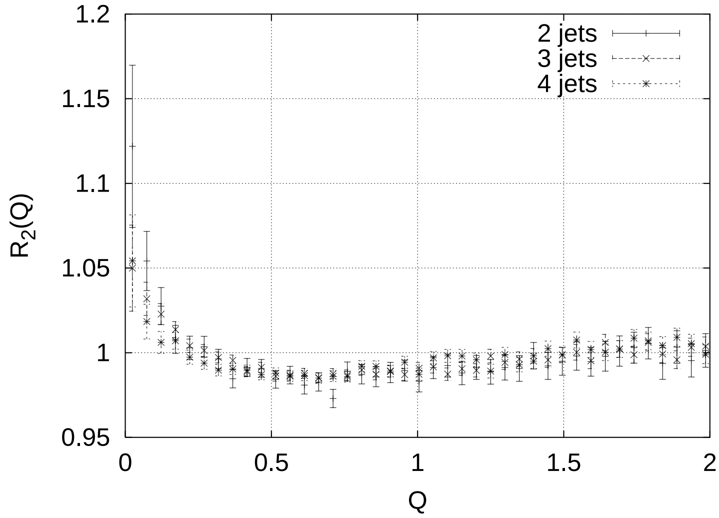

Figure 4.13: The figure shows the two particle correlation function for 2,3 and 4 jet events. $\sqrt{s} = 90$ GeV and $\delta^2 = 0.25$ GeV^2. Including pions from long-lived resonances screens the enhancement-effect shown in Fig.4.12 to a large extent.

have more chains. This would suggest that the tuning of 2-jet events would be special, but we find that tuning of weighted 3-jet multiplicity distribution is sufficient to restore not only multiplicity distributions of events with more jets, but also 2-jet multiplicity distributions.

In Fig.4.12, we show the plot of the two particle correlation function, obtained using our way of calculating the event weight. We separated the event into 2-jet, 3-jet and 4-jet events using the LUCLUS jet clustering algorithm in PYTHIA. The Bose-Einstein effect clearly becomes weaker for systems with more jets. This figure shows the correlation function for particles involved in the symmetrisation process. Relatively long-lived resonances like η and η' contribute with a rather large fraction of pions to the final state. These pions are not considered in our symmetrisation procedure. Consequently, their distribution is not affected by the weighting procedure and therefore they appear as background. In Fig.4.13, we show the correlation function including the pions from long-lived resonances. We see that the background caused by long-lived resonances screens the enhancement effect shown in Fig.4.12 to a large extent.

4.7 Summary and Conclusions

We have formulated a model for the description of Bose-Einstein correlations (BEC) inside the framework of the Lund string fragmentation model, for general multi-jet events. This is an extension of a similar attempt at modelling BEC for flat $q\overline{q}$ strings, presented earlier [12]. An amplitude is proposed for an underlying quantum mechanical process which would give rise to the Lund model formulae. The total amplitude for a final state with many identical particles is calculated by summing over contributions corresponding to permutations of identical particles in the final state. The effect of the interference terms are introduced into the Monte Carlo through an event weight. One signature of this re-weighting of the events is the enhancement of the probability of formation of identical pions a shade closer in phase space compared to a Monte Carlo without such a re-weighting procedure.

Our treatment of flat $\mathrm{q}\overline{\mathrm{q}}$ strings is largely similar to that in [12]. However, we use a different partitioning of the total probability among alternative configurations of final state particles, which is manifestly positive definite, in contrast to the weight used in [12]. We reformulated the treatment in the hadronisation scenario in ALFS, and observed that there was a possible generalisation to multi-gluon strings.

The properties of the hadronisation process in ALFS allow a symmetrisation procedure for fragmentation products of multi-gluon states; but they impose stringent constraints on possible contributions to the total amplitude from permuted configurations. Effectively, the result of these constraints is that the total amplitude and event weight can be factorised, and written as a product of contributions from local flat regions associated with the string. Consequently the correlation among particles comes out as a local effect in this approach.

The expression "local flat regions" for a string has to be understood in perspective. The multi-gluon strings considered in string fragmentation normally consist of a finite number of gluons with transverse momenta above a transverse momentum resolution scale. Such a resolution of the state results in a directrix consisting of a few light-like segments, and the resulting string world surface is a collection of planar regions. Choosing a smaller cut-off or resolution scale resolves smaller planar regions. Any choice of the scale is an approximation of the state, but the infrared stability of hadronisation process implies that it is possible to choose a scale such that properties of hadrons would be insensitive to any structure on the string at smaller scales. Moreover, different properties of the final state might be sensitive to structures at different resolution scales. Our approach to the Bose-Einstein correlations favours the use of a different resolution scale, which is based on the final state of hadrons, and does not introduce a new constraint on the resolution parameter used to define partonic states.

We defined structures called Coherence Chains (CCs) on the set of hadrons obtained as fragmentation products of multi-gluon strings, in the fragmentation scheme in ALFS. A CC is roughly a set of rank connected hadrons whose energy-momenta lie in a plane, up to small transverse fluctuations. Certain stability properties of the CCs with respect to global event properties like centre of mass energy, thrust, multiplicity of events etc, makes this structure an attractive basis upon which to base our BEC model.

Seen as a collection of coherence chains, the total BE weight for an event factorises into a set of independent contributions, one for each CC. Almost independent of the total energy, event topology, multiplicity, thrust etc, every event exhibits the same kind of coherence chains. The size of coherence chains is of course, determined by the maximum transverse momentum allowed in their definition. Once this scale is set however, events with larger multiplicity, or more complicated jet structure, merely appear as larger collections of CCs, each of which has more or less the same distributions in size. Consequently, BE weights for CCs are independent of the kind of events under consideration.

These properties allowed us to formulate a model for BEC using event weights which did not change the relative normalisations of different partonic configurations, using an event weight which did not average to unity. An average weight higher than 1 for CCs meant a shift of the multiplicity distributions for all kinds of events towards higher multiplicities, but a simple re-tuning of fragmentation related parameters to restore multiplicity distributions for CCs to their pre-weighting values resulted in an effective re-tuning of all kinds of events.

In this model for BEC, the pions in the final state which result from the decay of relatively long lived particles (eg. mesons containing c or b quarks, the pseudo-scalar states η, η') would not have correlations with the rest of the pions in the events. The decay of these resonances is thought of as a process independent of string fragmentation, and the decay products are not available at the time scale of string fragmentation to contribute to the symmetrised amplitude.

Short lived resonances like the ρ-mesons on the other hand decay on a time scale comparable to string decay. It is reasonable to expect that the decay products from such decays would play a role in the total symmetrised amplitude. We have treated these short lived resonances in the same way as in [12], i.e. we treated the resonance decay products as if they were results of string fragmentation, while evaluating the BE weight. A different treatment of short lived resonances might affect our results.

This model certainly results in an enhancement of the two particle correlation function for small momentum transfers. There is also an unambiguous trend for the correlation strength to go down for more complicated event topologies. However, the overall correlation strength, taking into account the background created by the decay of long lived resonances, appears to be rather low. We stress that the distributions in this paper should not be compared with those in [12], as they were correlations between "participant" pions on a flat string, whereas we have presented distributions from all pions, from events including parton showers. Naturally the correlation between direct pions is larger, but we believe that it is not possible to identify particular pions in the final state as decay products of particular resonances.

Though re-tuning of model parameters can affect the correlation strength and correlation length to a small extent, the signal remains small in the rather large background from resonance decays. Thus comparison with experimental data indicate that other physical processes contribute to the correlations. However, in particular the dependence of the matrix elements upon the transverse momenta is very uncertain. In the future we will study if a modification of the $k_\perp$-dependence or some other possible effect, may enhance the correlation strength in the model. If this turned out to be the case, the result could eventually lead to an increased understanding of the hadronisation process on a quantum mechanical level.

Acknowledgements

We are grateful towards the late Prof. Bo Andersson for his guidance in the initial stages of this project. We would like to thank G. Gustafson, L. Lönnblad and T. Sjöstrand for many valuable discussions.

References

[1] B. Andersson, G. Gustafson and C. Peterson, *Z. Phys.* **C1** (1979) 105.

[2] B. Andersson, G. Gustafson and B. Söderberg, *Z. Phys.* **C20** (1983) 317.

[3] B. Andersson, The Lund Model, Cambridge University Press, 1998.

[4] T. Sjöstrand, P. Edén, C. Friberg, L. Lönnblad, G. Miu, S. Mrenna and E. Norrbin, *Computer Phys. Commun.* **135** (2001) 238.

[5] T. Sjöstrand, *Nucl. Phys.* **B248** (1984) 469.

[6] B. Andersson, S. Mohanty and F. Söderberg, *Eur. Phys. J.* **C21** (2001) 631.

[7] S. Mohanty, LU TP 03-09 (2003).

[8] B. Andersson, S. Mohanty and F. Söderberg, *Nucl. Phys.* **B646** (2002) 102.

[9] B. Andersson, G. Gustafson and B. Söderberg, *Nucl. Phys.* **B264** (1986) 29.

[10] B. Andersson, P. Dahlqvist and G. Gustafson, *Z. Phys.* **C44** (1989) 455; *Z. Phys.* **C44** (1989) 461.

[11] B. Andersson and W. Hofmann, *Phys. Lett.* **B169** (1986) 364.

[12] B. Andersson and M. Ringnér, *Nucl. Phys.* **B513** (1998) 627.

[13] B. Andersson, G. Gustafson and T. Sjöstrand, *Z. Phys.* **C6** (1980) 235.

[14] Yu.L. Dokshitzer, V.A. Khoze, A.H. Mueller and S.I. Troyan, Basics of Perturbative QCD (Edition Frontières 1991).

[15] G. Gustafson and U. Pettersson, *Nucl. Phys.* **B306** (1988) 746.

[16] L. Lönnblad, *Computer Phys. Commun.* **71** (1992) 15.

[17] T. Sjöstrand, *Computer Phys. Commun.* **28** (1983) 227.

[18] B. Andersson, G. Gustafsson and J. Samuelsson, *Z. Phys.* **C64** (1994) 653.